
JSCSEN 75(3)297–422(2010)

Journal of the Serbian Chemical Society

e
Version
electronic

VOLUME 75

No 3

BELGRADE 2010

Available on line at



www.shd.org.rs/JSCS/

The full search of JSCS

is available through

DOAJ DIRECTORY OF

OPEN ACCESS

JOURNALS

www.doaj.org



CONTENTS

Editor's Note	297
Organic Chemistry	
<i>H. Ghasemnejad-Bosra, M. Faraje, S. Habibzadeh and F. Ramzanian-Lehmali:</i> An efficient one-pot synthesis of highly substituted furans catalyzed by <i>N</i> -bromosuccinimide	299
<i>A. Hasaninejad, M. A. Zolfigol, G. Chehardoli and M. Mokhlesi:</i> Molybdatephosphoric acid as an efficient catalyst for the catalytic and chemoselective oxidation of sulfides to sulfoxides using urea hydrogen peroxide as a commercially available oxidant.....	307
Biochemistry and Biotechnology	
<i>A. Divac, B. Tomic and J. Kušić:</i> The role of adenosine triphosphate in the function of human origin recognition complex 4 protein	317
<i>V. D. Dragičević, S. D. Šredojević and M. B. Spasić:</i> Introduction of the interdependence between the glutathione half-cell reduction potential and the thermodynamic parameters during accelerated aging of maize seeds	323
<i>M. Voicescu, R. Ion and A. Meghea:</i> Evaluation of the oxidative activity of some free base porphyrins by a chemiluminescence method	333
<i>R. S. Verma, L. U. Rahman, C. S. Chanotiya, R. K. Verma, A. Chauhan, A. Yadav, A. Singh and A. K. Yadav:</i> Essential oil composition of <i>Lavandula angustifolia</i> Mill. cultivated in the mid hills of Uttarakhand, India (Short communication)	343
Inorganic Chemistry	
<i>A. S. Munde, A. N. Jagdale, S. M. Jadhav and T. K. Chondhekar:</i> Synthesis, characterization and thermal study of some transition metal complexes of an asymmetric tetradentate Schiff base ligand	349
Theoretical Chemistry	
<i>A. R. Ashrafi and M. Ghorbani:</i> Enumeration of a class of IPR hetero-fullerenes	361
Polymers	
<i>Y. Liu, L. Wang, X. Tuo and S. Li:</i> An SEM and EDS study of the microstructure of nitrate ester plasticized polyether propellants	369
<i>J. Gao, Z. Ma, J. Guo, Y. Huai, Z. Deng and J. Suo:</i> Surface-charged polyacrylonitrile/poly(vinyl alcohol) (PAN/PVA) colloids used to prepare proton conducting materials (Short communication)	377
Materials	
<i>Z. Li, T. Shi and L. Guo:</i> Preparation and morphology of porous SiO ₂ ceramics derived from rice flour templates	385
Chemical Engineering	
<i>J. Ivanović, D. Mišić, M. Ristić, O. Pešić and I. Žižović:</i> Supercritical CO ₂ extract and essential oil of bay (<i>Laurus nobilis</i> L.) – chemical composition and antibacterial activity	395
Environmental	
<i>F. J. Rojas Moreno, J. M. Cardenete López, R. Marín Galván, M. J. Martínez Cordón and J. M. Rodríguez Mellado:</i> On the removal of <i>s</i> -triazine herbicides from waters using commercial low-cost granular carbons	405
<i>S. P. Agarwal, M. D. Khalid Anwer, R. Khanna, A. Ali and Y. Sultan:</i> Humic acid from Shilajit – a physico-chemical and spectroscopic characterization	413

Published by the Serbian Chemical Society
Karnegijeva 4/III, 11000 Belgrade, Serbia
Printed by the Faculty of Technology and Metallurgy
Karnegijeva 4, P.O. Box 35-03, 11120 Belgrade, Serbia

Available online at www.shd.org.rs/JSCS/



JSCS – OnLine First

The section “JSCS – OnLine First” at www.shd.org.rs/JSCS, starting March 1, 2010, and issue No. 3 of Vol. 75 (2010), displays peer reviewed and accepted articles to be published in the *Journal of the Serbian Chemical Society*. The articles are prepared for final technical work.

When the final article is assigned to an issue of the Journal, the “JSCS – OnLine First” version will be removed from this section and will appear in the associated printed Journal issue and in the electronic form at the Journal’s Web Site.

Please be aware that, although “JSCS – On Line First” versions do not have all bibliographic details available yet, they can already be cited using the year of OnLine publication and the DOI as follows: Author (s), Article Title, *Journal* (Year), DOI. Printed (or electronic) versions are to be cited in the usual way.

Please consult the Journal’s reference style for the exact appearance of these elements, abbreviation of journal names and the use of punctuation.



An efficient one-pot synthesis of highly substituted furans catalyzed by *N*-bromosuccinimide

HASSAN GHASEMNEJAD-BOSRA^{1*}, MOHAMMAD FARAJE¹,
SETAREH HABIBZADEH² and FARHAD RAMZANIAN-LEHMALI³

¹Islamic Azad University-Babol Branch, School of Science, P.O. Box 755, Babol, ²Industrial Noshiravani University, Babol and ³University of Payamnoor, Babol, Iran

(Received 24 August, revised 25 December 2009)

Abstract: *N*-Bromosuccinimide was found to efficiently catalyze the synthesis of highly functionalized, tetra-substituted furan derivatives in the one-pot reactions of but-2-ene-1,4-diones and acetoacetate esters in the presence of *i*-PrOH as solvent under mild and neutral conditions at 80–90 °C for 3–7 h in high yields (87–94 %).

Keywords: highly substituted furans; *N*-bromosuccinimide; but-2-ene-1,4-diones; acetoacetate esters.

INTRODUCTION

Highly substituted furans are a structural component of a vast number of biologically active natural and synthetic compounds.^{1–4} These compounds are found as structural units in many natural products, such as kallolides,⁵ combinatorialides,⁶ pheromones⁷ and polyether antibiotics.⁸ These heterocycles have found applications in many pharmaceuticals, fragrances and dyes.⁹ Furan subunits have also been used as building blocks for a large number of heterocyclic compounds and as synthons in natural product synthesis.¹⁰ As a consequence, the synthesis of furan derivatives has been a subject of research for over a century, and a variety of well-established classical methods are now available in the literature.^{11–14} The development of newer approaches for heterocyclic syntheses employing efficient and economic routes is a popular research area nowadays. The most common strategy involved in the synthesis of furans is the cyclization¹⁵ of 1,4-dicarbonyl compounds. Of the other various methods, syntheses involving transition-metal salts have recently been described for the preparation of substituted furan derivatives.^{16,17} Oh *et al.*¹⁸ synthesized highly substituted furans via Pt-catalyzed hydroxyl- or alkoxy-assisted cyclization of 2-(1-alkynyl)-2-alkene-1-ones. More recently, Dey and coworkers reported a novel method to

*Corresponding author. E-mail: h_ghasem2000@yahoo.it
doi: 10.2298/JSC090824025G

highly substituted furans by InCl_3 -catalyzed nucleophilic addition followed by cyclization reaction, although it is limited to specific substrate classes.¹⁹

EXPERIMENTAL

The employed chemicals were obtained from either Merck or Fluka. The IR spectra were recorded using a Shimadzu 435-U-04 spectrophotometer (KBr pellets) and the NMR spectra were obtained in CDCl_3 using a 90 MHz JEOL FT NMR spectrometer. All melting points were determined on a Büchi 530 melting point apparatus and are reported uncorrected.

Typical procedure for the synthesis of tetra-substituted furans

To a stirred solution of but-2-ene-1,4-dione, **1a** (0.24 g, 1.0 mmol), and methyl acetoacetate, **2a** (0.18 g, 1.0 mmol), in dry *i*-PrOH (7.0 ml) was added anhydrous *N*-bromosuccinimide, NBS (52 mg, 0.23 mmol). The reaction mixture was then stirred under reflux at 80–90 °C for 3.1 h. After complete disappearance of the starting materials (monitored by TLC using petroleum ether–chloroform (6:4)), the solvent was removed from the reaction mixture on a rotary evaporator. The residue was then diluted with water (15 ml) and extracted with CHCl_3 (4×15 ml). The organic layer was separated, washed with brine and then dried over anhydrous MgSO_4 . Removal of the solvent resulted in a solid which was chromatographed over silica gel using petroleum ether and an increasing proportion of ethyl acetate as eluent. Petroleum ether–ethyl acetate (96:4) eluent gave a solid which was recrystallized from chloroform–petroleum ether (2:8): **3a** (0.31 g, 93 %), white solid, m.p. 92 °C.

The products **3b–j** were obtained in a similar manner using the appropriate but-2-ene-1,4-dione and acetoacetate ester.

The products were characterized on the basis of their physical and spectral analysis (Table I) and by direct comparison with literature data.¹⁹

TABLE I. IR (KBr), ^1H -NMR and ^{13}C -NMR spectral data of the tetra-substituted furans **3a–j**

Product	IR, $\tilde{\nu}$ / cm^{-1}	^1H -NMR, δ / ppm	^{13}C -NMR, δ / ppm
3a	3068, 1712, 1610, 1452, 1058, 772	2.35 (3H, <i>s</i> , $-\text{CH}_3$), 3.28 (3H, <i>s</i> , $-\text{OCH}_3$), 4.45 (2H, <i>s</i> , $-\text{CH}_2-$), 7.36–7.55 (10H, <i>m</i> , Ar)	14.40 ($-\text{CH}_3$), 35.63 ($-\text{CH}_2-$), 51.12 ($-\text{OCH}_3$), 107.69 (C_3), 122.79 (C_4), 126.01–134.57 (Ph), 149.02 (C_5), 155.15 (C_2), 166.78 ($-\text{CO}_2\text{Me}$), 196.69 (CO)
3b	3063, 1716, 1625, 1460, 1050, 796	1.24 (3H, <i>t</i> , $-\text{CH}_2-\text{CH}_3$), 2.34 (3H, <i>s</i> , $-\text{CH}_3$), 4.12 (2H, <i>q</i> , $-\text{CH}_2-\text{CH}_3$), 4.42 (2H, <i>s</i> , $-\text{CH}_2-$), 7.30–7.57 (10H, <i>m</i> , Ar)	14.01 ($-\text{CH}_2-\text{CH}_3$), 16.49 ($-\text{CH}_3$), 37.57 ($-\text{CH}_2-$), 59.74 ($-\text{OCH}_2-$), 111.32 (C_3), 125.65 (C_4), 127.97–135.12 (Ph) 149.02 (C_5), 155.74 (C_2), 166.49 ($-\text{CO}_2\text{Et}$), 196.62 (CO)
3c	3058, 2933, 1783, 1678, 1509, 1316, 1050, 827	2.31 (3H, <i>s</i> , $-\text{CH}_3$), 2.35 (3H, <i>s</i> , $-\text{CH}_3$), 2.44 (3H, <i>s</i> , $-\text{CH}_3$), 3.62 (3H, <i>s</i> , $-\text{OCH}_3$), 4.43 (2H, <i>s</i> , $-\text{OCH}_3$), 4.73 (2H, <i>d</i> , Ar), 7.35 (2H, <i>d</i> , Ar), 7.96 (2H, <i>d</i> , Ar)	14.85 ($-\text{CH}_3$), 21.08 ($-\text{CH}_3$), 21.67 ($-\text{CH}_3$), 35.78 ($-\text{CH}_2-$), 51.38 ($-\text{OCH}_3$), 114.36 (C_3), 114.85 (C_4), 127.03–144.15 (Ph), 150.79 (C_5), 159.27 (C_2), 165.08 ($-\text{CO}_2\text{Me}$), 197.33 (CO)



TABLE I. Continued

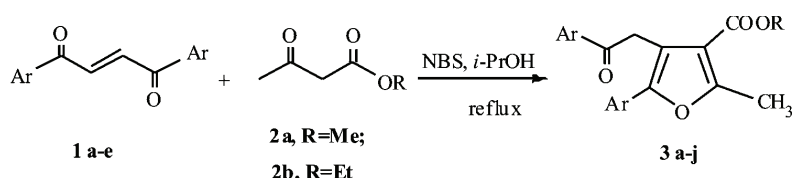
Product	IR, $\tilde{\nu}$ / cm ⁻¹	¹ H-NMR, δ / ppm	¹³ C-NMR, δ / ppm
3d	3070, 1710, 1609, 1448, 1250, 1108, 770	1.22 (3H, <i>t</i> , $-\text{CH}_2\text{CH}_3$), 2.32 (3H, <i>s</i> , $-\text{CH}_3$), 2.34 (3H, <i>s</i> , $-\text{CH}_3$), 2.37 (3H, <i>s</i> , $-\text{CH}_3$), 4.10 (2H, <i>q</i> , $-\text{CH}_2-$ CH_3), 4.45 (2H, <i>s</i> , $-\text{CH}_2-$), 7.03–7.19 (4H, <i>dd</i> , Ar), 7.76 (2H, <i>d</i> , Ar), 8.02 (2H, <i>d</i> , Ar)	14.15 ($-\text{CH}_2\text{CH}_3$), 16.58 ($-\text{CH}_3$), 21.10 ($-\text{CH}_3$), 21.82 ($-\text{CH}_3$), 35.79 ($-\text{CH}_2-$), 58.45 ($-\text{OCH}_2-$), 115.01 (C ₃), 114.97 (C ₄) 127.03–143.47 (Ph), 157.98 (C ₅), 164.35 (C ₂), 166.08 ($-\text{CO}_2\text{Et}$), 197.97 (CO)
3e	3080, 1704, 1605, 1442, 1238, 1025, 785	2.36 (3H, <i>s</i> , $-\text{CH}_3$), 3.30 (3H, $-\text{OCH}_3$), 4.47 (2H, <i>s</i> , $-\text{CH}_2-$), 7.48–7.56 (4H, <i>dd</i> , Ar), 7.70–7.81 (4H, <i>dd</i> , Ar)	15.32 ($-\text{CH}_3$), 31.29 ($-\text{CH}_2-$), 50.73 ($-\text{OCH}_3$), 118.49 (C ₃), 123.84 (C ₄), 126.03–141.49 (Ph), 149.02 (C ₅), 155.17 (C ₂), 165.23 ($-\text{CO}_2\text{Me}$), 196.70 (CO)
3f	3085, 1709, 1611, 1437, 1245, 1062, 788	1.24 (3H, <i>t</i> , CH_2CH_3), 2.41 (3H, <i>s</i> , $-\text{CH}_3$), 4.13 (2H, <i>q</i> , $-\text{CH}_2\text{CH}_3$), 4.48 (2H, <i>s</i> , $-\text{CH}_2-$), 7.41–7.50 (4H <i>dd</i> , Ar), 7.68–7.76 (4H, <i>dd</i> , Ar)	16.01 (CH_2CH_3), 17.07 ($-\text{CH}_3$), 36.11 ($-\text{CH}_2-$), 59.82 ($-\text{OCH}_2-$), 116.12 (C ₃), 116.97 (C ₄), 131.17–147.53 (Ph), 158.38 (C ₅), 165.25 (C ₂), 165.98 ($-\text{CO}_2\text{Et}$), 198.17 (CO)
3g	3100, 1705, 1610, 1450, 1248, 1055, 792	2.35 (3H, <i>s</i> , $-\text{CH}_3$), 3.28 (3H, $-\text{OCH}_3$), 4.45 (2H, <i>s</i> , $-\text{CH}_2-$), 7.39 (2H, <i>d</i> , Ar), 7.50–7.58 (4H, <i>dd</i> , Ar), 7.85 (2H, <i>d</i> , Ar)	14.68 ($-\text{CH}_3$), 31.57 ($-\text{CH}_2-$), 51.38 ($-\text{OCH}_3$), 116.33 (C ₃), 127.81 (C ₄), 129.10–142.40 (Ph), 151.03 (C ₅), 156.37 (C ₂), 167.03 ($-\text{CO}_2\text{Me}$), 196.19 (CO)
3h	3090, 1706, 1613, 1458, 1090, 838	1.20 (3H, <i>t</i> , $-\text{CH}_2\text{CH}_3$), 2.32 (3H, <i>s</i> , $-\text{CH}_3$), 4.08 (2H, <i>q</i> , $-\text{CH}_2-$), 59.01 ($-\text{OCH}_2-$), 116.57 (C ₃), 4.51 (2H, <i>s</i> , $-\text{CH}_2\text{CH}_3$), 7.31 (2H, <i>d</i> , Ar), 7.45–7.51 (4H, <i>dd</i> , Ar), 7.73 (2H, <i>d</i> , Ar)	15.01 ($-\text{CH}_2\text{CH}_3$), 17.19 ($-\text{CH}_3$), 34.24 ($-\text{OCH}_2-$), 115.87 (C ₄), 132.54–147.78 (Ph), 157.44 (C ₅), 166.05 (C ₂), 167.01 ($-\text{CO}_2\text{Et}$), 197.18 (CO)
3i	3110, 1703, 1606, 1451, 1100, 840	2.18 (3H, <i>s</i> , $-\text{CH}_3$), 2.21 (3H, $-\text{CH}_3$), 2.29 (3H, <i>s</i> , $-\text{CH}_3$), 3.32 (3H, <i>s</i> , $-\text{OCH}_3$), 4.56 (2H, <i>s</i> , $-\text{CH}_2-$) 7.24 (3H, <i>m</i> , Ar), 7.51 (3H, <i>m</i> , Ar)	14.11 ($-\text{CH}_3$), 25.98 ($-\text{CH}_3$), 26.29 ($-\text{CH}_3$), 37.12 ($-\text{CH}_2-$), 51.74 ($-\text{OCH}_3$), 116.30 (C ₃), 116.84 (C ₄), 129.14–145.35 (Ph), 159.70 (C ₅), 169.47 (C ₂), 170.22 ($-\text{CO}_2\text{Me}$), 198.35 (CO)
3j	3105, 1707, 1611, 1452, 1235, 1039, 770	1.23 (3H, <i>t</i> , CH_2CH_3), 2.17 (3H, <i>s</i> , $-\text{CH}_3$), 2.28 (3H, <i>s</i> , $-\text{CH}_3$), 2.31 (3H, <i>s</i> , $-\text{CH}_3$), 4.10 (2H, <i>q</i> , $-\text{CH}_2\text{CH}_3$), 4.53 (2H, <i>s</i> , $-\text{CH}_2-$), 7.12 (3H, <i>m</i> , Ar), 7.49 (3H, <i>m</i> , Ar)	14.15 ($-\text{CH}_2\text{CH}_3$), 16.58 ($-\text{CH}_3$), 26.78 ($-\text{CH}_3$), 27.27 ($-\text{CH}_3$), 37.48 ($-\text{CH}_2-$), 59.37 ($-\text{OCH}_2-$), 115.01 (C ₃), 116.13 (C ₄) 130.12–145.25 (Ph), 160.15 (C ₅), 170.31 (C ₂), 172.15 ($-\text{CO}_2\text{Et}$), 198.54 (CO)

RESULTS AND DISCUSSION

In continuation of on-going research on various transformations by halogenating agents and sydnone,^{20–26} and also in order to avoid the drawbacks generally resulting from the use of strong acidic media in nitrosation reactions, herein is reported the use of NBS as a more robust and efficient catalyst in the



one-pot synthesis of the highly functionalized tetra-substituted furan derivatives **3a–j** by reaction of but-2-ene-1,4-diones **1a–e** and acetoacetate esters **2a** or **2b** in *i*-PrOH in satisfactory yields (87–94 %) under neutral conditions (Scheme 1, Table II). As shown in Table II, the reactions occurred satisfactorily within 3.1–6.1 h under reflux conditions. The experimental results indicate that the most effective conversion occurred when a 1:0.23 substrate:NBS mole ratio was used. Longer reaction times were required when lower amounts of NBS were employed. It is important to note that no furan derivatives were afforded when the reactions were performed in the absence of NBS in the reaction mixture.



Scheme 1. Proposed mechanism for the synthesis of highly substituted furans.²⁶

TABLE II. NBS-catalyzed synthesis of furans **3a–j**

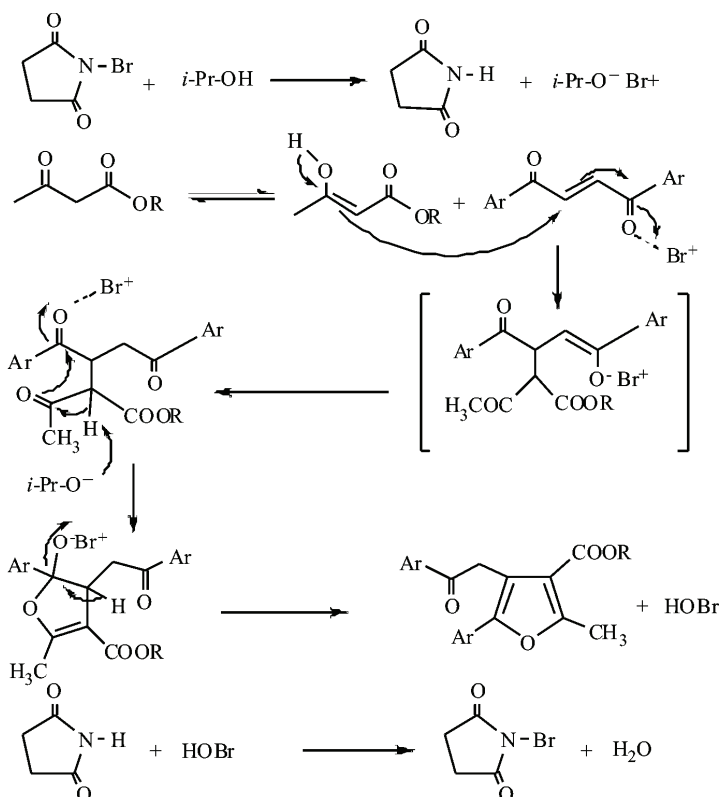
Entry	Product ^a	Ar	R	Time, h	Yield, % ^b	M.p., °C
1	3a	C ₆ H ₅ Me		3.1	93	92
2	3b	C ₆ H ₅ Et		3.9	91	89
3	3c	4-Me-C ₆ H ₄ Me		4.0	89	83
4	3d	4-Me-C ₆ H ₄ Et		3.8	87	80
5	3e	4-Br-C ₆ H ₄ Me		3.3	89	87
6	3f	4-Br-C ₆ H ₄ Et		5.2	94	85
7	3g	4-Cl-C ₆ H ₄ Me		4.7	90	96
8	3h	4-Cl-C ₆ H ₄ Et		5.5	91	94
9	3i	3-Cl,4-Me-C ₆ H ₃ Me		6.0	93	79
10	3j	3-Cl,4-Me-C ₆ H ₃ Et		6.1	94	77

^aAll the isolated products were characterized by their physical properties, by ¹H-NMR, ¹³C-NMR and IR spectra and by direct comparison with literature data;^{19 b} isolated yields

The mechanism shown in Scheme 2 is proposed for these reactions.²⁶ Thus, the 1,4-diarylbut-2-ene-1,4-diones act as Michael acceptors and the acetoacetates as nucleophiles resulting in a Michael adduct that under the influence of NBS forms a hemiketal, which undergoes spontaneous dehydration to afford the furans. It is important to note that no furan derivatives were formed when the reactions were performed in the presence of HBr as catalyst. Furthermore, no reaction was seen when the 1,4-diarylbüt-2-ene-1,4-diones and acetoacetates were used separately as substrates with NBS as the catalyst in the presence of *i*-PrOH under reflux.

The advantages or the characteristic aspects of the method described in this paper in comparison with other previously reported ones are the following: the yields of products were better than the previous reported yields and in addition, the catalyst NBS in comparison with 1,3-dibromo-5,5-dimethylhydantoin (DBH)

and InCl_3 is inexpensive, has no moisture sensitivity, and no special measures are required for the reaction.



Scheme 2.

The role of the solvent was also investigated. Among the various solvents tested, *i*-PrOH afforded the maximum yield of the furan derivative **3a** (Table III). It is well known that reactions of this type are more efficient in polar solvents, which was corroborated in this study (Table III). It was also observed that the inclusion of water had very little or no effect on this reaction.

TABLE III. Role of the solvent in the synthesis of furan **3a**

Solvent Ti me, h	Isolated yield of 3a , %
<i>i</i> -PrOH 3.0	93
<i>i</i> -PrOH–H ₂ O (6:4)	60
MeOH 9.0	52
CH ₃ CN 18	44
CH ₂ Cl ₂ 15	38
THF 14	61

^aExtension of the reaction did not improve the product yield

CONCLUSIONS

The present methodology shows that *N*-bromosuccinimide (NBS) is an efficient catalyst in the one-pot synthesis of highly functionalized tetra-substituted furan derivatives. The main advantages of the presented protocol are mild, clean and environmentally benign reaction conditions, as well as the high yields. Furthermore, this method is also expected to find application in organic synthesis due to the low cost of the reagent. It is believed that this method will be a useful addition to modern synthetic methodologies.

Acknowledgements. We wish to thank the Islamic Azad University-Babol Branch, Babol, Iran, for financial support during the realization of this research.

ИЗВОД

ЕФИКАСНА СИНТЕЗА У ЈЕДНОМ СУДУ ВИСОКО СУПСТИТУИСАНИХ ФУРАНА КАТАЛИЗОВАНА *N*-БРОМСУКЦИНИМИДОМ

HASSAN GHASEMNEJAD-BOSRA¹, MOHAMMAD FARAJE¹, SETAREH HABIBZADEH²
и FARHAD RAMZANIAN-LEHMALI³

¹*Islamic Azad University-Babol Branch, School of Science, P.O. Box 755, Babol, Industrial Noshiravani University, Babol* и ³*University of Payamnoor, Babol, Iran*

Утврђено је да *N*-бромсукцинимид ефикасно катализује синтезу високо функционализованих, тетрасупституисаних деривата фурана у реакцији у једном суду бут-2-ен-1,4-диона и ацатоацетатних естара у *i*-PrOH као растворачу под благим и неутралним условима на 80–90 °C током 3–7 h уз високе приносе (87–94 %).

(Примљено 24. августа, ревидирано 25. децембра 2009)

REFERENCES

1. a) Y. Guindon, M. Therien, Y. Girard, C. Yoakim, *J. Org. Chem.* **52** (1987) 1680; b) D. J. Goldsmith, E. Kennedy, R. J. Campbell, *J. Org. Chem.* **40** (1975) 3571; c) B. H. Lipschutz, *Chem. Rev.* **86** (1986) 795
2. K. S. Huang, *J. Chin. Chem. Soc.* **51** (2004) 1305
3. S. Solujić, S. Šukdolak, N. Vu ković, N. Niciforović, S. Stanić, *J. Serb. Chem. Soc.* **73** (2008) 1039
4. T. Shah, V. Desi, *J. Serb. Chem. Soc.* **72** (2007) 443
5. S. A. Look, M. T. Burch, W. Fenical, Q. Zheng, J. Clardy, *J. Org. Chem.* **50** (1985) 5741
6. W. Fenical, R. K. Okuda, M. M. Bandurraga, P. Culver, R. S. Jacobs, *Science* **212** (1981) 1512
7. a) K. Mori, *Tetrahedron* **45** (1989) 3233; b) D. L. Wright, *Chem. Innov.* **31** (2001) 17; c) B. A. Keay, P. W. Dibble, in *Comprehensive Heterocyclic Chemistry II*, Elsevier, Oxford, 1997, p. 395
8. J. W. Westley, *Polyether Antibiotics: Naturally Occurring Acid Ionophores*, Marcel Dekker, New York, 1982
9. X. L. Hou, H. Y. Cheung, T. U. Hon, P. L. Kwan, T. H. Lo, S. Y. Tong, H. N. C. Wong, *Tetrahedron* **54** (1998) 1955
10. D. L. Wright, *Prog. Heterocycl. Chem.* **17** (2005) 1

11. C.-T. Chunge, C.-H. Yen, H.-J. Wu, *J. Chin. Chem. Soc.* **45** (1998) 789
12. T.-W. Tsai, E.-C. Wang, S.-R. Li, Y.-H. Chen, Y.-L. Lin, Y.-F. Wang, K.-S. Huang, *J. Chin. Chem. Soc.* **51** (2004) 1307
13. K.-S. Huang, E.-C. Wang, H.-M. Chen, *J. Chin. Chem. Soc.* **51** (2004) 585
14. K. Yasutaka, T. Makoto, T. Kazuhiko, U. Kiitiro, *Tetrahedron* **48** (1992) 3495
15. a) J. A. Marshall, E. D. Robinson, *J. Org. Chem.* **55** (1990) 3450; b) J. A. Marshall, X. J. Wang, *J. Org. Chem.* **57** (1992) 3387; c) A. S. K. Hashmi, T. L. Ruppert, T. Knöfel, J. W. Bats, *J. Org. Chem.* **62** (1997) 7295; d) J. B. Sperry, C. R. Whitehead, I. Ghiviriga, R. M. Walczak, D. L. Wright, *J. Org. Chem.* **69** (2004) 3726; e) A. S. K. Hashmi, L. Schwarz, J.-H. Choi, T. M. Frost, *Angew. Chem. Int. Ed.* **112** (2000) 2382; f) A. S. K. Hashmi, P. Sinha, *Adv. Synth. Catal.* **346** (2004) 432
16. a) W. C. Christopf, L. L. Miller, *J. Org. Chem.* **51** (1986) 4169; b) F. Freeman, D. S. H. L. Kim, E. Rodriguez, *J. Org. Chem.* **57** (1992) 1722
17. a) B. M. Trost, M. C. McIntosh, *J. Am. Chem. Soc.* **117** (1995) 7255; b) M. Aso, A. Ojida, G. Yang, O.-J. Cha, E. Osawa, K. J. Kanematsu, *J. Org. Chem.* **58** (1993) 3960
18. C. H. Oh, V. R. Reddy, A. Kim, C. Y. Rhim, *Tetrahedron Lett.* **47** (2006) 5307
19. S. Dey, D. Nandi, P. K. Pradhan, V. S. Giri, P. Jaisankar, *Tetrahedron Lett.* **48** (2007) 2573
20. D. Azarifar, H. Ghasemnejad, F. Ramzanian, *Mendeleev Commun.* (2005) 209
21. D. Azarifar, H. Ghasemnejad-Bosra, M.-A. Zolfigol, M. Tajbaksh, *Heterocycles* **68** (2006) 175
22. D. Azarifar, H. Ghasemnejad-Bosra, *Synthesis* (2006) 1123
23. D. Azarifar, H. Ghasemnejad-Bosra, M. Tajbaksh, *J. Heterocycl. Chem.* **44** (2007) 467
24. H. Ghasemnejad-Bosra, M. Haghadi, I. Gholampour-Azizi, *Heterocycles* **75** (2008) 391
25. H. Ghasemnejad-Bosra, M. Haghdi, O. Khanmohamadi, M. Gholipour, G. Asghari, *J. Chin. Chem. Soc.* **55** (2008) 464
26. H. Ghasemnejad-Bosra, M. Faraje, S. Habibzadeh, *Helv. Chim. Acta* **92** (2009) 575.



Molybdatophosphoric acid as an efficient catalyst for the catalytic and chemoselective oxidation of sulfides to sulfoxides using urea hydrogen peroxide as a commercially available oxidant

ALIREZA HASANINEJAD¹, MOHAMMAD ALI ZOLFIGOL², GHOLAMABBAS CHEHARDOLI^{3*} and MOHAMMAD MOKHLESI²

¹Department of Chemistry, Faculty of Sciences, Persian Gulf University, Bushehr 75169,

²Faculty of Chemistry, Bu-Ali Sina University, P. O. Box 4135, Hamedan 6517838683

and ³School of Pharmacy, Hamedan University of Medical Sciences,
zip code 65178, Hamedan, Iran

(Received 10 December 2008, revised 16 October 2009)

Abstract: An efficient procedure for the chemoselective oxidation of alkyl (aryl) sulfides to the corresponding sulfoxides using urea hydrogen peroxide (UHP) in the presence of a catalytic amount of molybdatophosphoric acid at room temperature is described. The advantages of described method are: generality, high yield and chemoselectivity, short reaction time, low cost and compatibility with green chemistry protocols.

Keywords: molybdatophosphoric acid; urea hydrogen peroxide (UHP); chemoselective; oxidation; sulfides; sulfoxides.

INTRODUCTION

The development of efficient catalytic systems for selective organic transformations is currently one of the challenging tasks in synthetic organic chemistry.¹ In recent years, the search for environmentally benign chemical processes or methodologies has received much attention from chemists, because they are essential for the conservation of the global ecosystem. From this viewpoint, catalytic oxidation is a valuable process because the use of stoichiometric reagents, which are often toxic, poses inherent limitations from both economical and environmental viewpoints regarding product purification and waste management.²

Heteropolyacids (HPAs) are more active catalysts than conventional inorganic and organic acids for a variety of organic reactions.³ They have been used as the catalyst for several types of reactions such as Freidel-Crafts acylation,⁴ hetero-Michael addition reaction⁵ and the oxidation of anilines to their nitro com-

*Corresponding author. E-mails: chehardoli@umsha.ac.ir; cheh1002@gmail.com
doi: 10.2298/JSC081210001H

pounds.⁶ Among heteropolyacids, molybdatophosphoric acid is a good promoter due to its high acid strength, thermal stability, low reducibility and atom economy.⁷

Concentrated H₂O₂ is very dangerous to handle and not readily available. Hence this reagent has been replaced by its more stable and safe complexes. The strongly H-bonded urea hydrogen peroxide (UHP, H₂NCONH₂·H₂O₂)⁸ is nowadays commercially available,⁹ and its applications in organic and analytical chemistry, as well as in industry, are quickly widening. Its stability at room temperature, high hydrogen peroxide content (36.2 %) and the potential for releasing it in a controlled manner, as well as its solubility in organic solvents, make it a good and safe substitute as a “dry carrier” of the hazardous and unstable hydrogen peroxide in most oxidation reactions. Moreover, selectivity can be achieved by replacing the potentially explosive hydrogen peroxide with the safer crystalline UHP for the controlled release of the oxidant and it is a well-recognized source of oxygen.¹⁰

The selective oxidation of organic sulfides to sulfoxides without any over-oxidation to sulfones is a challenging research topic in synthetic organic chemistry, partly because of the importance of sulfoxides as intermediates in a range of biologically active molecules, including therapeutic agents such as anti-ulcer, antibacterial, antifungal, anti-atherosclerotic, antihypertensive and cardiotonic agents as well as psychotropic and vasodilators.¹¹ There are many reagents available for the oxidation of sulfides to sulfoxides.^{12–23} However, most of the existing methods use sophisticated reagents, complex catalysts, toxic metallic compounds, or rare oxidizing agents that are difficult to prepare. Many of these procedures also suffer from poor selectivity or undesirable products, such as aromatic halogenation, C–S bond cleavage and over-oxidation to sulfone. Hence, for the facile conversion of sulfides to sulfoxides, careful selection of the oxidizing agent and the reaction conditions are prerequisites.

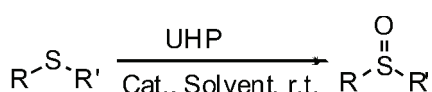
Before commencing the results and discussion section, a list of the employed abbreviations is given in Table I.

TABLE I. List of abbreviations

Abbreviation	Name
UHP	Urea hydrogen peroxide
MPA Moly	bdatophosphoric acid
TPA Tungstopho	sphoric acid
BTPPDC	<i>n</i> -Butyltriphenylphosphonium dichromate
CAN	Ceric ammonium nitrate
CPCC 3-Carboxy	pyridinium chlorochromate
NBS	<i>N</i> -Bromosuccinimide
THF Tetrahydrofura	<i>n</i>
DMF Di	methylformamide

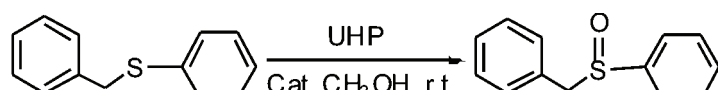
RESULTS AND DISCUSSION

In continuation of our interest in the development of synthetic methods for the transformation of organic functional groups, in particularly the application of heteropolyacids, H₂O₂ adducts and catalytic oxidation reactions,²⁴ urea hydrogen peroxide is introduced in this report as a safe and eco-friendly oxidant for the selective conversion of sulfides to sulfoxides in the presence of a catalytic amount of molybdatophosphoric acid (Scheme 1).



Cat.: Molybdatophosphoric acid Scheme 1.

In order to optimize the reaction conditions, the oxidation of benzyl phenyl sulfide using urea hydrogen peroxide (UHP) in methanol was chosen as a model reaction to provide the corresponding sulfoxide (Scheme 2).



Scheme 2.

The obtained results are summarized in Table II. First, a model run was performed with benzyl phenyl sulfide and UHP in the absence of catalyst in methanol at room temperature (Table II, Entries 1 and 2). It was found that the reaction did not go to completion even using a ten-fold excess of UHP and a long reaction time (4 h). Thus, the effect of various activators as promoter or catalyst on the reactivity of UHP for the oxidation of model compound was studied, Scheme 2. The results are summarized in Table II, from which it can be seen that although tungstophosphoric acid gave a good yield of benzyl phenyl sulfoxide (Table II, entry 8), an excellent yield of the product was obtained in the presence of molybdatophosphoric acid in a shorter reaction time (Table II, entry 3). The other tested catalysts or activators had one or more of the following disadvantages: long reaction time, low yield and selectivity and the use of large amount of activator. Therefore, molybdatophosphoric acid (MPA) is an effective catalyst for the oxidation of sulfide to sulfoxide and it was used as catalyst for all subsequent reactions. In this study, the effects of various amounts of molybdatophosphoric acid and various amounts of UHP were investigated (see, Table II, entries 3–7). The highest yield in an appropriate reaction time for the sulfoxidation reaction was obtained when 0.1 mmol MPA was used for the reaction of 1 mmol benzyl phenyl sulfide with 2 mmol UHP in 5 mL CH₃OH at room temperature (Table II, entry 3).

TABLE II. Oxidation of benzyl phenyl sulfide (1 mmol) to the corresponding sulfoxide using UHP in the presence of various catalysts/activators in CH₃OH (5 mL) at room temperature

Entry	Catalyst (amount) ^b	UHP, mmol	Time	Yield of sulfoxide, % ^a
1	Abs	2	4	h
2	Abs	10	4	30
3	MPA (0.1 mmol)	2	17 min	100
4	MPA (0.2 mmol)	2	10 min	100
5	MPA (0.05 mmol)	2	2 h	97
6	MPA (0.1 mmol)	1	3 h	80
7	MPA (0.1 mmol)	1.5	2 h	86
8	TPA ^c (0.1 mmol)	2	3 h	80
9	TPA (0.3 mmol)	2	2 h	90
10	AlCl ₃ (0.5 mmol)	2	3 h	nc ^d
11	Al(HSO ₄) ₃ (0.5 mmol)	2	3 h	nc
12	Na ₂ HPO ₄ (0.5 mmol)	2	3 h	trace
13	ZnCl ₂ (0.3 mmol)	2	3 h	30
14	CaCl ₂ .2H ₂ O (0.5 mmol)	2	3 h	20
15	Al ₂ O ₃ (0.5 g)	2	3 h	trace
16	SiO ₂ (0.5 g)	2	3 h	20
17	ZrCl ₄ (0.2 mmol)	2	3 h	trace
18	NaHSO ₄ 2		3 h	trace
19	ZnO (0.5 mmol)	2	3 h	trace
20	MgO (0.5 mmol)	2	3 h	trace
21	NH ₂ SO ₃ H 2		3 h	nc

^aIsolated yield; ^bin the absence of catalyst; ^ctungstophosphoric acid; ^dreaction did not go to completion

In the next step, the effect of various solvents on the progress of the reactions was investigated. As illustrated in Table III, methanol was the solvent of choice for the above-mentioned reaction.

TABLE III. Solvent effect on the oxidation of benzyl phenyl sulfide using UHP in the presence of MPA as catalyst

Entry	Solvent	Time	Conversion, %
1	CH ₂ Cl ₂	6	0
2	CH ₂ Cl ₂	5	0
3	EtOAc	3 h	70
4	Acetone	6 h	50
5	n-Hexane	5	0
6	THF	5 h	45
7	CH ₃ CN	3	60
8	DMF	3 h	45
9	CH ₃ OH	17	100
10	H ₂ O	2	65
11	O ₂	2	0



To determine the scope of this procedure, the oxidation of other sulfides to sulfoxides was studied. A wide range of substrates, *i.e.*, aryl alkyl, diaryl and dialkyl sulfides were selectively oxidized to their corresponding sulfoxides (Table IV).

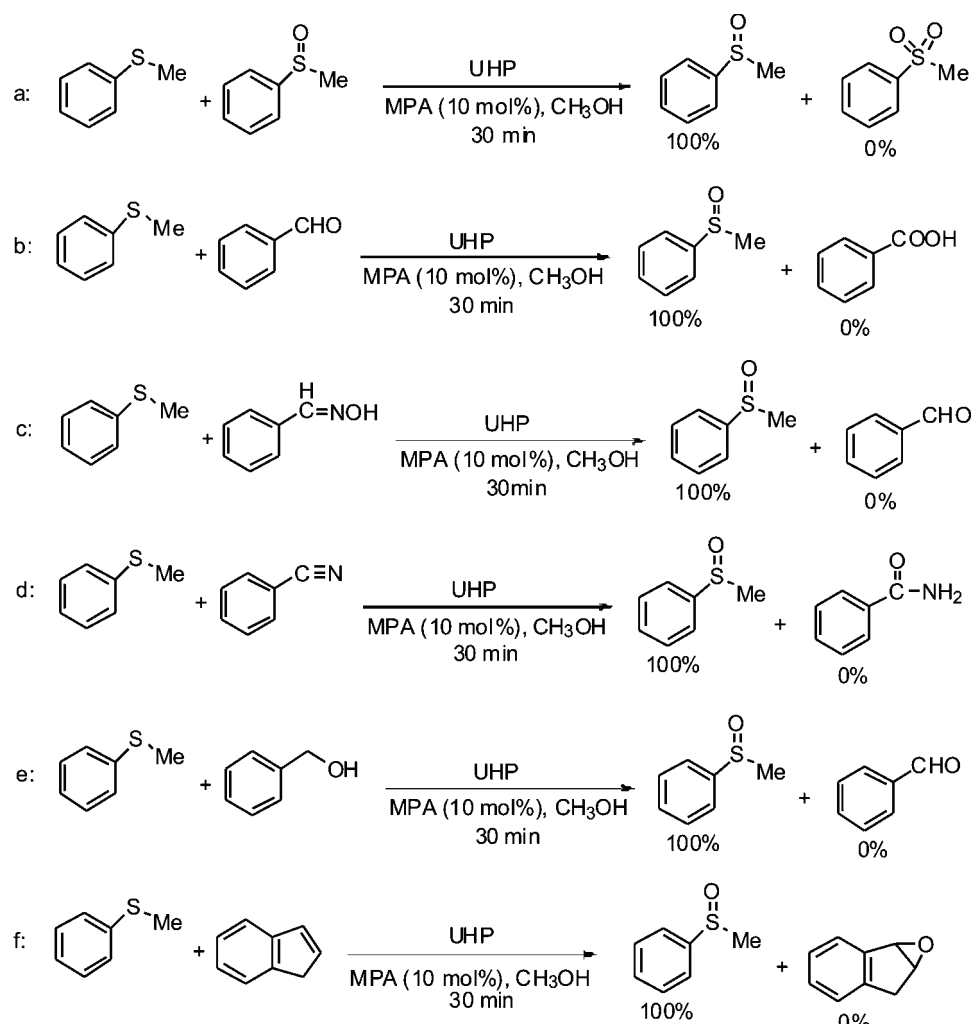
TABLE IV. Chemoselective oxidation of sulfide (1.0 mmol) to the corresponding sulfoxide using UHP (2.0 mmol) in the presence of MPA (0.10 mmol) as catalyst in CH_3OH at room temperature

Entry	Substrate	Time	Yield, % ^a
1		17 min	100
2		10 min	90
3		18 min	91
4		6.5 h	95 ^c
5		15 min	90
6		10 min	undp ^b
7		3 h	100
8		13 min	100
9		17 min	92
10		40 min	80
11		90 min	91
12		20 min	87

^aIsolated yields, UHP (1 mmol), MPA (0.2 mmol), 50 °C; ^bundesired products

It is noteworthy that sulfides containing functional groups, such as alcohol, aldehyde and ester, were selectively oxidized without any interference from these

groups (Table IV, entries 5, 9 and 11). To further determine the chemoselectivity of the described system, some competitive reactions were designed. Thus, the competitive oxidation of sulfides in the presence of sulfoxide, aldehyde, oxime, nitrile, benzylic alcohol and alkene was monitored. These observations clearly show that the method is applicable for the chemoselective oxidation of sulfides to sulfoxides in the presence of the previously mentioned functional groups and can be considered as a useful practical method for the oxidation of sulfides to sulfoxides without general oxidation (Scheme 3).



Scheme 3.

In order to assess the capability of the present method with respect to the reported methods for the oxidation of sulfide to sulfoxide, the oxidation of benzyl phenyl sulfide by the present method was compared with oxidation by the reported methods (Table V). It is clear from Table V that the present method is superior to some previously reported methods in terms of chemoselectivity, yield, reaction time and amount of the catalyst and reagent required for successful oxidation without having to resort to complex catalysts, a hazardous and unstable oxidant, microwave heating or toxic metallic compounds.

TABLE V. Comparison of the oxidation of benzyl phenyl sulfide (1.0 mmol) by UHP/MPA with some reagents reported in the literature

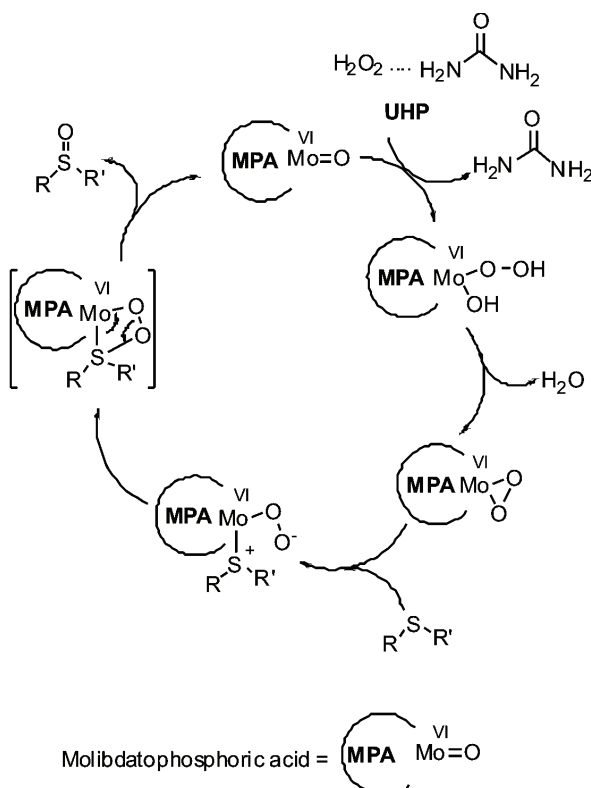
Entry	Reagent (oxidant/substrate)	Time	Yield, %		Ref.
			Sulfoxide	Sulfone	
1	UHP/MPA/CH ₃ OH/rt (2:0.1)	17 min	100	0	—
2	BT PPDC/AlCl ₃ /CH ₃ CN/reflux (1.5:1)	90 min	93	nr ^a	14
3	BT PPDC/AlCl ₃ /MW (1.2:1)	2 min	94	nr	14
4	NaIO ₄ /wet SiO ₂ /MW (1.7:1)	2.5 min	83	nr	15
5	PhCH ₂ PPh ₃ HSO ₅ /CH ₃ CN/reflux (1.5:1)	12 h	88	nr	16
6	Ba(MnO ₄) ₂ /CH ₃ CN/reflux (6:1)	4 h	88	nr	13
7	CAN/wet SiO ₂ /CH ₂ Cl ₂ /rt (2:1)	45 min	96	nr	17
8	BT PPDC/AlCl ₃ /MW (2.5:1)	2.5 min	nr	97	14
9	CPCC/Al Cl ₃ /CH ₃ CN/reflux (1:1)	75 min	93	nr	18
10	CPCC/Al Cl ₃ /MW (0.8:1)	1.5 min	92	nr	18
11	H ₂ O ₂ /Silica sulfuric acid/CH ₃ CN/rt (1:0.1 g)	40 min	96	nr	19
12	H ₂ O ₂ /Amberlyst 15/CH ₃ OH/rt (2:0.5)	6.5 h	95	nr	20
13	H ₂ O ₂ /Amberlyst IR-400/CH ₃ OH/rt (3:0.5)	7.5 h	92	nr	20
14	HIO ₃ /wet SiO ₂ /solvent-free 50 °C (1:3)	170 min	93	nr	21
15	H ₂ O ₂ /Silica-based tungstate/CH ₂ Cl ₂ :CH ₃ OH (4:0.1)	3 h	85	nr	22
16	H ₂ O ₂ /NBS/CH ₃ CN (3:0.1)	15 h	90	nr	22 ^b
17	H ₂ O ₂ /ZrCl ₄ /CH ₃ OH (7:2)	2 min	96	nr	23

^aNot reported

The observation that the oxidation of benzyl phenyl sulfide and dibenzyl sulfide yields the corresponding sulfoxide (Table IV, entries 1 and 2) indicates that the reaction proceeds via an oxygen transfer mechanism. If the reaction involved electron transfer instead of oxygen transfer, substantial amounts of benzaldehyde would have been formed.²⁵ According to a literature survey,^{26–33} a reasonable mechanism for the oxidation of sulfide to the corresponding sulfoxide using UHP in the presence of MPA is outlined in Scheme 4. This observation



probably indicates that molybdenum ions generate Mo⁵⁺-peroxy species on interaction with UHP, which is possibly the active intermediate species.²⁶ Then the reaction can proceed *via* the 1,3-dipolar mechanism.



Scheme 4.

EXPERIMENTAL

General

The employed chemicals were purchased from Fluka, Merck or Aldrich. The quoted yields refer to isolated pure products. The oxidation products were characterized by comparison of their spectral (IR and ¹H-NMR) and physical data with those of authentic samples, which were synthesized by other reported procedures.¹²⁻²³

General procedure for the oxidation of sulfides

A mixture of sulfide (1.0 mmol), UHP (2.0 mmol) and molybdatophosphoric acid (0.10 mmol) in methanol (5.0 mL) was vigorously stirred for the required time (see Table III). The progress of the reaction was monitored by TLC. After completion of the reaction, the CH₃OH was evaporated and the crude product was purified by short column chromatography on silica gel with EtOAc/n-hexane (1:5 to 1:2) as the eluent.

CONCLUSIONS

In summary, it was found that molybdatophosphoric acid efficiently catalyzed the selective oxidation of sulfides to sulfoxides by the urea hydrogen peroxide adduct (UHP) at room temperature. This method offers the following advantages: a) the procedure is highly efficient, b) the yield of sulfoxide is high, c) the reagent is cheap, safe, and available and d) the selectivity of the method is remarkable with regards to sulfides. Also, its compatibility with sensitive functionalities, such as ester, aldehyde, oxime, nitrile and double bonds, with regards to economic and ecological considerations allows the belief that this method represents a valuable alternative to the existing reagents reported in the literature for the oxidation of sulfides to sulfoxides.

Acknowledgements. Financial support for this work by the Center of Excellence of the Development of Chemical Methods, (CEDCM), Bu-Ali Sina University, Hamedan, the Hamedan University of Medical Sciences, and also the Persian Gulf University, Bushehr, Iran, is gratefully acknowledged.

ИЗВОД

МОЛИБДАТОФОСФОРНА КИСЕЛИНА КАО ЕФИКАСАН КАТАЛИЗATOR ЗА
КАТАЛИТИЧКУ И ХЕМОСЕЛЕКТИВНУ ОКСИДАЦИЈУ СУЛФИДА У
СУЛФОКСИДЕ КОРИШЋЕЊЕМ АДУКТА УРЕЕ И ВОДОНИК-ПЕРОКСИДА
КАО КОМЕРЦИЈАЛНО ДОСТУПНОГ ОКСИДАНТА

ALIREZA HASANINEJAD¹, MOHAMMAD ALI ZOLFIGOL², GHOLAMABBAS CHEHARDOLI³
и MOHAMMAD MOKHLESI²

¹Department of Chemistry, Faculty of Sciences, Persian Gulf University, Bushehr 75169, ²Faculty of Chemistry, Bu-Ali Sina University, P. O. Box 4135, Hamedan 6517838683 и ³School of Pharmacy, Hamedan University of Medical Sciences, zip code 65178, Hamedan, Iran

Описан је ефикасан поступак хемоселективне оксидације алкил-(арил)-сулфида до одговарајућих сулфоксида помоћу водоник-пероксида на собној температури у присуству катализичке количине молибдатофосфорне киселине. Предности описаног поступка, које га чине упоредивим са еколошки чистим методама, јесу општост методе, висок принос, хемоселективност, кратко реакционо време, као и ниска цена поступка.

(Примљено 10. децембра 2008, ревидирано 16. октобра 2009)

REFERENCES

1. S. S. Kim, G. Rajagopal, *Synth. Commun.* **34** (2004) 2237
2. D. Choudhary, S. Paul, R. Gupta, J. H. Clark, *Green Chem.* **8** (2006) 479
3. a) R. S. Drago, J. A. Dias, T. Maier, *J. Am. Chem. Soc.* **119** (1997) 7702; b) A. Corma *Chem. Rev.* **95** (1995) 559
4. H. Firouzabadi, N. Iranpoor, F. Nowrouzi, *Tetrahedron* **60** (2004) 10843
5. H. Firouzabadi, N. Iranpoor, A. A. Jafari, *Synlett* (2005) 299
6. H. Firouzabadi, N. Iranpoor, F. Nowrouzi, K. Amani, *Green Chem.* **3** (2001) 131
7. H. Firouzabadi, A. A. Jafari, *J. Iran. Chem. Soc.* **2** (2005) 85
8. C. S. Lu, E. W. Hughes, P. A. Giguere, *J. Am. Chem. Soc.* **63** (1941) 1507

9. *Aldrich Handbook of Fine Chemicals and Laboratory Equipment*, Aldrich, Milwaukee, WI, 2003–2004, p. 1898
10. S. Taliinsky, *Synlett* (2005) 1962
11. a) I. Fernandez, N. Khiar, *Chem. Rev.* **103** (2003) 3651 and references cited therein; b) A. M. Khenkin, R. Neumann, *J. Am. Chem. Soc.* **124** (2002) 4198
12. K. Kaczorowska, Z. Kolarska, K. Mitka, P. Kowalski, *Tetrahedron* **61** (2005) 8315, and references cited therein
13. H. Firouzabadi, M. Seddighi, *Synth. Commun.* **21** (1991) 211
14. I. Mohammadpoor-Baltork, H. R. Memarian, K. Bahrami, K. Esmayilpour, *Phosphorus Sulfur Silicon Relat. Elem.* **180** (2005) 2751
15. R. S. Varma, R. K. Saini, H. M. Meshram, *Tetrahedron Lett.* **38** (1997) 6525
16. A. R. Hajipour, S. E. Mallakpour, H. Adibi, *J. Org. Chem.* **67** (2002) 8666
17. M. H. Ali, D. R. Leach, C. E. Schmitz, *Synth. Commun.* **28** (1998) 2969
18. I. Mohammadpoor-Baltork, H. R. Memarian, K. Bahrami, *Can. J. Chem.* **83** (2005) 115
19. A. Shaabani, A. H. Rezayan, *Catal. Commun.* **8** (2007) 1112
20. M. M. Lakouraj, M. Tajbakhsh, H. Tashakkorian, *Monatsh. Chem.* **138** (2007) 83
21. M. M. Lakouraj, M. Tajbakhsh, F. Shirini, M. V. A. Tamami, *Synth. Commun.* **35** (2005) 775
22. (a) B. Karimi, M. Ghoreishi-Nezhad, J. H. Clark, *Org. Lett.* **7** (2005) 625; (b) B. Karimi, D. Zareyee, *J. Iran. Chem. Soc.* **5** (2008) 103
23. a) K. Bahrami, *Tetrahedron Lett.* **47** (2006) 2009; b) M. A. Zolfogol, K. Amani, A. Ghorbani-Choghamarani, M. Hajjami, R. Ayazi-Nasrabadi, S. Jafari, *Catal. Commun.* **9** (2008) 1739
24. a) M. A. Zolfogol, M. Shiri, *Mendeleev Commun.* (2005) 165; b) M. A. Zolfogol, G. Chehardoli, M. Shiri, *React. Funct. Polym.* **67** (2007) 723; c) M. A. Zolfogol, F. Shirini, G. Chehardoli, E. Kolvari, *J. Mol. Catal. A: Chem.* **265** (2007) 272; d) M. A. Zolfogol, M. Bagherzadeh, S. Mallakpour, G. Chehardoli, A. Ghorbani-Choghamarani, N. Koukabi, M. Dehghanian, M. Doroudgar, *J. Mol. Catal. A: Chem.* **270** (2007) 219; e) K. Niknam, M. A. Zolfogol, T. Sadabadi, A. Nejati, *J. Iran. Chem. Soc.* **3** (2006) 318; f) A. Bamoniri, B. F. Mirjalili, M. A. Zolfogol, I. Mohammadpoor-Baltork, *J. Iran. Chem. Soc.* **4** (2007) 332
25. E. Baciocchi, O. Lanzalunga, S. Malandrucco, *J. Am. Chem. Soc.* **118** (1996) 8973
26. H. Mimoun, S. De Roch, L. Sajus, *Tetrahedron* **26** (1970) 37
27. J. M. Khurana, A. Agrawal, S. Kumar, *J. Braz. Chem. Soc.* **20** (2009) 1256
28. N. K. K. Raj, A. V. Ramaswamy, P. Manikandan, *J. Mol. Catal. A: Chem.* **227** (2005) 37
29. H. Mimoun, L. Saussine, E. Daire, M. Postel, J. Fischer, R. Weiss, *J. Am. Chem. Soc.* **105** (1983) 3101
30. A. E. Gekhman, I. P. Stolarov, N. I. Moiseeva, V. L. Rubaijlo, M. N. Vargaftik, I. I. Moiseev, *Inorg. Chim. Acta* **276** (1998) 453
31. K. I. Matveev, I. V. Kozhevnikov, *Kinet. Katal.* **21** (1980) 1189
32. K. Jeyakumar, D. K. Chand, *J. Chem. Sci.* **121** (2009) 111
33. L. Marosi, C. OteroAreán, *J. Catal.* **213** (2003) 235.





The role of adenosine triphosphate in the function of human origin recognition complex 4 protein

ALEKSANDRA DIVAC*, BRANKO TOMIĆ and JELENA KUŠIĆ

Institute of Molecular Genetics and Genetic Engineering,
University of Belgrade, Belgrade, Serbia

(Received 24 July, revised 13 October 2009)

Abstract: Human origin recognition complex 4 (ORC4) protein, a subunit of the origin recognition complex, belongs to the AAA+ superfamily of adenosine triphosphate (ATP)ases. Proteins belonging to this family require ATP for their function and interactions with ATP lead to conformational changes in them or in their partners. Human ORC4 protein induces structural changes in DNA substrates, promoting renaturation and formation of non-canonical structures, as well as conversion of single-stranded into multi-stranded oligonucleotide structures. The aim of this study was to further investigate the role of ATP in the function of human ORC4 protein. For this purpose, a mutant in the conserved Walker B motif of ORC4, which is able to bind but not to hydrolyze ATP, was constructed and its activity in DNA restructuring reactions was investigated. The obtained results showed that ATP hydrolysis is not necessary for the function of human ORC4. It is proposed that ATP has a structural role as a cofactor in the function of human ORC4 as a DNA restructuring agent.

Keywords: origin recognition complex (ORC); adenosine triphosphate (ATP); DNA structure; origin selection.

INTRODUCTION

The origin recognition complex (ORC) is a universal eukaryotic initiator and an essential complex for the selection of active origins during the cycle of cells.¹ The ORC consists of six subunits, three of which (ORC1, ORC4 and ORC5) belong to the superfamily of adenosine triphosphate (ATP)ases associated with various cellular activities (AAA+ superfamily).^{2,3} Members of this superfamily play crucial roles in transforming chemical energy into biological events, from protein remodeling, transport, complex assembly and disassembly to DNA replication, recombination, repair and transcription. They all require ATP for their function and binding and/or hydrolysis of ATP induces structural changes in these pro-

* Corresponding author. E-mail: aleksandradivac@imgge.bg.ac.rs
doi: 10.2298/JSC090724019D

teins or in their partners.⁴ All AAA+ superfamily members have several conserved motifs: an $\alpha\beta\alpha$ core domain structure and Walker A and B motifs. The Walker B motif has the consensus sequence hhhhDE (h – hydrophilic amino acid). The carboxy group of the glutamate residue is believed to act as a catalytic base, abstracting a proton from a molecule of water, thereby priming it for nucleophilic attack on the γ -phosphate of bound ATP. The conserved aspartate residue is involved in the coordination of Mg²⁺.⁵

The human ORC4 subunit, a typical AAA+ superfamily protein, was shown to play a critical role in human ORC assembly and maintenance.^{6–8} It was demonstrated that human ORC4 has sequence-unspecific DNA binding activity.⁹ In addition, it was previously shown that human ORC4 acts as a DNA restructuring agent; it catalyses the formation of non-canonical DNA structures in origin DNA.¹⁰ The most intriguing feature of human ORC4 is its unique ability to promote the formation of homodimeric structures, such as duplexes and even larger structures.¹⁰ Human ORC4 belongs to the family of AAA+ ATPases, the aim was to further elucidate the role of ATP in the function of human ORC4 as a DNA restructuring agent.

EXPERIMENTAL

Expression and purification of mutant human ORC4 protein (WB protein)

Site directed mutagenesis of D159A and E160A in the Walker B motif of human ORC4 was performed by polymerase chain reaction (PCR) amplification of the pQE-30 plasmid (Qiagen, Valencia, CA), containing a fragment encoding the full-length human protein (1311 bp), with the mutagenic primer 5'-GCCAGTGATCTTCATATTAGCTGCATTGATC-TTTTGCTCATC-3' and using the QuikChange Multi Site-directed Mutagenesis kit (Stratagene, La Jolla, CA). The PCR products were treated with DpnI to digest the parental DNA template and used to transform M15 (pREP4)-competent cells. The presence of the mutated sequence, coding for a protein containing an active Walker B motif (WB protein), was confirmed by direct DNA sequencing.

The recombinant human ORC4 was expressed in *Escherichia coli* and purified over a metal affinity resin as essentially described previously.⁹ To improve the yield of the active protein, treatment of bacterial lysates with DNase I was also included in the purification procedure. In addition, to minimize aggregation during purification and improve the yield, detergents, NP 40 and CHAPS, were used, as well as 1 M NaCl and 10 mM ATP. An improvement was observed when ATP was used; hence, this step was incorporated into the protocol for the purification of the mutant protein. All other steps were the same for the mutant and wild type proteins. To remove insoluble aggregates, the protein was repurified by glycerol gradient centrifugation. The centrifugation was realized in 10 to 30% glycerol gradients prepared in buffer A (20 mM HEPES (pH 7.9), 30 mM NaCl, 2 mM ZnCl₂, 6 mM MgCl₂, 0.1 mM ATP, 0.1 mM EDTA, 1 mM DTT, and 0.1 mM PMSF). The gradients were centrifuged in an SW 41 Beckman rotor at 38000 rpm, for 20 h at 8 °C. Gradient fractions were collected from the bottom and analyzed using an Agilent 2100 Bioanalyzer and Protein 200 Plus LabChip kit, in combination with Protein 200 Plus assay software. The glycerol gradient fractions containing human ORC4 were pooled and kept at -80 °C.

Protein-mediated conversion of single-stranded oligonucleotides into multi-stranded structures

For protein-mediated conversion of single-stranded oligonucleotides into multi-stranded structures, 4 fmols of end-labeled single-stranded oligonucleotides d(A)₃₄ were dissolved in buffer A1 (20 mM HEPES (pH 7.9), 30 mM NaCl, 2 mM ZnCl₂, 20 mM MgCl₂, 0.1 mM ATP, 0.1 mM EDTA, 1 mM DTT, 0.1 mM PMSF) and incubated for 15 min at 37 °C with 50 ng, 100 ng or 150 ng of an appropriate protein. The typical reaction volume was 25 µL. At the end of the incubation, the reaction mixtures were quickly cooled on ice, adjusted to 1 M NaCl and 1% SDS, and deproteinized with chloroform and isoamyl alcohol. Alternatively, the protein was digested with 1–5 µg of proteinase K dissolved in 0.1–0.5% SDS. Protein digestion was performed for 15 min at 37 °C. The deproteinized samples were analyzed by TBM-PAGE in a cold room, followed by autoradiography.

RESULTS AND DISCUSSION

The WB protein, a mutated form of human ORC4 protein, was successfully cloned, expressed and purified from an *E. coli* M15 (pREP4) bacterial strain. The coding gene sequence of human ORC4 was previously cloned in pQE30 vector (Promega) and its sequence was confirmed by DNA sequencing. Mutagenesis of the wild type coding sequence was performed using a QuikChange Multi Site-Directed Mutagenesis Kit (Stratagene, USA). The sequence of the mutated gene was confirmed by direct sequencing and the appropriate vector was used for transformation of *E. coli* M15 (pREP4) competent cells. Purification of the mutant protein was performed using the same protocol as for the wild type protein, with the addition of 100 mM ATP, and resulted in a single band assayed by Coomassie Blue staining or an Agilent Bioanalyzer 2100 (Fig. 1).¹⁰

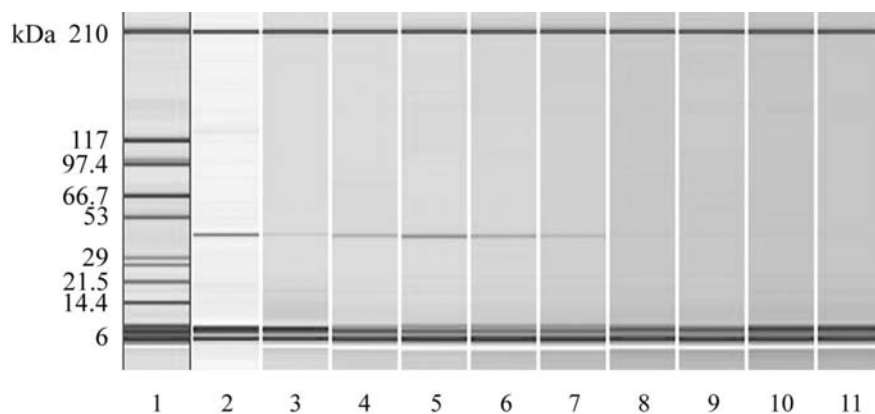


Fig. 1. Gel-like image of the purified mutant ORC4 analyzed with an Agilent 2100 Bioanalyzer (Protein 200 Plus assay). The mutant ORC4 was purified by cobalt affinity chromatography (lane 2) and separated by glycerol gradient centrifugation. Glycerol gradient odd fractions are presented in lanes 3–11. Upper and lower marker bands of the protein ladder (lane 1) are seen in all lanes.

The WB protein was assayed for its ability to convert single-stranded oligonucleotides, d(A)34, into multi-stranded structures. In these restructuring reactions, wild type human ORC4 and mutated form of ORC4 (WA protein) were used as controls. The WA protein is a mutated form of ORC4 where the Walker A (GKT) motif of the wild type protein is changed (K73A) so that it cannot bind ATP.¹⁰ In the presence of Walker B mutant protein, there was almost complete conversion of the single-stranded substrate into a multi-stranded structure, very similar to the wild type protein (Fig. 2).

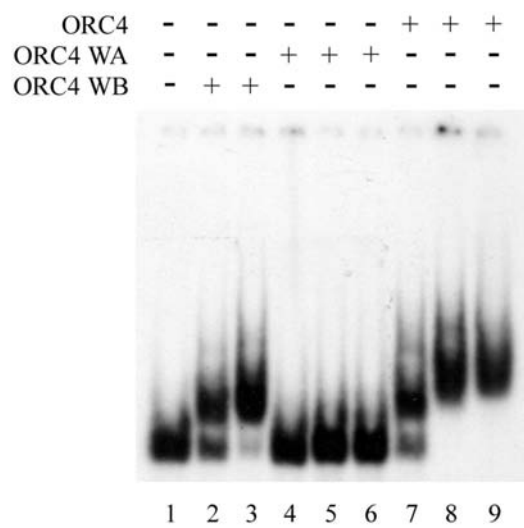


Fig. 2. ATP is not necessary for AA pairing catalyzed by human ORC4. Single stranded oligoadenine (lane 1) incubated with increasing amounts of WB mutant (lanes 2–3), WA mutant (lanes 4–6) or wild type human ORC4 (lanes 7–9).

Human ORC4 is a typical member of AAA+ protein superfamily, hence the aim was to investigate the role of ATP in its function in DNA restructuring reactions. The function of ATP could be twofold, as a source of energy for the restructuring reactions or as a cofactor for ORC4. It was previously shown that the mutant protein is unable to bind ATP (WA protein) and also does not function in oligonucleotide restructuring.¹⁰ To further elucidate the role of ATP in the function of human ORC4, a mutated protein unable to hydrolyze ATP was constructed and its activity in conversion reactions was tested. The mutant that does not hydrolyze ATP shows similar activity as the wild type protein (Fig. 2).

Binding of ATP is essential for ORC4 function in ORC assembly and maintenance.^{7,8} Mutant ORC4 protein that does not bind ATP (WA mutant) is also unable to form the complex. Mutant ORC4 protein that does not hydrolyze ATP, but can bind it (WB mutant) shows similar activity to wild type protein.⁸ It is postulated that ATP has a structural role, as a cofactor, in the ORC complex assembly and that its presence is necessary for preservation of the integrity of the complex.⁸ Additional experiments with a non-hydrolysable ATP analog (ATPγS)

showed that hydrolysis is not necessary for complex formation, because it has the same activity as ATP. The human ORC4 subunit seems to play a crucial role in the mediation of the effect of ATP in subunit interactions and complex stability.⁷ Although the binding of the whole complex to DNA is stimulated and stabilized by ATP, it was shown that DNA binding of the recombinant ORC4 is independent of the presence of ATP.^{6,9}

It was shown that recombinant human ORC4 protein preferentially binds AT-rich DNA, both double-stranded and triple-stranded. Additionally, human ORC4 stimulates renaturation of origin fragments and oligonucleotides. For these interactions, it is essential that DNA fragments are able to form Hoogsteen bonds.¹⁰ Human ORC4 also stimulates intra- and intermolecular TAT triplex formation. Also, it has a very intriguing feature that it is able to create homoadenine structures, such as duplexes and even higher structures. The action of human ORC4 in all of these reactions was dependent on the presence of magnesium ions and ATP.

The role of ATP in the function of ORC4 seems to be structural in both complex assembly and actions on DNA. Once bound, ATP could function as a source of energy in some downstream ORC functions. One of these could be the formation of a pre-replicative complex (pre-RC), which is a result of ORC-dependent loading of the Cdc6, Cdt1 and Mcm 2-7 DNA replicative helicase onto DNA. It was shown that ATP hydrolysis by ORC is required for multiple rounds of Mcm2-7 loading and requires the coordinate function of the ORC1 and ORC4 subunits.^{11,12}

CONCLUSIONS

The results of this study show that ATP plays a role as a cofactor in the function of human ORC4. Human ORC4 protein does not require ATP hydrolysis for activity in DNA restructuring reactions. Taking into consideration previous studies, it is concluded that the action of recombinant human ORC4 in DNA restructuring reactions is dependent on the presence of magnesium ions and ATP.

Acknowledgements. This work was supported by the Ministry of Science and Technological Development of the Republic of Serbia, Grant 143051.

ИЗВОД

УЛОГА АТР-а У ФУНКЦИЈИ ХУМАНОГ ПРОТЕИНА ORC4

АЛЕКСАНДРА ДИВАЦ, БРАНКО ТОМИЋ и ЈЕЛЕНА КУШИЋ

Институт за молекуларну генетику и генетичко инжењерство, Универзитет у Београду, Београд

Хумани протеин ORC4, подјединица ORC комплекса (енг. *Origin Recognition Complex*), припада фамилији AAA+ аденоzin-трифосфат (ATP)-аза повезаних са различитим функцијама у ћелији. За припаднике ове фамилије протеина је карактеристично да је ATP неопходан за њихову функцију и да по везивању ATP-а пролазе кроз конформациону промену или је индукују у својим партнерима. Хумани протеин ORC4 индукује структурне промене у суп-

стратним ДНК, тако што промовише ренатурацију и формирање неканонских структура, као и конверзију једноланчаних олигонуклеотида у вишеланчане структуре. ATP је неопходан за ове функције ORC4 протеина, што је показано анализом активности мутанта који не може да веже ATP, и који није активан у овим реакцијама. Да бисмо ближе испитали улогу ATP-а у активности ORC4 направљен је протеин са мутацијом у домену за хидролизу ATP-а (Вокер Б мотив), који има очувану ATP-везивну активност. Овај мутант је био активан у реакцијама реструктурирања ДНК, тако да се може закључити да је улога ATP-а структурна, као кофактора, и да његова хидролиза није неопходна за функцију хуманог протеина ORC4.

(Примљено 24. јула, ревидирано 13. октобра 2009)

REFERENCES

1. S. P. Bell, B. Stillman, *Nature* **357** (1992) 114
2. T. Ogura, A. J. Wilkinson, *Genes Cells* **6** (2001) 575
3. B. P. Duncker, I. N. Chesnokov, B. J. McConkey, *Genome Biol.* **10** (2009) 214
4. M. J. Davey, D. Jeruzalimi, J. Kariyan, M. O'Donnell, *Nat. Rev. Mol. Cell Biol.* **3** (2002) 826
5. J. Snider, A. Walid, *Biochem. Soc. Trans.* **36** (2008) 72
6. J. Giordano-Coltart, C. Y. Yi ng, J. Gautier, J. Hurwitz, *Proc. Natl. Acad. Sci. USA* **102** (2005) 69
7. A. Ranjan, M. Gossen, *Proc. Natl. Acad. Sci. USA* **103** (2006) 4864
8. K. Siddiqui, B. Stillman, *J. Biol. Chem.* **282** (2007) 32370
9. D. Stefanović, S. Stanojčić, A. Vindigni, A. Ochem, A. Falaschi, *J. Biol. Chem.* **278** (2003) 42737
10. D. Stefanović, J. Kusić, A. Divac, B. Tomić, *Biochemistry* **47** (2008) 8760
11. J. L. Bowers, J. C. Randell, S. Chen, S. P. Bell, *Mol. Cell* **16** (2004) 967
12. J. C. Randell, J. L. Bowers, H. K. Rodríguez, S. P. Bell, *Mol. Cell* **21** (2006) 29.



Introduction of the interdependence between the glutathione half-cell reduction potential and thermodynamic parameters during accelerated aging of maize seeds

VESNA D. DRAGIČEVIĆ^{1*}, SLOBODANKA D. SREDOJEVIĆ¹ and MIHAJLO B. SPASIĆ²

¹Maize Research Institute, Slobodana Bajića 1, 11185 Belgrade-Zemun and ²Institute for Biological Research "Siniša Stanković", Bld. Despota Stefana 142, 11060 Belgrade, Serbia

(Received 30 June, revised 16 September 2009)

Abstract: Two maize hybrids with a different ability to maintain seed germination were examined during the course of a ccelerated aging (AA). Initially, the similar seed reduction potential of the GSSG/2GSH half-cell increased in H1 (dent hybrid) without influencing the seed germination ability up to the 6th day of AA, while in H2 (sweet corn hybrid), it was not changed up to the 6th day of AA but with a significant later loss of seed germination ability. During the AA course, the amount of free thiol decreased in H1 and increased in H2. Irrespective of the continual increase of the differential Gibbs energy during AA, the characteristics of the examined hybrids are possibly connected to the different metabolic pathways of the seed s: H1 is characterised by higher entropy and positive enthalpy values, while H2 has negative entropy values and a decreasing trend of enthalpy, indicating a shift of the system from a relatively ordered to a disordered state. The different types of nanomolecular switches, resulting in a faster decrease of GSH in the H2 than in the H1 hybrids, indicate that a combination of the GSSG/2GSH half-cell potential and thermodynamics could be a useful tool to quantify plant stress.

Keywords: aging; glutathione; maize seeds; free thiols; seed germination ability; thermodynamics.

INTRODUCTION

Despite the fact that the germination percentage is still the most important parameter that describes and integrates germination ability¹, the seed germination process, by itself, has many different aspects. The trend of loosing viability during long-term storage has two phases: the first is slower and longer lasting and the second, faster and shorter lasting.^{2,3} Kittock and Law⁴ and Anderson⁵ ascertained that seed respiration, as the main producer of reactive oxygen species (ROS), could increase during storage, due to exogenous and endogenous factors:

*Corresponding author. E-mail: vdragicevic@mrizp.rs
doi: 10.2298/JSC090630017D

temperature, air humidity, *etc.*⁶ During oxidative stress, ROS damage first the mitochondria and then the other cell components, leading to respiration reduction and membrane disintegration,⁷ which could be assumed as the moment of irreversible injuring. Accelerated aging induces changes in the naturally occurring seed antioxidants, such as glutathione,² which are integrated into the cellular redox status. Some ROS species and NO⁸ are capable of modulating transmembrane receptors and cytoplasmic signal transduction routes.⁹ Molecular sensors with free thiols mainly react *via* their oxidation, forming disulphides,^{10,11} having different redox and transcriptional signals. Although seeds represent relatively dry systems, the relations are even more complex, including the facts that most of the endosperm and a smaller part of the embryo represent dead cells, made through programmed cell death during seed formation.^{12,13}

The theoretical basis of the energy concept, *i.e.*, thermodynamics, gives the possibility of quantification of biological vitality,^{14,15} considering that a change in the internal energy of a system represents the maximal work available for achievement. The vitality of seeds is maintained by the formation of a glass structure, which is thermodynamically unstable, while aging induces structural changes,² as a consequence of metabolic unbalance, originating from gradual desiccation and high oxidative activity.¹⁶ Subsequently, the observed equilibrium shift, induced by oxidative activity during long-term desiccation or ageing, also leads to the breakdown of the antioxidants, *i.e.*, when major parts of the GSH pool are converted into GSSG, the half-cell potential increases and becomes a signal that initiates programmed cell death.¹⁷

The objective of study was to investigate the changes in seed germination ability during accelerated aging of two maize hybrids (H1 – dent hybrid and H2 – sugary hybrid) consequently through alterations of the half-cell redox potential of the GSSG/2GSH couple, the amount of free thiols and the thermodynamic parameters of differential Gibbs energy, entropy and enthalpy.

EXPERIMENTAL

The seeds of two maize hybrids with different abilities of germination (ZP SC 580 – H1, and ZP SC 504_{su} – H2, originating from the same location and year, stored at 4 °C), were subjected to accelerated ageing treatment¹⁸ at a temperature of 42 °C and a relative air humidity of 100 % for 3, 6 or 9 days (down to an economical limit of 80 %). Subsequently, the germination capacity was determined by ISTA Rules in four replications of 100 uniform seeds¹ after 7 days, on filter towels, used as the medium.

The contents of free thiol (PSH), reduced (GSH) and oxidised glutathione (GSSG) in the seeds were determined according to the method of de Kok *et al.*¹⁹ After homogenisation of 1 g of a sample with 10 mL of 0.15 % Na-ascorbate, the sample was centrifuged at 20,000 g for 20 min. Then, the free thiol content was determined: 1.5 ml of 0.20 M potassium phosphate buffer (pH 8.0) and 0.20 ml of 10 mM DTNB reagent (5,5'-dithio(2-nitrobenzoic acid) solved into 0.020 M potassium phosphate buffer (pH 7.0)) were added to 1.5 ml of the extract. The absorbance was measured at 415 nm. Then, the supernatant was deproteinised in the water

bath at 95 °C for 3 min. After repeated centrifugation at 15000 g for 15 min, the content of total glutathione from the supernatant was analysed. After repeated centrifugation at 15000 g for 15 min, the content of total glutathione in the supernatant was analysed as described above: to 1.5 mL of supernatant, 1.5 mL of 0.20 M potassium phosphate buffer (pH 8.0) and 0.20 mL of 10 mM DTNB reagent (pH 7.0) were added. The absorbance was read at 415 nm. In the other 1.5 mL of supernatant, 0.5 mL of 0.25 M potassium phosphate buffer (pH 6.8), 0.3 mL of albumin, 0.020 mL of glyoxalase I (Sigma grade IV) and 0.08 mL of 0.10 M methylglyoxal are added. After incubation at 30 °C for 15 min, the content of reduced glutathione (GHS) was determined in the above described manner. GSH (Sigma Ultra 98–100 %) was used as the standard. The content of oxidised glutathione (GSSG) was calculated as the difference between the total and reduced glutathione.

The redox capacity of the GSSG/2GSH couple was estimated by the method of Schafer and Buettner.²⁰

$$E_{hc} = -240 - \frac{59.1}{2} \log \frac{[GSH]^2}{[GSSG]} \quad (1)$$

The thermodynamic parameters were calculated from the water content, which was determined after drying at 130 °C,²¹ by a modified model proposed by Davies¹⁴ and Sun:^{22,23}

$$G^0 = -RT \ln Wc \quad (2)$$

$$\Delta G = -G^0 + RT \ln \frac{Wc_1}{Wc_2} \quad (3)$$

$$\Delta H = \frac{RT_1 T_2}{T_2 - T_1} \ln \frac{Wc_1}{Wc_2} \quad (4)$$

$$\Delta S = \frac{\Delta H - \Delta G}{T} \quad (5)$$

where G^0 is the starting Gibbs energy, R is the universal gas constant ($8.314 \text{ J K}^{-1} \text{ mol}^{-1}$), T is the sum of the average daily temperatures, in K, Wc is the water content (whereby, 1 g = 1 mL), ΔG is the Gibbs energy change, ΔH is the enthalpy change and ΔS is the entropy change.

It is important to stress that the time factor is insignificant in thermodynamics, while it is important for living systems; this paradox was surpassed by the introduction of daily temperature sums (obtained on the days of AA). The results of germination test, the GSH, GSSG and PSH contents were statistically calculated with the Anova T-test ($LSD = 5\%$); the E_{hc} , ΔG , ΔH and ΔS values were calculated with SD value; the dependence between the germination percentage, E_{hc} , ΔG , ΔH and ΔS were expressed by multiple regressions and correlation coefficients, calculated with Statistica 7.0 software (StatSoft Inc.).

RESULTS AND DISCUSSION

Redox signals are key regulators of various plant metabolic processes, including morphogenesis and growth. Glutathione is the major redox regulating substance in seeds. More tolerant genotypes have higher quantities of total glutathione, with different relations between reduced and oxidised glutathione (2GSH/GSSG).^{24,25} During the AA treatment, similar and significant decreases of GSH were found in the seeds of both hybrids, down to 55 and 56 % in H1 and H2, respectively (Table I), while the percentage germination was significantly decreased by 11 %

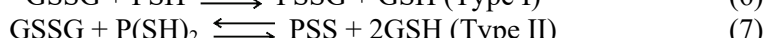
in H1 and by 19 % in H2. The decreased GSH amount correlates with the significant increase in GSSG amount, which is in agreement with the results of De Paula *et al.*²⁶ and Torres *et al.*,²⁷ although their ratio was shifted to a greater extent in H2. Generally, the relationship between seed viability and GSH decrease does not coincide with a GSSG increase, with the values increasing by only to 28 % in H1 and over 3.6 times in H2 (Table I), signifying an irreversible loss of GSH from the system.²⁸ This is an indication of its reaction with other seed biomolecules, which could, moreover, be linked to a reaction shift to necrotic processes²⁹ *i.e.*, to programmed cell death.^{13,17} It seems that the protective role of GSSG,³⁰ was emphasized in H2, having a 3.5 times higher GSSG content after 9 days of AA, with only a 7.6 % loss of total glutathione.

TABLE I. Changes in the germination percentage, GSH, GSSG and PSH in maize seeds (H1 – dent hybrid, H2 – sugary hybrid) during accelerated (AA) aging treatment for 3, 6 and 9 days

Property Hy	brid	AA / days			LSD 0.05
		0	3	6	
Germination, %	H1	98.0	97.7	96.0	87.7
	H2	95.5	95.0	83.0 ^a	77.5
GSH / nmol	H1	296.8	277.1	232.4	132.4
	H2	265.4	260.9	246.5	116.0
GSSG / nmol	H1	154.9	159.6	165.2	216.0
	H2	49.0	50.9	57.3	174.1
PSH / nmol	H1	91.3	87.8	80.4	25.9
	H2	78.4	88.9	98.1	133.2

^aLeast significant difference, Student's *T*-test, *P* = 0.05

Seeds contain most of the thiols and disulphides in proteins,^{31,32} which are liable to aging changes owing to their role in the regulation of the cell redox environment. Pukacka³³ found a decrease in PSH during the aging of *Acer platanoides* seeds, which is in agreement with the changes in the H1 seeds (decrease of 72 %, Table I). The significant increase in the PSH content was accompanied by a considerable decrease in GSH and germination ability during AA treatment in H2, compared to H1, which may develop from proteins undergoing dethiolation, although the similar changes were already established by Seres and co-workers.³⁴ The observed mechanism was suggested by Grant *et al.*,³⁵ as the last defence in the irreversible oxidation of cysteine residues, the occurrence of which would otherwise lead to polypeptide aggregation. It is also possible that two different types of nanomolecular switches:²⁰



are present in H1 and H2, resulting in different alterations of the GSH/PSH ratio, which had a sigmoid trend in H1, decreasing from 3.2 to 2.9 (up to 6th day of



AA) and the n increasing, up to 5.1, underlining intensive PSH consumption to GSH, while in H2, the ratio had a more continual decrease to the 6th day of AA (from 3.4 to 2.5) and then a steeper reduction to 0.9, emphasising intensive GSH expenditure.

However, Schafer and Bueettner²⁰ used the GSSG/2GSH half-cell potential (E_{hc}), which gave the opportunity to quantify the physiological status influencing plant growth. The changes in the E_{hc} of the maize seeds shown in Fig. 1 clearly illustrate the changes developed during the course of AA. In the seeds of both hybrids, the GSSG increased due to GS H oxidation, as was also evidenced in other seeds.^{26,27} In the initial maize hybrid seeds, the value of E_{hc} was similar, i.e., -158.2 and -157.8 mV in H2 and H1, respectively, with negligible changes after 9 days of AA, i.e., -119.1 and -118.5 mV, respectively. The slight variation in E_{hc} accompanied with intensive changes in GSH and GSSG (Table I), as well as a decrease in the total glutathione to 55 and 56 % in H1 and H2, respectively, were similar to the results obtained by De Vos *et al.*²⁸ indicating that the glutathione redox system is not a closed one and that GSH reacts with other macromolecules in the seeds during aging. Dean and Devarajene³⁶ suggested conjugation of GSH with soluble phenolic compounds as the mechanism of its elimination from cells, while the significant amount of GSH in H2 may serve for disulphide dethiolation.^{34,35}

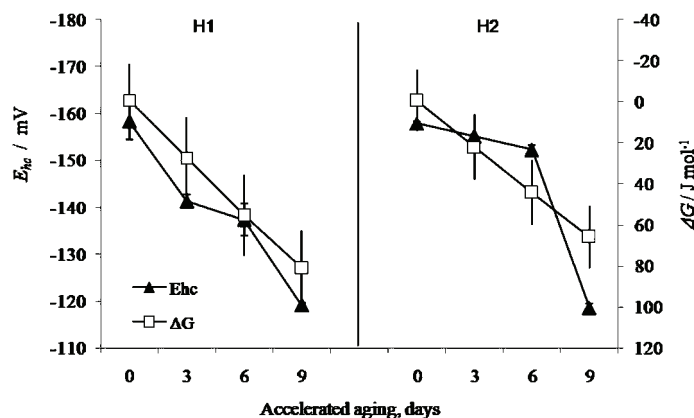


Fig. 1. Changes of the GSSG/2GSH half cell potential (E_{hc}) and Gibbs energy change (ΔG), as a result of accelerated aging for 3, 6 or 9 days (H1 – dent hybrid, H2 – sugary hybrid); vertical bars represent the SD values.

The found E_{hc} values were higher than the results obtained by Kranner *et al.*,¹⁷ which could be connected to the level of the Gibbs energy change (ΔG , Fig. 1). Thus, ΔG negatively correlates with the germination decrease ($R = -0.66$) to a higher degree than the E_{hc} increase ($R = -0.59$). The thermal treatment (aging

mode)⁶ elevated the Gibbs energy, but to a higher degree in H1 (81 J mol^{-1}) than in H2 (66 J mol^{-1}). The relatively parallel changes in the ΔG and E_{hc} of the seeds ($R = 0.90$) are indicative of an intensification of endergonic reactions and a larger energy expenditure.^{14,23} Furthermore, the ΔG increase does not correspond with the ΔS change, which was decreased by a maximum of 0.06 J m ol^{-1} in H1 (Fig. 2). Considering that entropy presents capacity, *i.e.*, the presence of energy unavailable for work, the system is under conditions of restricted energetic capacity (thermodynamic equilibrium, $\Delta S \approx 0$) and lower molecular mobility,^{23,37} from the 3rd day of AA. It is necessary to emphasise that the lower entropy values of the H1 seeds indicate an enhanced capacity to tolerate change with respect to H2 seeds. Only for the ΔH , *i.e.*, measurement of the total energy change, were significant alterations observed, which had a sigmoid shape with the H1 seeds and a maximum ($\Delta H > 0$) on the 3–6th day of accelerated aging, while for H2, ΔH had a general decreasing trend, with the negative values indicating a shift of the system from a relatively ordered to a disordered state.^{14,23}

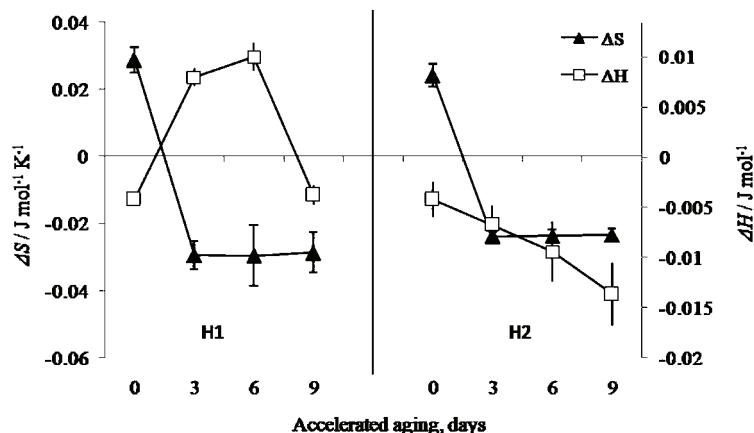


Fig. 2. Changes of entropy (ΔS) and enthalpy (ΔH) due to accelerated aging for 3, 6 or 9 days (H1 – dent hybrid, H2 – sugary hybrid); vertical bars represent the SD values.

The observed dynamics could be connected to a possible melting of the glass matrix and irreversible metabolic changes, attributed to desiccation.^{16,22,38} Additionally, the trends of the ΔH and ΔS changes indicate a different organisation structure of the dent and sugary hybrids, irrespective of their positive correlation with germination reduction (Fig. 3) and the observed correlation between them ($R = 0.71$ for ΔH ; $R = 0.38$ for ΔS). Namely, the rapid increase in enthalpy, followed by a negligible increase in entropy for the H1 seeds could be related to glass relaxation,³⁹ followed by a later domination of stronger bonds, as consequence of desiccation²³ and furthermore impairment of metabolism by free radicals.¹⁶ Moreover, the H2 seeds could be characterised by weaker molecule move-

ments and stronger bonds, hence the system is above the edge of enthalpy equilibrium, with a relatively weak relaxation, characteristic for seeds with a lower germination ability.³⁹ It could be assumed that desiccation tolerance and prolonged seed longevity in the desiccated state depend on the ability of the system to scavenge free radicals. The failure of the antioxidant system during long-term desiccation appears to trigger programmed cell death, causing ageing and eventual death of the organism.^{13,16}

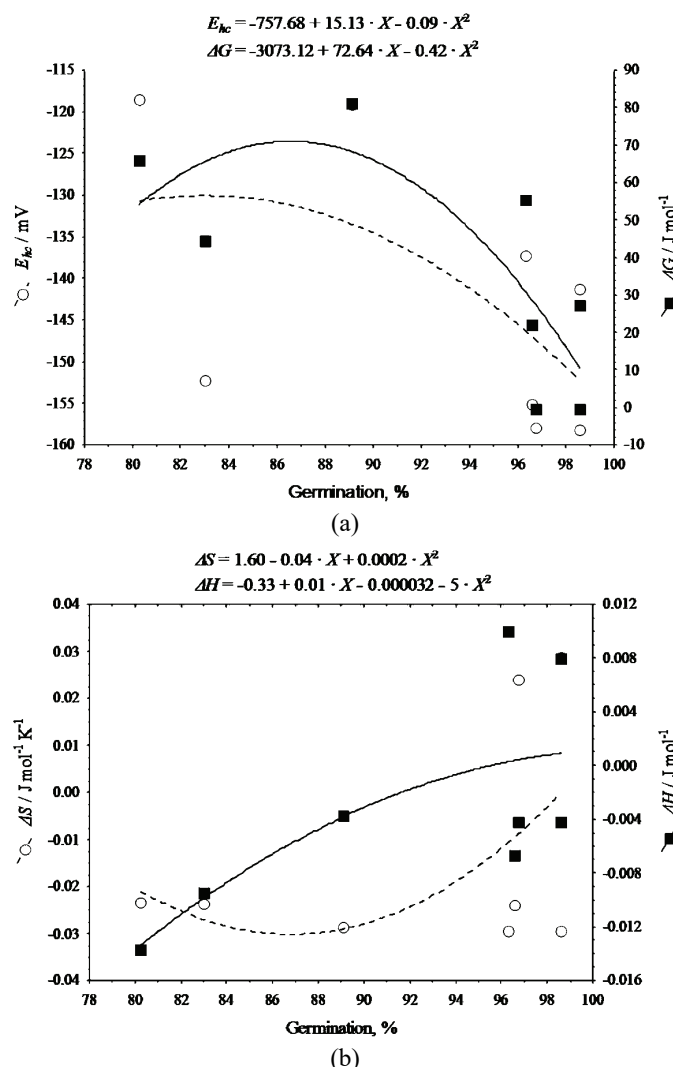


Fig. 3. Correlation between the maintenance of germination (percentage) ability;
a) changes of the redox potential, E_{hc} , and Gibbs energy change, ΔG , and
b) changes in enthalpy, ΔH , and entropy ΔS .

CONCLUSIONS

The genotypic characteristics of the two examined hybrids indicated possible different metabolic pathways of the seeds, which is connected to different trends of the changes in the thermodynamic parameters (ΔG , ΔH and ΔS) and different types of nanomolecular switches, resulting in relative faster decrease of GSH in the H2 hybrid than in the H1 hybrid, emphasizing that the GSSG/2GSH half cell potential is a useful tool for quantifying plant stress, but it cannot be alone a measure for seed germination ability. The observed changes in the seeds could be described from the viewpoint of thermodynamics by the enthalpy: $\Delta H = 0 \text{ J mol}^{-1}$ might be considered as the border between reversible and irreversible injuries in seeds. The combination of the GSSG/ 2GSH half-cell potential with thermodynamic parameters may possibly be a more effective tool for determination of seed germination ability and the physiological status of seeds.

Acknowledgments. This work was supported by the scientific project “Development of Maize Cropping Technology with an Ecological Approach”(Ev. No. TR-20007) of the Ministry of Science and Technological Development of the Republic of Serbia.

ИЗВОД

УВОД У МЕЂУСОБНУ ЗАВИСНОСТ ЂЕЛИЈСКОГ РЕДОКС ПОТЕНЦИЈАЛА ГЛУТАТИОНА И ТЕРМОДИНАМИКЕ ТОКОМ УБРЗАНОГ СТАРЕЊА СЕМЕНА КУКУРУЗА

ВЕСНА Д. ДРАГИЧЕВИЋ¹, СЛОБОДАНКА Д. СРЕДОЈЕВИЋ¹ и МИХАЈЛО Б. СПАСИЋ²

¹Институут за кукуруз, Слободана Бајића 1, 11185 Београд-Земун и ²Институут за биолошка истраживања
“Синиша Станковић”, Булевар Десетога Септембра 142, 11060 Београд

Проучавано је убрзано старење семена два хибрида кукруза која имају другачију способност очувања клијавости. Сличан почетни редукциони потенцијал GSSG/2GSH паре је код H1(зубан) растао без утицаја на способност клијања до шестог дана убрзаног старења, док се код H2 (шећерац) није мењао до шестог дана старења, уз каснији значајан пад клијавости. Количина PSH се смањивала код H1, док је расла код H2 током третмана старења. Без обзира на континуиран пад слободне енергије током убрзаног старења, особине семена испитиваних хибрида су можда биле везане за другачије метаболичке путеве: H1 карактерише висока ентропија и позитивне вредности енталпије, док је за H2 карактеристична релативно ниска ентропија, уз негативне вредности енталпије, указујући на помењање система из релативно уређеног у неуређено стање. Другачији типови наномолекулских прекидача, утичући на бржи пад GSH код H2 у односу на H1, истичу да се комбинација GSSG/2GSH ђелијског потенцијала и термодинамике могу користити при квантификацији биљног стреса.

(Примљено 30. јуна, ревидирано 16. септембра 2009)

REFERENCES

1. ISTA, *International rules for seed testing*, ISTA, Bassersdorf, 2007, p. 5A
2. C. Walters, *Seed Sci. Res.* **8** (1998) 223
3. M. R. Munamava, A. S. Goggi, L. Pollak, *Crop Sci.* **44** (2004) 542



4. D. L. Kittock, A. G. Law, *Agron. J.* **60** (1968) 286
5. J. D. Anderson, *Crop Sci.* **10** (1970) 36
6. S. Tang, D. M. Tekrony, D. B. Egli, P. L. Cornelius, *Crop Sci.* **40** (2000) 463
7. A. Benamar, C. Tallon, D. Macherel, *Seed Sci. Res.* **13** (2003) 35
8. Z. Giba, D. Grubišić, R. Konjević *Seed Sci. Res.* **13** (2003) 187
9. D. Pavlović, V. Djordjević, G. Kocić, *Facta Universit. Med. Biol.* **9** (2002) 131
10. L. Xiong, J. K. Zhu, *Plant Cell Environ.* **25** (2002) 131
11. M. S. B. Paget, M. J. Buttner, *Annu. Rev. Genet.* **37** (2003) 91
12. C. Giuliani, G. Consoni, G. Gavazzi, M. Colombo, S. Dolfini, *Ann. Bot.* **90** (2002) 287
13. H. El-Maarouf-Bouteau, C. Bailly, *Plant Signal. Behavior* **3** (2008) 175
14. D. D. Davies, *Intermediary metabolism in plants*, Cambridge University Press, Cambridge, 1961, p. 35
15. J. S. Boyer, *Annu. Rev. Plant Physiol.* **20** (1969) 35
16. C. Bailly, H. El-Maarouf-Bouteau, F. Corbineau *C R Biol.* **331** (2008) 806
17. I. Kranner, S. Birtic, K. M. Anderson, H. W. Pritchard, *Free Rad. Biol. Med.* **40** (2006) 2155
18. J. M. Woltz, D. M. Tekrony, *Seed Technol.* **23** (2001) 21
19. L. J. de Kok, P. J. L. de Kan, G. Tanczos, J. C. Kupier, *Physiol. Plant.* **53** (1981) 435
20. F. Q. Schafer, G. R. Buettner, *Free Rad. Biol. Med.* **30** (2001) 1191
21. ISTA, *Seed Sci. Technol.* 27, Suppl. 47–59 and Annex, 1999, Zürich, p. 271
22. W. Q. Sun, *Plant Physiol.* **124** (2000) 1203
23. W. Q. Sun, *Desiccation and survival in plants: drying without dying*, M. Black, H. W. Pritchard, Eds., CABI Publishing, Wallingford, 2002, p. 47
24. G. Kocsy, M. Brunner, A. Rüegsegger, P. Stamp, C. Brunold, *Planta* **198** (1996) 365
25. L. Xiong, K. S. Schumaker, J. K. Zhu, *Plant Cell* **14** (2002) s165
26. M. De Paula, M. Pérez-Otaola, M. Darder, M. Torres, G. Frutos, C. J. Martínez-Hondurilla, *Physiol. Plant.* **96** (1996) 543
27. M. Torres, M. De Paula, M. Pérez-Otaola, M. Darder, G. Frutos, C. J. Martínez-Hondurilla, *Physiol. Plant.* **101** (1997) 807
28. C. H. R. De Vos, H. L. Kraak, R. J. Bino, *Physiol. Plant.* **92** (1994) 131
29. C. Ju, K. N. Yoon, Y. K. Oh, H. C. Kim, C. Y. Shin, J. R. Ryu, K. H. Ko, W. K. Kim, *J. Neurochem.* **74** (2000) 1989
30. I. Kranner, G. Grill, *Bot. Acta* **109** (1996) 8
31. T. Leustek, M. N. Martin, J. A. Bick, J. P. Davies, *Annu. Rev. Plant Physiol. Plant Mol. Biol.* **51** (2000) 141
32. P. Schürmann, J. P. Jacquot, *Annu. Rev. Plant Physiol. Plant Mol. Biol.* **51** (2000) 371
33. S. Pukacka, *Physiol. Plant.* **8** (1991) 306
34. T. Seres, V. Ravichandran, T. Moriguchi, T. Rokutan, J. A. Thomas, R. B. Johnston, *J. Immunol.* **156** (1996) 1973
35. C. M. Grant, K. A. Quinn, I. W. Dawes, *Mol. Cell. Biol.* **19** (1999) 2650
36. J. V. Dean, T. P. Devarenne, *Physiol. Plant.* **99** (1997) 271
37. J. Buitink, C. Walters-Vertucci, F. A. Hoekstra, O. Leprince, *Plant Physiol.* **111** (1996) 235
38. O. Leprince, F. A. Hoekstra, *Plant Physiol.* **118** (1998) 1253
39. P. Krishnan, D. K. Joshi, M. Mahe swari, S. Nagarajan, A. V. Moharir, *Biol. Plant.* **48** (2004) 117.





Evaluation of the oxidative activity of some free base porphyrins by a chemiluminescence method

MARIANA VOICESCU^{1*}, RODICA ION² and AURELIA MEGHEA³

¹Institute of Physical Chemistry, Romanian Academy, Splaiul Independentei 202, 060021

Bucharest, ²Research and Development National Institute for Chemistry and

Petrochemistry –ICECHIM, 202 Splaiul Independentei, 060021, Bucharest and

³University Politehnica of Bucharest, Department of Applied Physical Chemistry
and Electrochemistry, Polizu 1, 78126 Bucharest, Romania

(Received 9 August, revised 16 September 2009)

Abstract: Due to their spectral characteristics, phototoxicity and high affinity for tumour tissues, porphyrins and their derivatives are widely used in modern medicine as contrast agents for cancer diagnostics and as sensitizers in photodynamic therapy, where they kill tumours *via* enhancement of tumour oxidative stress. The aim of this work was to simulate *in vitro* the effects caused by oxidation of two free base porphyrins, 5,10,15,20-tetraphenylporphyrin (TPP) and 5,10,15,20-tetra(4-methoxyphenyl)porphyrin (TMOPP). The kinetic study was monitored using spectral techniques and chemiluminescence. The effect of both porphyrins on an oxidation process was evidenced using the chemiluminescent system, luminol–hydrogen peroxide, in a phosphate buffer at pH 7. It was found that at low concentration, TPP exerts the anti-oxidative effect in the employed chemiluminescent system, while at higher concentrations, its effect is pro-oxidative. TMOPP exerts a pro-oxidant effect, which was more pronounced than TPP. The results are discussed with respect to oxidative stress.

Keywords: free base porphyrins; chemiluminescence; oxidative activity; luminol.

INTRODUCTION

Porphyrins, free base and metallocomplexes,^{1,2} play an important role in many energy transfer processes from photochemistry,³ photobiology⁴ and photomedicine.^{5,6} Porphyrins can be oxidized chemically, electrochemically, photochemically (photosensitization) to form porphyrin-ring centred oxidized products.⁷

Recently, importance was granted to oxidative stress (a common state in most pathological conditions, such as cancer, diabetes, radiation injury and disorders of the central nervous system), especially regarding the role of synthetic antioxidants, such as Mn porphyrins, in the treatment of oxidative stress.^{8,9} Chemi-

*Corresponding author. E-mail: voicescu@icf.ro
doi: 10.2298/JSC090809021V

luminescence detection reactions have become popular in analytical biochemistry, essentially due to their high sensitivity. In this way, a synthetic chemiluminescent system (luminol/porphyrin) was conveniently employed to measure serum oxalate by determination of the hydrogen peroxide generated through oxalate oxidase.^{10–12} In order to use metalloporphyrins as labels in immunoassays or in nucleic probes, a detection method based on luminol chemiluminescence (CL) at alkaline pH was developed.¹³ The generation of the free radicals HO[•] and O₂^{•-} was found to be the result of luminol oxidation by metalloporphyrins. In these respects, using 5,5'-dimethyl-1-pyrroline-N-oxide as a spin trap agent, electron spin resonance (ESR) evidenced the production of HO[•] and O₂^{•-}. The role of O₂^{•-} was confirmed by the almost complete inhibition of light emission when superoxide dismutase was added to the CL reaction. The contribution of oxygen was also confirmed by the large decrease in the CL emission when deaerated solutions were used.^{7,13} Owing to their redox properties, FMN and NAD enhancers could act at this level through an increase of the exchange rate between Fe²⁺ and Fe³⁺. In the presence of FMN, a significant red shift and shape change of the luminol emission spectrum was observed, which arises from an energy transfer phenomenon in the final luminescent step of the reaction.¹³

It is known that several synthetic metalloporphyrins associated with oxygen atom donors are potent catalysts for the chemiluminescent oxidation of luminol or isoluminol. In these respects, the luminescence produced at pH 7.5 in the presence of isoluminol, H₂O₂ and metalated water-soluble porphyrins (Fe³⁺ or Mg²⁺) derivatives of tetra-sodium *meso*-tetrakis(*p*-sulphonatophenyl)porphyrin and *meso*-tetrakis(4-*N*-methyl-pyridiniumyl)porphyrin] to tracetate was of the same order of magnitude as that produced by horseradish peroxidase under the same conditions.^{14,15} Many porphyrins catalyze luminol chemiluminescence at pH 13 without addition of peroxide. The most active catalyst was Mn-*meso*-tetrakis(*p*-sulphonatophenyl)porphyrin. It was found that Tween-20 enhanced the activity of this catalyst best at a Tween-20 to luminol ratio of 74:1. Dodecyl sulphate enhanced best at the optimum dodecyl sulphate to luminol ratio of over 100:1 and both detergents enhanced the reaction when present below their critical micelle concentrations. Moreover, negatively charged aliphatic compounds, such as fatty acids, enhanced the reaction but positively charged aliphatic compounds inhibited it.¹¹

The Mn and Fe porphyrins that were shown to have broad antioxidant properties are, in effect, analogues of naturally occurring haeme (iron protoporphyrin IX). It was shown that the reactivities of the synthetic metalloporphyrins were not constrained by the microenvironment of protein-bound haeme.¹⁶ Moreover, Ferrer-Sueta *et al.*¹⁷ and Crow¹⁸ reported that some metalloporphyrins appear to be capable of scavenging the CO₂ adduct of peroxynitrite. In addition, metalloporphyrins were shown to be protective in a number of cell and animal models of

oxidative injury¹⁹ and models of stroke.²⁰ Such evidence that these redox active porphyrins were effective *via* peroxy nitrite scavenging was provided by showing that protein nitration was prevented.^{21,22} In these regards, prevention of protein nitration strongly suggests that other deleterious reactions of peroxy nitrite were also prevented. However, new evidence suggests that metalloporphyrins have protective effects independent of antioxidant activities, namely that they are potent inducers of haeme oxygenases and other heat shock proteins – proteins which are known to enhance survivability to oxidative stress.

Recently, the lipophilicity of potent porphyrin-based antioxidants, by a comparison between *ortho*- and *meta*-isomers of Mn³⁺-N-alkylpyridylporphyrins was studied.²³

This work follows a previous study²⁴ and deals with the effects of two free base porphyrins (5,10,15,20-tetra-*p*-phenylporphyrin (TPP) and 5,10,15,20-tetra-(*p*-methoxyphenyl)porphyrin (TMOPP)) in an oxidation process studied by a chemiluminescence method using the chemiluminescent system luminol-hydrogen peroxide in phosphate buffer at pH 7. It was found that at low concentrations, TPP exerted an anti-oxidative effect in the employed CL system, while its effect was pro-oxidative at higher concentrations. TMOPP exerted a pro-oxidant effect, which was more pronounced than TPP. These findings could be important regarding oxidative stress as a function of concentration. The studied free base porphyrins could have a protective effect against reactive oxygen species.

EXPERIMENTAL

Materials

The system luminol (LH₂) (8.80×10^{-5} M)-hydrogen peroxide (H₂O₂) (30 mM) in 50 mM phosphate buffer at pH 7 was considered the reference system. LH₂ and H₂O₂ were from Merck and the phosphate buffer from Sigma. TPP, in which R = C₆H₅ (5,10,15,20-tetraphenylporphyrin) and TMOPP, in which R = C₆H₅-OCH₃ (5,10,15,20-tetra(4-methoxyphenyl)porphyrin) (Fig. 1) were synthesized by Prof. Ion's team and the solutions for this study were prepared in dimethyl sulphoxide (DMSO).²⁵

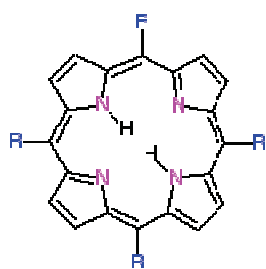


Fig. 1. Chemical structure of the studied porphyrins.

Methods and apparatus

The chemiluminescence (CL) measurements were realized with a chemiluminescence instrument TD 20/20 Turner Design, USA. The points on the plot were obtained by integrating the light signal at periods of 4 s. Five measurements were made and an average value

calculated, obtaining a maximum 10 % relative scattering of the results from the mean value. The working volume was 1000 µl.

The extinction of the CL emission, S , was calculated according to the equation:

$$S = 100 \frac{I_0 - I}{I_0}$$

where I_0 and I represent the CL intensity measured for the reference system and for the reference system in the presence of antipyrine, respectively; both values were measured 5 s after the beginning of the reaction.

The $I_{CL} = f(t)$ variation enable the determination of the rate constant of the reaction, for the upward part of the plot, $-k_2$ (attributed to the consumption of free radicals reaction), as well as for the downward part of the curve, k_1 (attributed to the formation of free radicals reaction), considering that the CL reaction is first order. The values of k_1 and k_2 were determined using the following equation:

$$k = \frac{1}{\Delta t} \ln \frac{I_i}{I_0}, \Delta t = t_i - t_0$$

in which t_i represents the time at the moment i , t_0 represents the initial time, I_i is the intensity of CL signal at the moment i and I_0 is the intensity of the CL signal at the initial moment. The value of the rate constants were calculated in time range 5–60 s ($-k_2$) for the LH_2 /phosphate at pH 7/ H_2O_2 , at pH 7/ H_2O_2 /TPP and TMOPP systems.

The visible absorption spectra were recorded on a SPECORD M400 Carl Zeiss Jena spectrophotometer. The mass spectra were obtained with an HP 5985 spectrometer (Hewlett-Packard), using a silica column. The final product of the photodegradation reaction of TPP was identified with a Perkin Elmer spectrometer, from CCl_4 solution.

The FTIR spectra were acquired using a Jasco FT/IR-470 plus or a FT/IR-4200 spectrometer as KBr pellets.

Carlo Erba FTV 4160 gas chromatograph, incorporating Grob-type split/splitless and on-column injectors, was employed throughout this work. The same type of instrument was also linked to an AEI MS 30 magnetic sector mass spectrometer. A flexible silica interface was employed to prevent adsorption and decomposition of the porphyrins.

Several WCOT capillary columns, coated with apolar phases, were employed. A 20 m × 0.34 mm i.d. glass capillary column coated with CP Sil 5 (Chrompak) was adequate for the analysis of the porphyrin derivatives. The less volatile porphyrin derivatives were analysed on a 6 m × 0.3 mm i.d. Hewlett-Packard flexible fused silica capillary column coated with OV-1 stationary phase. Hydrogen was usually employed as the carrier gas, typically at an inlet pressure of 0.2 kg cm⁻², producing an average gas velocity of approximately 100 cm s⁻¹. All analyses were temperature programmed.

The ketone and peroxide concentrations were determined by colorimetric methods as indicated in the literature.²⁶

RESULTS AND DISCUSSION

The chemiluminescence (CL) technique is based on generating free radicals (HO^\bullet , $O_2^\bullet-$, 1O_2 , ROO^\bullet) in a luminescence system and is followed by the study of pro- and anti-oxidative actions on a specific molecule.^{13,14} CL is a concerted chemical and physical process which occurs after an exergonic chemical reaction, releasing the energy as light. In this way, a molecule in the excited state un-

dergoes a structural arrangement process of an electronic level, showing physical and chemical properties that are different compared to those of the ground state. It is well known that $\text{LH}_2\text{-H}_2\text{O}_2$ in alkaline solution yields an excited amine-phthalate dianion species, which leads to the appearance of oxygen free radicals, such as: the superoxide anion, singlet oxygen and hydroxyl radical.^{13,14} The result of the multiple interactions is light emission, as luminol is consumed. In the presence of an antioxidant compound (which consumes free radicals), the CL intensity decreases, while the effect of a pro-oxidant compound (which increases the concentration of free radicals) is an increase in the CL intensity.

The CL measurements were recorded in order to evaluate the anti-oxidative ability of TPP and TMOPP in various systems. Chemiluminescence, already evidenced for some porphyrins by Wasser and Fuhrhop²⁷ was evaluated at 430–440 nm in this study. Usually, the degradation of porphyrins involves a macrocycle break with an energy release of 60–70 kcal/mol, sufficient for light emission. In DMSO and hydrogen peroxide, the proton from inside the porphyrin macrocycle can leave the macrocycle and the porphyrin becomes an anion with a strong electronic density at the methine carbon position.^{28–30} Under such conditions, the anionic form of the porphyrin could aggregate (Fig. 2, 2), in good agreement with literature data,³¹ Fig. 2.

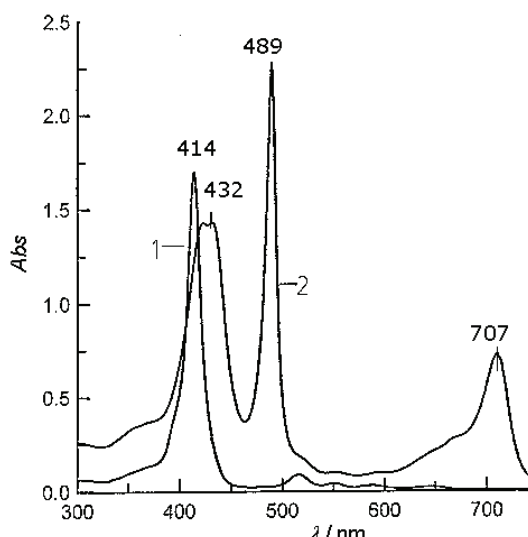


Fig. 2. UV-Vis spectra of TPP in the monomeric form (1) and the aggregated form (2).

The variation of the CL intensity as a function of time (Fig. 3) allows the determination of the quenching of the CL reaction for systems that contain porphyrins. It was found that the profiles of the CL in the presence of TPP and TMOPP porphyrins were almost the same and the peak intensities of the CL increased with increasing concentration of the employed porphyrin. At small concentrations, TPP

acts as a trap for free radicals produced in the system $\text{LH}_2\text{--H}_2\text{O}_2$. At higher concentrations, 0.50–1.5 μM , TPP leads to a strong increase of the CL intensity, which in fact could be the result of a process of aggregation of porphyrins in DMSO and in the presence of H_2O_2 . An oxidation of lum inol by the porphyrin occurs. This is a consequence of the photo generation of hydrogen peroxide by the porphyrins.³²

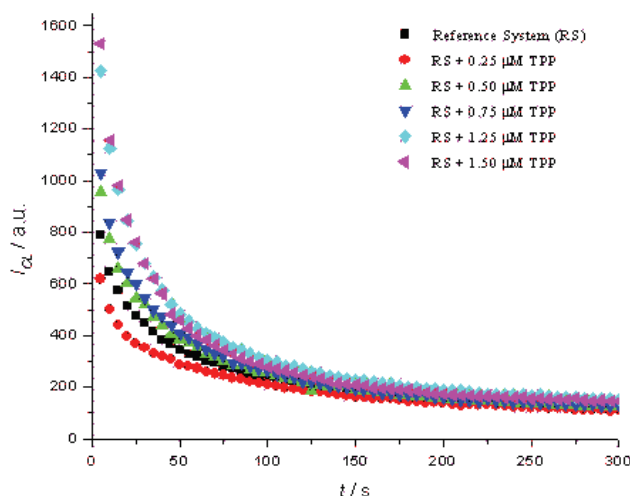


Fig. 3. The effect of TPP concentration on the CL intensity of the LH_2 ($8.80 \times 10^{-5}\text{M}$)– H_2O_2 (30 mM) system in 50 mM phosphate buffer at pH 7 (reference system).

Similarly, in the case of TMOPP (the results are not shown), an increase in the CL intensity, more pronounced than in the case of TPP, was evidenced. These are according to the efficiency of CL quenching ($S / \%$) and reaction rate values, Table I. Moreover, it can be observed that the results also corroborate with the concentration of ketones and peroxides.

The responsible species for chemiluminescence are dioxetane species, via ketone and peroxide species evidently, as determined by IR spectroscopy, the stretching vibrational bands $\nu(\text{C}=\text{O})$ at 1600 and 980 cm^{-1} (Fig. 4), and by mass spectrometry (Fig. 5).

TABLE I. The kinetic parameters of the CL process (efficiency of CL quenching, reaction rate and rate constants) in the $\text{LH}_2\text{--H}_2\text{O}_2$ –phosphate buffer at pH 7 system (reference system, RS), in the presence of TPP and TMOPP, 5 s after the beginning of the chemiluminescence reaction

System	$S / \%$	v / s^{-1}	$k \times 10^2 / \text{s}^{-1}$	Ketone concentration, $\mu\text{l ml}^{-1}$	Peroxide concentration, $\mu\text{l ml}^{-1}$
RS	–150		3.1	–	–
RS + 1.50 μM TPP	–93.8	306	4.2	5.12	3.13
RS + 1.50 μM TMOPP	–130.1	364	4.0	23.46	17.45

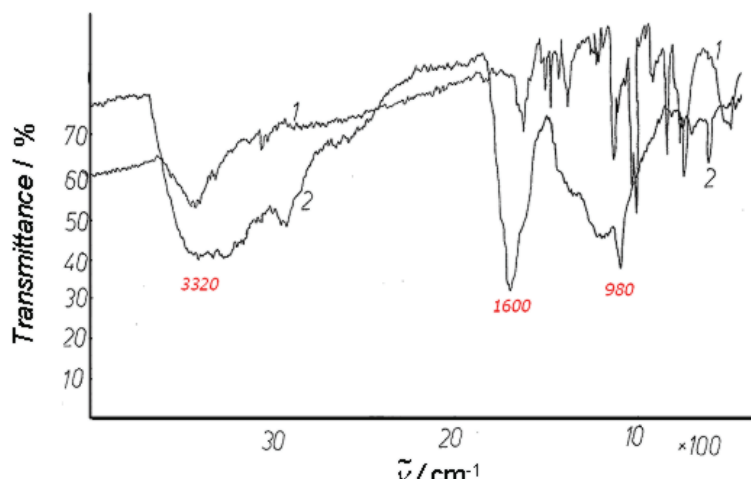


Fig. 4. IR spectra of TPP, initial (1) and final (2).

It was possible to determine the ketone and peroxide concentrations, as a proof for the above-mentioned porphyrin degradation, Table I. It can be observed that, in the case of TMOPP, the found concentration of ketone, 23.5 $\mu\text{M}/\text{ml}$ was higher than that in the case of TPP porphyrin, 5.12 $\mu\text{M}/\text{ml}$. With regards to the peroxide concentration, a higher value was also found, 17.4 $\mu\text{M}/\text{ml}$ in the case of TMOPP compared with 3.13 $\mu\text{M}/\text{ml}$ in the case of TPP.

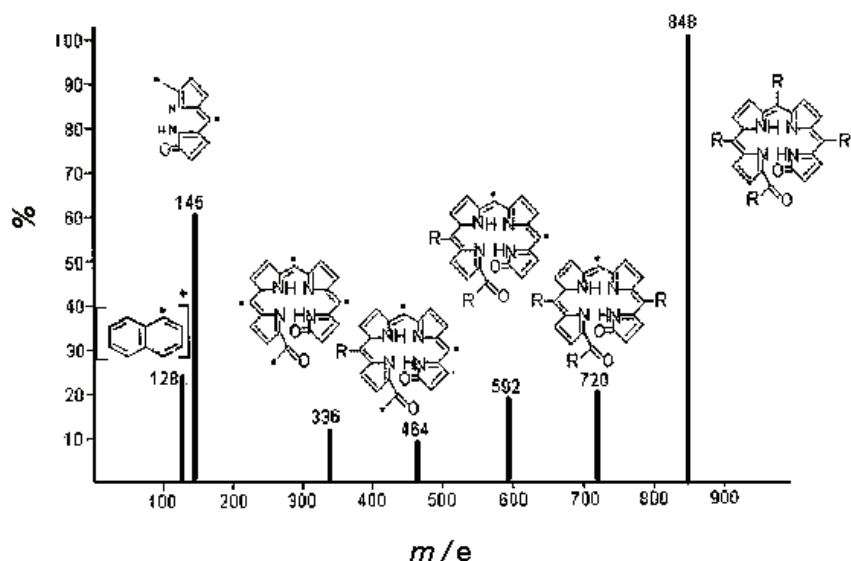


Fig. 5. The fragmentation diagram for TPP degradation.

CONCLUSIONS

The study was aimed at simulating *in vitro* the effects of 5,10,15,20-tetraphenylporphyrin (TPP) and 5,10,15,20-tetra(4-methoxyphenyl)porphyrin (TMOPP) in the oxidative system luminol–hydrogen peroxide, in phosphate buffer at pH 7. The kinetic study was monitored by the evolution of the chemiluminescence intensity as a function of time. It was found that at a low concentration (0.25 µM) TPP exerted an anti-oxidative effect in the employed chemiluminescent system while at higher concentrations (0.50–1.5 µM), its effect was pro-oxidant. TMOPP, for the same range of concentrations, exerted a pro-oxidant effect, which was more pronounced than that of TPP.

The ketone and peroxide concentrations were found to be higher in the case of TMOPP than in the case of TPP.

These aspects are important and could be an indication in future investigations with regard to the oxidative stress process. Moreover, the results are an additional tool to predict a possible protective effect of free base porphyrins in an oxidation process. These free base porphyrins may have a protective effect that could work independently of anti-oxidant activities.

ИЗВОД

ОДРЕЂИВАЊЕ ОКСИДАТИВНЕ АКТИВНОСТИ НЕКИХ СЛОБОДНИХ БАЗА ПОРФИРИНА ХЕМИЛУМИНЕСЦЕНТНОМ МЕТОДОМ

MARIANA VOICESCU¹, RODICA ION² и AURELIA MEGHEA³

¹*Institute of Physical Chemistry, Romanian Academy, Splaiul Independentei 202, 060021 Bucharest, ²Research and Development National Institute for Chemistry and Petrochemistry –ICECHIM, 202 Splaiul Independentei, 060021, Bucharest и ³University Politehnica of Bucharest, Department of Applied Physical Chemistry and Electrochemistry, Polizu 1, 78126 Bucharest, Romania*

Порфирини и њихови деривати се, захваљујући својим спектралним карактеристикама, фототоксичности и великим афинитету према ткиву тумора, широко користе у модерној медицини као контрастни агенси у дијагнози тумора и терапији. Они убијају туморе повећавајући оксидативни стрес у њима. Циљ овог рада је да *in vitro* симулира ефекте које изазивају две слободне базе порфирина, 5,10,15,20-тетрафенилпорфирин (TPP) и 5,10,15,20-тетра(4-метоксифенил)порфирин (TMOPP). Кинетичка студија је праћена спектралним и хемилуминесцентним методама. Ефекат порфирина у процесу оксидације је одређиван у хемилуминесцентном систему, луминол–водоник–пероксид, у фосфатном пуферу, pH 7. При ниским концентрацијама TPP има антиоксидативни ефекат, док при вишим концентрацијама има прооксидативно дејство. TMOPP испорава прооксидативни ефекат и то израженије него TPP. Резултати су дискутовани у односу на оксидативни стрес.

(Примљено 9. августа, ревидирано 16. септембра 2009)

REFERENCES

1. P. Hambright, *Coord. Chem. Rev.* **6** (1971) 247
2. D. Frackowiak, A. Planner, R. M. Ion, in *Near-infrared dyes for high technology applications*, S. Daehne, U. Resch-Genger, O. Wolfbeis, Eds., NATO ASI Series, Vol. 3/52, Kluwer Academic Publishers, Dordrecht/Boston/London, 1998, p. 87



3. R. M. Ion, in *Porfirinele si terapia fotodinamica a cancerului*, FMR, Ed., Bucuresti, Ch. 8, 2003, p. 113 (In Romanian)
4. G. Barrett, *Nature* **215** (1967) 533
5. M. S. Rana, *Saudi Pharm. J.* **13** (2005) 97
6. M. S. Rana, K. Tomagake, *Chim. Pharm. Bull.* **53** (2005) 604
7. C. Poupon- Fleuret, J.-P. Steghens, J.-C. Bernengo, *Analyst* **121** (1969) 1539
8. B. Halli well, J. Gutteridge, *Free Radical Biology and Medicine*, 4th Ed., O xford Univ. Press, London, 2007
9. I. Batinic-Haberle, L. Benov, I. Spasojevic, P. Hambright, A. L. Fridovich, *Inorg. Chem.* **38** (1999) 4011
10. Y. Adam, J. Bernadou, B. Meunier, *New J. Chem.* **16** (1992) 525
11. M. A. Motsenbocker, K. Oda, Y. Ichimori, *J. Biolumin. Chemilum.* **9** (1994) 7
12. K. Komagoe, T. Katsu, *Anal. Sci.* **22** (2006) 255
13. R. Olinescu, M. Greabu, *Chemiluminescenta si bioluminescenta*, Ed. Tehnica, Bucuresti, 1987 (in Romanian)
14. A. K. Campbell, *Chemiluminescence – Principle and applications in biology and medicine*, Ellis Horwood Ltd., Chichester, 1988
15. G. Merenyi, J. Lind, T. E. Erickson, *J. Biolumin. Chemilumin.* **5** (1990) 53
16. J. P. Crow, in *Neurodegenerative Diseases*, M. Flint Beal, A. E. Lang, A. Ludolph, Eds., Cambridge University press, Cambridge, 2005
17. G. Ferrer-Sueta, I. Batinic-Haberle, I. Spasojevic, I. Fridovich, R. Rodi, *Chem. Res. Toxicol.* **12** (1999) 442
18. J. P. Crow, *Arch. Biochem. Biophys.* **371** (1999) 41
19. X. Liu, J. M. Miller, M. S. Joshi, D. D. Thomas, J. R. Lancaster Jr., *Proc. Natl. Acad. Sci. USA* **95** (1998) 2175
20. G. B. Mackensen, M. Patel, H. Sheng, C. L. Calvi, I. Batinić-Haberle, B. J. Day, L. P. Liang, I. Fridovich, J. D. Crapo, R. D. Pearlstein, D.S. Warner, *J. Neurosci.* **21** (2001) 4582
21. D. Salvemini, D. P. Riley, P. J. Lennon, Z.-Q. Wang, M. G. Currie, H. Macarthur, T. P. Misko, *Br. J. Pharmacol.* **127** (1999) 685
22. T. P. Misko, M. K. Highkin, A. W. Veenhulzen, P. T. Manning, M. K. Stern, M. G. Currie, D. Salvemini, *J. Biol. Chem.* **273** (1998) 15646
23. I. Kos, J. S. Rebouças, G. De Freitas-Silva, D. Salvemini, Z. Vujskovic, M. W. Dewhirst, I. Spasojević, I. Batinić-Haberle, *Free Rad. Biol. Med.* **47** (2009) 72
24. R. M. Ion, A. Planner, K. Wiktorowicz, D. Frackowiak, *Acta Biochim. Pol.* **45** (1998) 833
25. R. M. Ion, C. Mandravel, *South. Braz. J. Chem.* **5** (1996) 111
26. F. Snell, C. Snell, *Colorimetric methods of analysis*, Vol. III, D. Van Nostrand Company Inc., Princeton, New York, 1953.
27. P. K. W. Wasser, J.-H. Fuhrhop, *Ann. N.Y. Acad. Sci.* **206** (1973) 533
28. H. Fuhrhop, D. Mauzerall, *Photochem. Photobiol.* **13** (1971) 453
29. R. M. Ion, *Rev. Chim.* **9** (1994) 789
30. R. M. Ion, L. Teodorescu, C. Mandravel, E. Volanschi, M. Hillebrand, *Rev. Chim.* **41** (1990) 129
31. L. Teodorescu, R. M. Ion, *Rev. Chim.* **41** (1990) 312
32. R. M. Ion, *Rev. Chim.* **44** (1993) 431.





SHORT COMMUNICATION

**Essential oil composition of *Lavandula angustifolia* Mill.
cultivated in the mid hills of Uttarakhand, India**

RAM S. VERMA^{1*}, LAIQ U. RAHMAN², CHANDAN S. CHANOTIYA²,
RAJESH K. VERMA¹, AMIT CHAUHAN¹, ANJU YADAV²,
ANAND SINGH¹ and AJAI K. YADAV¹

¹Central Institute of Medicinal and Aromatic Plants, Resource Centre, Purara,
P.O. – Gagrigole, Bageshwar, Uttarakhand – 263688 and ²Central Institute of
Medicinal and Aromatic Plants, PO CIMAP, Lucknow – 226015, India

(Received 16 June, revised 28 August 2009)

Abstract: The essential oil content in the inflorescence of lavender (*Lavandula angustifolia* Mill.) cultivated in the mid hills of Uttarakhand was found to be 2.8 % based on the fresh weight. The oil was analysed by capillary GC and GC-MS. Thirty seven constituents, representing 97.81 % of the oil were identified. The major components of the oil were linalyl acetate (47.56 %), linalool (28.06 %), lavandulyl acetate (4.34 %) and α -terpineol (3.75 %). The quality of lavender oil produced in India was found to be comparable to that produced in Hungary, France, China, Bulgaria, Russia and the USA.

Keyword: *Lavandula angustifolia*; Lamiaceae; inflorescence; essential oil; GC-MS.

INTRODUCTION

True lavender (*Lavandula angustifolia* Mill. syn. *L. officinalis* Chaix) is a perennial shrub of the family Lamiaceae. It is native to southern Europe and the Mediterranean area and is commercially cultivated in France, Spain, Portugal, Hungary, the UK, Bulgaria, Australia, China and the USA.¹ In India, it was introduced in the Kashmir Valley in 1983, where its commercial cultivation was found to be successful.² This plant is cultivated primarily for its aromatic inflorescence from which the essential oil is isolated, although its fresh and dried flowers are also marketed.³ Lavender oil is known for its excellent aroma and is extensively used in the perfumery, flavor and cosmetic industries. The oil is known to possess sedative, carminative, anti-depressive and anti-inflammatory properties.⁴ It was also found to be active against many species of bacteria, including those resistant to antibiotics, such as methicillin-resistant *Staphylococcus*

*Corresponding author. E-mail: rswaroop1979@yahoo.com
doi: 10.2298/JSC090616015V

aureus and vanco mycin-resistant Enterococcus.⁴ Lavender oil was also reported to be an effective antifungal agent against *Aspergillus nidulans* and *Trichophyton mentagrophytes*.⁵ The essential oil compositions of lavender grown in different countries were investigated.^{6–8}

Oil from lavender cultivated in India may become a significant competitor with historical sources of lavender oil due to the favourable climatic conditions for commercial cultivation in the hill tracks of northern India.⁸ At present, the cultivation of lavender is mainly confined to Jammu and Kashmir. However, the possibilities of commercial cultivation of lavender in other states of North and Northeast India have not yet been explored. Therefore, with the aim of exploring new ecological areas for cultivation of lavender, the crop was introduced in the Kumaon region of the western Himalaya during 2002. The purpose of this study was to investigate the essential oil composition of lavender produced in this region.

EXPERIMENTAL

Plant material

The fresh inflorescence (spikes) of *L. angustifolia* was collected from an experimental field of the Central Institute of Medicinal and Aromatic plants, Resource Centre Bageshwar, Uttarakhand in the month of June when the crop was in full bloom. The experimental site is located in the Kattyur Valley at an altitude of 1250 m, where a sub-temperate mild climate prevails. The voucher specimen of the plant was submitted to the Herbarium division of the Centre.

Essential oil isolation

Freshly harvested plant material (100 g) was immediately subjected to hydrodistillation in a Clevenger's apparatus for 3 h for the extraction of the essential oil. The oil was dried over anhydrous sodium sulphate and stored in a refrigerator at 5 °C prior to analysis.

Gas chromatography (GC)

The GC analyses of the oil sample were realised on a Perkin-Elmer Auto XL GC and a Nucon gas chromatograph model 5765, both equipped with an FID using two different stationary phases, PE-5 (60 m × 0.25 mm; 0.25 µm film coating) and BP-20 (coated with a Carb o-wax 20M, 30 m × 0.32 mm × 0.25 µm film thickness), fused silica columns, respectively. Hydrogen was the carrier gas at 1.0 ml/min. The column temperature programming was from 70–250 °C at 3 °C/min (for PE-5) and from 70–230 °C at 4 °C/min (for BP-20). The injector and detector temperatures were 200 and 230 °C on BP-20 and 220 and 300 °C on PE-5 column, respectively. The injection volume was 0.02 µL neat and the split ratio was 1:30.

Gas chromatography-mass spectrometry (GC-MS)

The GC-MS analysis of the oil was performed on a Perkin-Elmer Turbo mass Quadrupole mass spectrometer fitted with an Equity-5 (Perkin-Elmer) fused silica capillary column (60 m × 0.32 mm; 0.25 µm film coating). The column temperature was programmed 70 °C, initial hold time of 2 min, to 250 °C at 3 °C/min with a final hold time of 3 min, using helium as the carrier gas at a flow rate of 1 ml/min. The injector and source temperatures were 250 °C. The injection volume was 0.06 µL neat with a split ratio 1:30. The MS were taken at 70 eV with an EI source with mass range of *m/z* 40–400. The identification was realised based on the retention indices, an MS Library search (NIST and WILEY), *n*-alkane (C₉–C₂₂) hydrocarbon series (Nile, Italy) and by comparing the mass spectra with MS literature data^{8–10}. The relative

amount of the individual components was calculated from the peak area without applying an FID response factor correction.

RESULTS AND DISCUSSION

The essential oil content in the fresh inflorescence of *L. angustifolia* cultivated in the sub-temperate region, the Kumaon region of the western Himalaya was found to be 2.8 %. However, the essential oil content in the inflorescence of different accessions of lavender grown in temperate parts of Kashmir was only 0.80 to 1.3 %.¹¹ These variations could either be due to difference of the plant genotype³ or to the altitude and microclimate of the cultivation area.

The results of GC and GC-MS analyses of the essential oil together with the European Pharmacopoeia 5.0 standards (EP 5) are given in Table I. The major constituents (> 1.0 %) of the oil were linalyl acetate (47.56 %), linalool (28.06 %), lavandulyl acetate (4.34 %), α -terpineol (3.75 %), geranyl acetate (1.94 %), caryophyllene oxide (1.38 %) and 1,8-cineole (1.14 %). Other minor components (< 1.0 and > 0.10 %) identified in the oil were β -caryophyllene (0.93 %), borneol (0.85 %), *epi*- α -cadinol (0.70 %), nerol (0.59 %), terpinen-4-ol (0.56 %), β -myrcene (0.55 %), limonene (0.55 %) and 1-octen-3-ol (0.53 %). However, the major components reported in the lavender oil from different countries were linalool (27.3–42.2 %), linalyl acetate (27.2–46.6 %), (*Z*)- β -ocimene (0.2–11.6 %), terpinen-4-ol (0.70–4.6 %), lavandulyl acetate (0.50–4.8 %), β -caryophyllene (1.8–5.1 %), (*E*)- β -ocimene (0.30–3.8 %), α -terpineol (0.30–2.0 %) and 1,8-cineole (0.10–1.2 %).⁸

TABLE I. GC-MS analysis of the essential oil of *Lavandula angustifolia* from Uttarakhand, India

Compound	<i>KI</i> ^a	<i>KI</i> ^b	Area, %	EP 5 ^c , %
Tricyclene 924		921	0.03	—
α -Pinene 935		932	0.09	—
Camphepane	951	946	0.23	—
Sabinene 974		969	0.04	—
1-Octen-3-ol 995		974	0.53	—
β -Myrcene 998		988	0.55	—
1-Hexyl acetate	1015	1007	0.11	—
<i>p</i> -Cymene 1025		1020	0.09	—
Limonene	1030	1024	0.55	< 1.0
1,8-Cineole 1035		1026	1.14	< 2.5
(<i>E</i>)- β -Ocimene 1047		1044	0.08	—
(<i>Z</i>)-Linalool oxide (furanoid)	1072	1067	0.22	—
(<i>E</i>)-Linalool oxide (furanoid)	1090	1084	0.24	—
Linalool	1098	1095	28.06	20–45
1-Octen-3-yl acetate	1106	1110	0.35	—
Camphor 1146		1141	0.11	< 1.2
Lavandulol	1162	1165	0.25	> 0.1

TABLE I. Continued

Compound	<i>KI</i> ^a	<i>KI</i> ^b	Area, %	EP 5 ^c , %
Borneol	1165	1165	0.85	—
Terpinen-4-ol 1177		1174	0.56	0.1–6
<i>p</i> -Cymen-8-ol 1183		1179	0.06	—
α -Terpineol 1189		1186	3.75	< 2.0
Myrtenol 1195		1194	0.13	—
Nerol	1225	—	0.59	—
Geraniol 1237		1254	0.21	—
Linalyl acetate	1257	1257	47.56	25–46
Lavandulyl acetate	1285	1288	4.34	> 0.2
<i>p</i> -Menthyl-8-acetate 1346		—	0.42	—
Thymol acetate	1355	—	0.13	—
Neryl acetate	1356	1359	1.07	—
Geranyl acetate	1373	1379	1.94	—
β -Cadinene 1416		—	0.11	—
β -Caryophyllene 1419		1417	0.93	—
(<i>E</i>)-Isoeugenol	1449	—	0.17	—
γ -Cadinene 1511		1513	0.12	—
Elemol	1552	—	0.12	—
Caryophyllene oxide	1584	1582	1.38	—
<i>epi</i> - α -Cadinol 1639		1638	0.70	—
Total identified, %			97.81	

^aKovats index experimental (PE-5 column; relative to *n*-alkane); ^bKovats index, literature^{8,10}; ^cEuropean Pharmacopoeia 5.0

On comparison of the present results with those reported from other parts of India, it is quite evident that the concentrations of 1,8 cineole, camphor, β -caryophyllene and caryophyllene oxide were slightly higher, whereas the concentrations of α -terpineol, linalyl acetate, geranyl acetate, neryl acetate and lavandulyl acetate were relatively lower in the Kashmir oil than in the present oil.¹² However, the lavender oil reported from the Kashmir valley contained large amounts of limonene (11.0 %), citronellol (10.0 %) and α -terpineol (7.6 %) and low contents of linalool (10.0%).² Furthermore, the concentrations of (*E*)- β -ocimene, 1-octen-3-yl acetate, α -terpineol and β -caryophyllene were slightly higher in the oil produced in Kodaikanal when compared to the present oil.¹³ These variations could be due to differences in location, elevation, genetic makeup of the plant or due to an adaptive process to particular ecological conditions. Lawrence also observed a wide variation in the quantitative composition of lavender oil depending on plant genotype and cultivation area, and the composition of the oil from lavenders were recognized to vary significantly according to altitude, microclimate and region.^{14–16}

CONCLUSIONS

In the oil from *L. angustifolia* growing in Uttarakhand, the components linalool, limonene, 1,8-cineole, camphor, lavandulol, lavandulyl acetate and terpinen-4-ol were found to be well within the desired limit mentioned in EP 5, while the concentration of linalyl acetate and α -terpineol slightly exceeded the EP 5 specifications. However, 3-octanone was not detected in the present oil (0.10–2.5 % in EP 5). Thus, the composition of the lavender oil produced in Uttarakhand was comparable to the oils produced in Hungary, France, China, Bulgaria, Russia and the US A.⁸ Finally, this study suggested that the agro-climatic conditions of Uttarakhand are ideal for growing lavender of international standards, and can be exploited by giving proper opportunities to the farmers.

Acknowledgements. The authors are thankful to CSIR for providing the financial support. We would also like to express our special thanks to the Director, CIMAP Lucknow for providing the necessary facilities and encouragement.

ИЗВОД

САСТАВ ЕТАРСКОГ УЉА БИЉКЕ *Lavandula angustifolia* Mill. ГАЈЕНЕ У ПЛАНИНСКОМ ПОДРУЧЈУ УТАРАКАНДА, ИНДИЈА

RAM S. VERMA¹, LAIQ U. RAHMAN², CHANDAN S. CHANOTIYA², RAJESH K. VERMA¹, AMIT CHAUHAN¹, ANJU YADAV², ANAND SINGH¹ и AJAI K. YADAV¹

¹*Central Institute of Medicinal and Aromatic Plants, Resource Centre, Purara, P.O. – Gagrigole, Bageshwar, Uttarakhand – 263688* и ²*Central Institute of Medicinal and Aromatic Plants, PO CIMAP, Lucknow – 226015, India*

Етарско уље лаванде (*Lavandula angustifolia* Mill.), гајене у планинском подручју Утараканда, чини 2,8 % свеже масе биљке. Уље је анализирано методама капиларне GC и GC–MS. Идентификовано је тридесет седам састојака, који су чинили 97,81 % уља. Главни састојци уља су линалил-ацетат (47,56 %), линалол (28,06 %), лавандул-ацетат (4,34 %) и α -терпинеол (3,75 %). Квалитет овог лавандиног уља је сличан квалитету уља произведеног у Мађарској, Француској, Кини, Бугарској, Русији и САД.

REFERENCES

1. A. S. Shawl, S. Kumar, *J. Med. Arom. Plant Sci.* **22** (2000) 319
2. Tajuddin, A. S. Shawl, M. C. Nigam, A. Hussain, *Indian Perf.* **41** (1983) 56
3. E. N. C Renaud, D. J. Charles, *J. Essent. Oil Res.* **13** (2001) 269
4. H. M. A. Cavanagh, *Aust. Infect. Control* **10** (2005) 35
5. T. Moon, Y. F. Chan, J. M. Wilkinson, H. M. A. Cavanagh, in *Proceeding of AICA National Conference*, Adelaide, Australia, 2004, 46
6. A. Tucker, M. J. Maciarello, J. T. Howell, *Perf. Flav.* **9** (1984) 49
7. B. M. Lawrence, *Essential Oils, 1995–2000*, Allured Publishing, Carol Stream, IL, 2003
8. R. P. Adams, T. Yanke, *Perf. Flav.* **32** (2007) 40
9. W. Jennings, T. Shibamoto, *Qualitative analysis of flavour and fragrance volatile by glass capillary gas chromatography*, Academic Press, New York, 1980
10. R. P. Adams, *Identification of essential oil components by Gas chromatograph/quadrupole mass spectroscopy*, Allured Publishing Corp., Carol Stream, IL, 2001

11. A. K. Dhar, D. Sharma, B. K. Bhat, C. K. Atal, *Pafai J.* **4** (1982) 20
12. A. S. Shawl, T. Kumar, S. Shabir, N. Chishti, Z. A. Kaloo, *Indian Perf.* **49** (2005) 235
13. G. R. Mallavarapu, V. K., Mehta, K. P. Sastry, R. K. Krishnan, S. Ramesh, S. Kumar, *J. Med. Arom. Plant Sci.* **22** (2000) 768
14. B. M. Lawrence, *Essential Oils, 1991–1994*, Allured Publishing Corp., Wheaton, IL, 1994
15. B. M. Lawrence, *Perf. Flav.* **18** (1993) 58
16. B. M. Lawrence, *Perf. Flav.* **19** (1994) 33.



Synthesis, characterization and thermal study of some transition metal complexes of an asymmetrical tetradentate Schiff base ligand

ACHUT S. MUNDE¹, AMARNATH N. JAGDALE², SARIKA M. JADHAV³
and TRIMBAK K. CHONDHEKAR^{3*}

¹Department of Chemistry, Milind College of Science, Aurangabad-431 004, Maharashtra,

²Department of Chemistry, D. P. College, Karjat, Dist. Ahemdナー, Maharashtra and

³Department of Chemistry, Dr. Babasaheb Ambedkar Marathwada University,
Aurangabad-431 004, Maharashtra, India

(Received 8 April, revised 16 October 2009)

Abstract: Complexes of Cu(II), Ni(II), Co(II), Mn(II) and Fe(III) with an asymmetric tetradentate Schiff base ligand derived from dehydroacetic acid, 4-methyl-*o*-phenylenediamine and salicylic aldehyde were synthesized and characterized by elemental analysis, conductometry, magnetic susceptibility, UV-Vis, IR, ¹H-NMR spectroscopy, X-ray diffraction analysis of powdered samples and thermal analysis, and screened for antimicrobial activity. The IR spectral data suggested that the ligand behaves as a bis-diaxial tetradentate ligand towards the central metal ion with an O NNO donor sequence. From the microanalytical data, the stoichiometry of the complexes 1:1 (metal:ligand) was found. The physico-chemical data suggested square planar geometry for the Cu(II) and Ni(II) complexes and octahedral geometry for the Co(II), Mn(II) and Fe(III) complexes. The thermal behaviour (TGA/DTA) of the complexes was studied and kinetic parameters were determined by Horowitz-Metzger and Coats-Redfern methods. The powder X-ray diffraction data suggested a monoclinic crystal system for the Co(II), Mn(II) and Fe(III) complexes. The ligand and their metal complexes were screened for antibacterial activity against *Staphylococcus aureus* and *Escherichia coli* and fungicidal activity against *Aspergillus niger* and *Trichoderma viride*.

Keywords: dehydroacetic acid; asymmetrical tetradentate Schiff base; transition metal complexes; thermal analysis; powder X-ray diffraction; antimicrobial activity.

*Corresponding author. E-mail: as_munde@yahoo.com
doi: 10.2298/JSC090408009M

INTRODUCTION

Schiff bases are most widely used as chelating ligands in coordination chemistry.¹ They are also useful in catalysis and in medicine as antibiotics, antiallergic and antitumor agents.² The metal complexes of Schiff bases derived from heterocyclic compounds have been the centre of attraction for many workers in recent years.^{3–7} Tetradebate Schiff bases are well known for their coordination with various metal ions, forming stable compounds.⁸ Many symmetrical bis tetradebate Schiff bases of 1,2-diamines with *o*-hydroxyaldehydes/ketones have been prepared and studied intensively. However, much less attention has been focused on unsymmetrical tetradebate Schiff bases derived from 1,2-diamines and different aldehydes/ketones. In particular those derived from aromatic 1,2-diamines have been under-investigated.⁹ It is worthwhile to mention that asymmetrical Schiff bases of this type are difficult to obtain and not easy to isolate.¹⁰

One of the oxygen heterocyclic compounds 3-acetyl-1,6-methyl-2H-pyran-2,4(3H)-dione (dehydroacetic acid or DHA) was reported to be an excellent chelating agent and to possess promising fungicidal, bactericidal, herbicidal and insecticidal activities.^{11–14} It is also a versatile starting material for the synthesis of a wide variety of heterocyclic ring systems.¹⁵ A search of the literature revealed that no work has been done on transition metal complexes of the unsymmetrical Schiff bases derived from aromatic 1,2-diamine, dehydroacetic acid and salicylic aldehyde. The synthesis of an unsymmetrical tetradebate Schiff base formed by the condensation of 4-methyl-*o*-phenylenediamine, dehydroacetic acid and salicylic aldehyde (Fig. 1) is reported. The complexes of Cu(II), Ni(II), Co(II), Mn(II) and Fe(III) with this ligand were also prepared in the solid state and characterized by different physico-chemical methods.

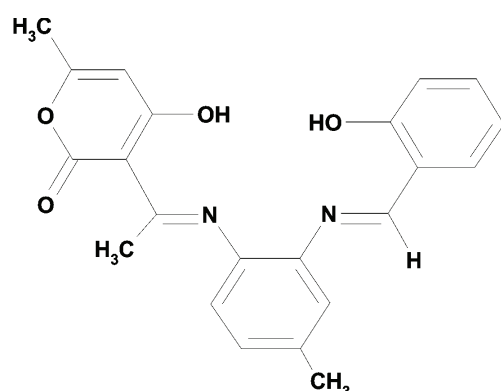


Fig. 1. Structural formula of the prepared unsymmetrical ligand.

EXPERIMENTAL

Dehydroacetic acid (purity ≥ 99 %) for synthesis was obtained from Merck, Germany, and used as supplied. 4-Methyl-*o*-phenylenediamine and salicylic aldehyde of A.R. grade, obtained from Acros Organics and Sigma, respectively, were used for the synthesis of the li-

gand. A.R. grade hydrated metal chlorides from S. D. Fine Chemicals were used for the preparation of the complexes. The C, H and N contents were determined on a Perkin Elmer (2400) CNS analyzer. The IR spectra were recorded on an FTIR spectrometer, Perkin Elmer Company using KBr pellets. The $^1\text{H-NMR}$ spectrum of the ligand was measured in CDCl_3 using TMS as the internal standard. The TG/DTA curves and XRD patterns were recorded on a Perkin Elmer TA/SDT-2960 and a Philips 3701, respectively. The UV-Vis spectra of the complexes were recorded on a Shimadzu UV-1601 spectrometer. The magnetic susceptibility measurements of the metal chelates were determined on a Gouy balance at room temperature using $\text{Hg}[\text{Co}(\text{SCN})_4]$ as the calibrant. The molar conductance of the complexes was measured on an Elico CM 180 conductivity meter using 10^{-3} M solutions in DMF. The microorganisms were collected from the Biotechnology Department, Milind College of Science, Aurangabad and the strains were maintained on nutrient agar at 4°C .

Synthesis

The asymmetric tetradeятate Schiff base ligand was synthesized via a stepwise approach.¹⁶ In the first step, the mono-Schiff base compound was prepared by refluxing 50 mL solution of 1.0 mmol (0.168 g) of dehydroacetic acid and 1.0 mmol (0.12 g) 4-methyl-*o*-phenylenediamine in super dry ethanol for about 3 h. The thus-formed mono-Schiff base was then refluxed with 1.0 mmol (0.12 g) salicylic aldehyde to prepare the asymmetric ligand *viz.* 4-hydroxy-3-(1-{2-[{(2-hydroxybenzylidene)amino]-4-methylphenyl}imino}ethyl)-6-methyl-2*H*-pyran-2-one (H_2L). The thus-formed asymmetric Schiff base was cooled to room temperature and collected by filtration, followed by recrystallization in ethanol (yield: 70%).

To a hot methanolic solution (25 ml) containing 1.0 mmol (0.38 g) of the ligand, a methanolic solution (25 ml) of a metal chloride (hydrate) (1.0 mmol) was added under constant stirring. The pH of the reaction mixture was adjusted to 7.5–8.5 by adding 10% alcoholic ammonia solution and refluxed for about 3 h. The precipitated solid metal complex was filtered off under hot conditions and washed with hot methanol, petroleum ether (40 – 60°C) and dried over anhydrous CaCl_2 in a vacuum desiccator (yield: 50–60%).

Antimicrobial activity

The antimicrobial activity of the ligand and metal complexes were tested *in vitro* against bacteria *Staphylococcus aureus* and *Escherichia coli* by the paper disc plate method.¹⁷ The compounds were tested at the concentration 0.50 and 1.0 mg mL⁻¹ in DMF and compared with known antibiotics *viz.* ciprofloxacin. For fungicidal activity, the compounds were screened *in vitro* against *Aspergillus niger* and *Trichoderma viride* by the mycelia dry weight method,¹⁸ using glucose nitrate media. The compounds were tested at the concentration 250 and 500 ppm in DMF and compared with the control.

RESULTS AND DISCUSSION

The physical characteristics, microanalytical, and molar conductance data of the ligand and its metal complexes are given in Table I. The analytical data of the complexes revealed 1:1 mole ratio (metal:ligand) and corresponds well with the general formula [ML] ($M = \text{Cu(II)}$ and Ni(II)) and [ML(H_2O)₂] ($M = \text{Co(II)}$, Mn(II) or Fe(III)). The magnetic susceptibilities of the Cu(II) and Ni(II) complexes at room temperature were found to be consistent with square-planar geometry and those of the Co(II), Mn(II) and Fe(III) complexes with high-spin octahedral structures having two water molecules coordinated to the metal ion. The



presence of two coordinated water molecules was confirmed by TG/DT analysis. The metal chelate solutions in DMF showed low conductance, supporting the non-electrolyte nature of the complexes.

TABLE I. Physical characterization and analytical and molar conductance data of the prepared compounds

Compound F.	W.	M.p. °C	Colour	Λ S cm ² mol ⁻¹	Found (Calcd.), %		
					C H	N	M
[C ₂₂ H ₂₀ N ₂ O ₄] (H ₂ L) 376.42		178	Yellow	—	70.12 (70.20)	5.40 (5.36)	7.38 (7.44)
[Cu(C ₂₂ H ₁₈ N ₂ O ₄)] 437.974		>300	Green	20.13	60.58 (60.28)	3.90 (4.11)	6.50 (6.39)
[Ni(C ₂₂ H ₁₈ N ₂ O ₄)] 433.13		>300	Red	28.70	61.24 (60.95)	4.52 (4.16)	6.20 (6.46)
[CoC ₂₂ H ₁₈ N ₂ O ₄ (H ₂ O) ₂] 469.35	245	Reddish brown		18.20	56.50 (56.25)	4.88 (4.69)	6.25 (5.97)
[MnC ₂₂ H ₁₈ N ₂ O ₄ (H ₂ O) ₂] 465.36	255	Brown		17.55	56.25 (56.73)	5.00 (4.73)	12.04 (6.02)
[FeC ₂₂ H ₁₈ N ₂ O ₄ (H ₂ O) ₂] 466.27	>300	Brown		42.63	56.30 (56.62)	4.26 (4.72)	5.75 (6.01)
							12.00 (11.98)

¹H-NMR spectrum of the ligand

The ¹H-NMR spectra of the free ligand in CDCl₃ at room temperature showed the following signals at δ (ppm): 2.15 (3H, s, C₆-CH₃), 2.45 (3H, s, phenyl-CH₃), 2.55 (3H, s, N=C-CH₃), 5.82 (1H, s, C₅-H), 6.9–7.4 (8H, m, phenyl), 11.1 (1H, s, phenolic OH), 8.60 (1H, s, N=C-H) and 15.80 (1H, s, enolic OH of the DHA moiety).

IR spectra

The IR spectrum of the free ligand showed characteristic bands at 3100–3400, 1703, 1662, 1362, and 1223 cm⁻¹, assignable to ν(OH) (intramolecular hydrogen bonded), ν(C=O) (lactone carbonyl), ν(C=N) (azomethine), ν(C–N) (aryl azomethine) and ν(C–O) (phenolic) stretching modes, respectively.¹⁹ The absence of a weak broad band in the 3100–3400 cm⁻¹ region, noted in the spectra of the metal complexes, indicates deprotonation of the intramolecular hydrogen bonded OH group on complexation and subsequent coordination of phenolic oxygen to the metal ion. This is further supported by the upward shift of ν(C–O) (phenolic)¹⁸ by 35–70 cm⁻¹. On complexation, the ν(C=N) band is shifted to lower wave numbers with respect to the free ligand, suggesting that the nitrogen of the azomethine group is coordinated to the metal ion. This is supported by the upward shift in ν(C–N) by 15–55 cm⁻¹.²⁰ The IR spectra of the metal chelates showed new bands in the 542–580 and 460–513 cm⁻¹ regions, which can be assigned to ν(M–O) and ν(M–N) vibrations, respectively.²¹ The IR spectra of Co(II),

Mn(II) and Fe(III) complexes show a strong band in the 3200–3600 cm⁻¹ region, indicating the presence of coordinated water in these complexes. The presence of coordinated water was further confirmed by the appearance of a non-ligand band in the 830–840 cm⁻¹ region, assignable to the rocking mode of water.²² The presence of coordinated water was also established and supported by TG/DT analysis of these complexes. Hence, coordination occurred *via* the phenolic oxygen and the azomethine nitrogen of the ligand molecule.

Magnetic measurements and electronic absorption spectra

The magnetic and electronic spectral data are given in Table II. The electronic absorption spectrum of the Cu(II) complex in DMSO solution shows three bands at 17813, 26525 and 30487 cm⁻¹, assignable to the transition $^2\text{B}_{1g} \rightarrow ^2\text{A}_{1g}$ and two intra-ligand charge transfer bands. These data and the magnetic moment value of 1.72 μ_{B} suggest square-planar geometry around Cu(II).^{21,23} The electronic absorption spectrum of the Ni(II) complex in DMSO solution consisted of two bands at about 17985 and 26595 cm⁻¹ assignable to the transition $^1\text{A}_{1g} \rightarrow ^1\text{T}_{2g}$ and a charge transfer transition, respectively. These data, the diamagnetic nature and red colour of the complex are in accordance with square-planar geometry for the Ni(II) complex.^{24,25} The electronic absorption spectrum of the Co(II) complex in DMSO solution had three bands at 10869, 19157 and 26954 cm⁻¹, which may be attributed to the transitions $^4\text{T}_{1g} \rightarrow \text{T}_{2g}(\text{F})$, $^4\text{T}_{1g} \rightarrow ^4\text{A}_{2g}(\text{F})$ and charge transfer, respectively. Together with the magnetic moment value of 4.70 μ_{B} , a high-spin octahedral geometry for the Co(II) complex^{26,27} was proposed. The octahedral geometry was further supported by the ratio $v_2/v_1 = 1.762$,

TABLE II. Magnetic and electronic absorption spectral data (in DMSO) of the compounds

Compound	$\mu_{\text{eff}} / \mu_{\text{B}}$	ν / cm^{-1}	B and assignment	Geometry
[C ₂₂ H ₂₀ N ₂ O ₄] (H ₂ L) –		31347	INCT ^a	–
		40816	INCT	
[Cu(C ₂₂ H ₁₈ N ₂ O ₄)] 1.72		17813	$^2\text{B}_{1g} \rightarrow ^2\text{A}_{1g}$	Square-planar
		26525	INCT	
		30487	INCT	
[Ni(C ₂₂ H ₁₈ N ₂ O ₄)] Dia magnetic		17985	$^1\text{A}_{1g} \rightarrow ^1\text{T}_{2g}$	Square-planar
		26595	INCT	
[CoC ₂₂ H ₁₈ N ₂ O ₄ (H ₂ O) ₂] 4.70		10869	$^4\text{T}_{1g} \rightarrow \text{T}_{2g}(\text{F})$	Octahedral
		19157	$^4\text{T}_{1g} \rightarrow ^4\text{A}_{2g}(\text{F})$	
		26954	INCT	
[MnC ₂₂ H ₁₈ N ₂ O ₄ (H ₂ O) ₂] 5.77		16051	$^6\text{A}_{1g} \rightarrow ^4\text{T}_{1g}$	Octahedral
		23640	$^6\text{A}_{1g} \rightarrow ^4\text{T}_{2g}$	
		29411	INCT	
[FeC ₂₂ H ₁₈ N ₂ O ₄ (H ₂ O) ₂] 5.79		12694	$^6\text{A}_{1g} \rightarrow ^4\text{T}_{1g} (^4\text{D})$	Octahedral
		18761	$^6\text{A}_{1g} \rightarrow ^4\text{T}_{1g}$	
		31250	INCT	

^aIntra-ligand charge transfer band



which is close to the value expected for octahedral geometry. The electronic absorption spectrum of the Mn(II) complex in DMSO solution contained three bands at 16051, 23640 and 29411 cm⁻¹, assignable to the transitions ${}^6A_{1g} \rightarrow {}^4T_{1g}$, ${}^6A_{1g} \rightarrow {}^4T_{2g}$ and charge transfer, respectively. The electronic transitions together with a magnetic moment value 5.77 μ_B , which is close to the spin-only value (5.92 μ_B) suggests high spin octahedral geometry for the Mn(II) complex.^{26,28} The electronic absorption spectrum of Fe(III) complex shows three weak bands at 12694, 18761 and 31250 cm⁻¹, which may be assigned to the transitions ${}^6A_{1g} \rightarrow {}^4T_{1g}(4D)$, ${}^6A_{1g} \rightarrow {}^4T_{1g}$ and charge transfer, respectively. The electronic transitions together with the magnetic moment value of 5.79 μ_B suggested high-spin octahedral geometry for the Fe(III) complex.^{26,29}

Thermal analysis

The simultaneous TG/DTA analysis of the Cu(II), Ni(II), Co(II) and Mn(II) metal complexes was studied from ambient temperature to 1000 °C under a nitrogen atmosphere using α -Al₂O₃ as the reference. The TG curve of the Cu(II) and Ni(II) complexes exhibited no mass loss up to 270 °C, indicating the absence of coordinated water²⁰ and the high thermal stability of the complexes. On the TG curve of Cu(II) complex, the first step of decomposition from 295 to 352 °C, with a mass loss 21.75 % (calcd. 22.83 %), accompanied by an exothermic peak with $t_{\max} = 309$ °C on the DTA curve, may be attributed to the removal of the non-coordinated part of the ligand. The second step, from 485 to 650 °C with mass loss 49.30 % (calcd. 49.10 %), corresponds to the decomposition of the coordinated part of the ligand. An exothermic peak with $t_{\max} = 505.7$ °C on the DTA curve was observed for this step. The mass of the final residue corresponded to stable CuO, 20.85 % (calcd. 18.37 %).

The TG curve of the Ni(II) complex shows a two-step decomposition. The first step from 360 to 410 °C with a mass loss of 24.50 % (calcd. 23.08%), accompanied by an endothermic peak with $t_{\max} = 319$ °C on the DTA curve, may be attributed to the decomposition of the non-coordinated part of the ligand. The second step, from 460 to 835 °C with a mass loss of 50.24 % (calcd. 49.43 %), corresponds to the removal of the coordinated part of the ligand. For this step, a broad endothermic peak in the DTA was observed. The mass of the final residue 12 % (calcd. 17.05 %) does not correspond to any stoichiometry of the end product, as the residue obtained is not close to that expected for metal oxide.

The thermogram of the Co(II) complex shows a mass loss of 7.5 % (calcd. 7.6 %) in the temperature range 190–216 °C and an endothermic DTA peak in this region, $t_{\min} = 207$ °C, indicates the loss of two coordinated water molecules.^{30,31} The anhydrous complex first showed decomposition from 240–550 °C, with a 21 % (calcd. 21.32 %) mass loss and a broad exothermic peak with $t_{\max} = 255$ °C in the DTA, which may be attributed to the removal of the non-coordinated part of the ligand. The second step of the decomposition from 545–

–860 °C, with a mass loss of 54.0 % (calcd. 54.58%) corresponds to the decomposition of the coordinated part of the ligand. A broad endothermic peak in the DTA was observed for this step. The mass of the final residue corresponded to stable CoO, 13.85 % (calcd. 15.09 %).

The TG curve for the Mn(II) complex showed a first mass loss of 7.30 % (calcd. 7.73 %) in the temperature range 190–200 °C and an endothermic peak in this region with $t_{\min} = 195.7$ °C, indicating the removal of two coordinated water molecules. The anhydrous complex exhibited a single-step decomposition from 240 to 900 °C, with a 62 % mass loss and a broad endothermic peak in the DTA.

Kinetic calculations

The kinetic and thermodynamic parameters *viz.* the order of the reaction (n), the energy of activation (E_a), the pre-exponential factor (Z), the entropy of activation ($\Delta S^\#$) and the Gibbs energy change ($\Delta G^\#$), together with the correlation coefficient (r) for the non-isothermal decomposition of the metal complexes, were determined by the Horowitz–Metzger (HM) approximation method³² and the Coats–Redfern integral method.³³ The obtained data are given in Table III. The results showed that the values obtained by two methods are comparable. The calculated values of the activation energy of the complexes are relatively low, indicating the autocatalytic effect of the metal ion on the thermal decomposition of the complex.^{34,35} The negative activation entropy value indicates that the activated complexes were more ordered than the reactant and that the reactions were slow. The more ordered nature may be due to the polarization of bonds in the activated state, which might occur through charge transfer electronic transitions.

TABLE III. The kinetic parameter of degradation of the metal complexes calculated by the Horowitz–Metzger (HM) and Coats–Redfern (CR) methods

M(II) complex	Step	n	Method	E_a kJ mol ⁻¹	Z s ⁻¹	$\Delta S^\#$ J K ⁻¹ mol ⁻¹	$\Delta G^\#$ kJ mol ⁻¹	r
Cu(II) I	I	1.01	HM	267.95	1.8×10^{27}	271.67	248.67	0.9948
			CR	264.73	1.94×10^{23}	195.28	250.86	0.9948
	II	1.42	HM	97.15	1.9×10^6	–133.07	110.39	0.9982
			CR	93.34	6.06×10^5	–142.73	113.55	0.9951
Ni(II) I	I	0.85	HM	136.36	8.7×10^{11}	–22.99	138.18	0.9909
			CR	132.82	2.1×10^9	–73.47	138.68	0.9890
	II	1.05	HM	47.17	68.1	–219.38	71.92	0.9977
			CR	46.37	41.04	–223.60	71.59	0.9892
Co(II) I	I	1.1	HM	12.53	0.7368	–253.36	30.90	0.9855
			CR	12.52	0.8983	–251.71	30.77	0.9912
	II	0.95	HM	37.16	4.290	–242.78	65.91	0.9995
			CR	33.34	4.756	–241.93	62.93	0.9995
Mn(II) –	I	0.65	HM	16.13	0.325	–263.26	43.83	0.9982
			CR	18.87	1.090	–253.16	45.51	0.9836



Powder X-ray diffraction analysis

The X-ray diffractograms of the Co(II), Mn(II) and Fe(III) complexes were scanned in the range 5–100° at a wavelength of 1.543 Å. The diffractograms and associated data depict the 2θ value for each peak, the relative intensity and inter-planar spacing (*d*-values). The X-ray diffraction pattern of these complexes with respect to major peaks of relative intensity greater than 10 % were indexed using a computer programme.³⁶ This indexing method also yields the Miller indices (*hkl*), the unit cell parameters and the unit cell volume. The unit cell of Co(II) complex yielded values of lattice constants: *a* = 8.9706 Å, *b* = 8.6441 Å and *c* = 4.7755 Å, and a unit cell volume *V* = 369.2291 Å³. The unit cell of the Mn(II) complex yielded values of lattice constants: *a* = 24.5882 Å, *b* = 4.4656 Å, *c* = 5.8676 Å, and a unit cell volume *V* = 627.2087 Å³. The unit cell of the Fe(III) complex yielded values of lattice constants: *a* = 7.0696 Å, *b* = 14.8954 Å, *c* = 5.3504 Å, and a unit cell volume *V* = 830.4539 Å³. In concurrence with these cell parameters, conditions such as *a* ≠ *b* ≠ *c* and $\alpha = \gamma = 90^\circ \neq \beta$ required for a monoclinic sample were tested and found to be satisfactory. Hence, it can be concluded that the Co(II), Mn(II) and Fe(III) complexes were monoclinic crystal systems. The experimental density values of the complexes were determined using the specific gravity method³⁷ and found to be 2.1908, 2.5002, and 2.0522 g cm⁻³ for the Co(II), Mn(II) and Fe(III) complexes, respectively. Using the experimental density values, ρ , the molecular weight of the complexes, *M*, Avogadro's number, *N*, and the volume of the unit cell, *V*, the number of molecules per unit cell, *n*, were calculated using the equation $\rho = nM/NV$ and they were found to be one for Co(II) and two for the Mn(II) and Fe(III) complexes. With these values, the theoretical densities were computed and found to be 2.1824, 2.4637 and 2.0645 g cm⁻³ for the respective complexes. Comparison of experimental and theoretical density value shows good agreement within the limits of experimental error.³⁸

Antimicrobial activity

The results of the *in vitro* antimicrobial activity of the ligand and metal complexes against the bacteria *Staphylococcus aureus* and *Escherichia coli*, determined by the paper disc plate method,¹⁷ are presented in Table IV, in which the activity of a known antibiotic viz. ciprofloxacin is included for comparison. The results of the *in vitro* fungicidal activity of the compounds against *Aspergillus niger* and *Trichoderma viride* determined by the mycelia dry weight method¹⁸ with glucose nitrate media, are given in Table V, in which the results of the control are also presented. From Tables IV and V, it is clear that the inhibition by the metal chelates was higher than that of the free ligand and results are in good agreement with previous findings with respect to comparative activity of free ligand and its complexes.^{17,18} The inhibition of growth (%) of both fungi due to metal com-

plexes decreased in the order Cu (II) > Ni (II) > Co (II) > Mn (II) > Fe (II). Such enhanced activity of metal chelates is due to the lipophilic nature of the metal ions in the complexes.³⁹ The increase in activity with concentration is due to the effect of metal ions on the normal metabolic function of the cell. The action of compounds may involve the formation of hydrogen bonds with the active centre of cell constituents, resulting in interference with the normal function of the cell.⁴⁰

TABLE IV. Antibacterial activity of the compounds

Test compound	Inhibition zone, mm			
	<i>E. coli</i>		<i>S. aureus</i>	
	500 ppm	1000 ppm	500 ppm	1000 ppm
Ciprofloxin	29	32	31	35
[C ₂₂ H ₂₀ N ₂ O ₄] (H ₂ L)	10	12	12	15
[CuC ₂₂ H ₁₈ N ₂ O ₄]	15	18	16	19
[NiC ₂₂ H ₁₈ N ₂ O ₄]	12	16	14	16
[CoC ₂₂ H ₁₈ N ₂ O ₄ (H ₂ O) ₂]	13	16	15	17
[MnC ₂₂ H ₁₈ N ₂ O ₄ (H ₂ O) ₂]	11	12	12	15
[FeC ₂₂ H ₁₈ N ₂ O ₄ (H ₂ O) ₂]	11	13	14	15

TABLE V. Yield of mycelial dry weight in mg and inhibition in % (in parentheses)

Test compound	<i>A. niger</i>		<i>T. viride</i>	
	250 ppm	500 ppm	250 ppm	500 ppm
Control	79	79	70	70
[C ₂₂ H ₂₀ N ₂ O ₄] (H ₂ L)	60 (24)	22 (72)	38 (46)	17 (76)
[CuC ₂₂ H ₁₈ N ₂ O ₄]	38 (52)	09 (89)	19 (73)	01 (99)
[NiC ₂₂ H ₁₈ N ₂ O ₄]	40 (49)	12 (85)	20 (71)	02 (97)
[CoC ₂₂ H ₁₈ N ₂ O ₄ (H ₂ O) ₂]	49 (38)	14 (82)	25 (64)	04 (94)
[MnC ₂₂ H ₁₈ N ₂ O ₄ (H ₂ O) ₂]	45 (43)	16 (80)	28 (60)	07 (90)
[FeC ₂₂ H ₁₈ N ₂ O ₄ (H ₂ O) ₂]	52 (34)	17 (78)	32 (54)	09 (87)

CONCLUSIONS

Based on the physicochemical and spectral data discussed above, square-planar geometry for Cu(II) and Ni(II) complexes and octahedral geometry for Co(II), Mn(II) and Fe(III) complexes are proposed. It is assumed that the ligand behaves as dibasic, ONNO tetradeятate, coordinating via the phenolic oxygen and the imino nitrogen as illustrated in Fig. 2. The complexes are biologically active and showed enhanced antimicrobial activities compared to the free ligand. A thermal study revealed that the complexes are thermally stable. An XRD study suggested the monoclinic crystal system for the Co(II), Mn(II) and Fe(III) complexes.



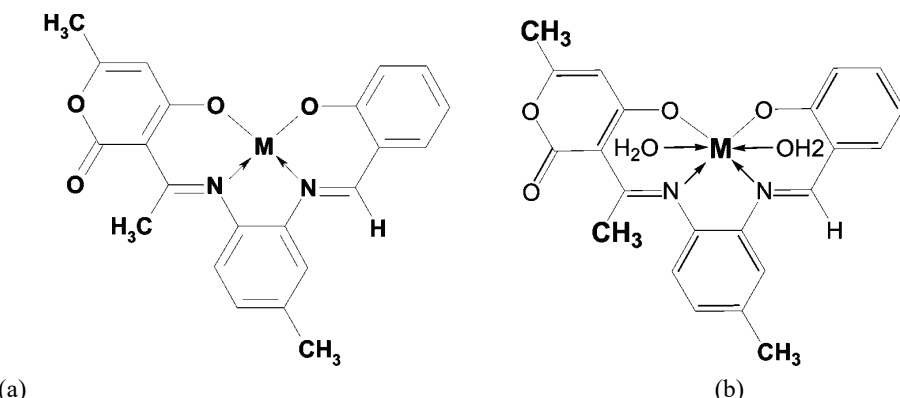


Fig. 2. The proposed geometry of the complexes; a) M(II) = Cu(II) or Ni(II) and b) M = Co(II), Mn(II) or Fe(III).

ИЗВОД

СИНТЕЗА, КАРАКТЕРИЗАЦИЈА И ТЕРМИЧКА СТУДИЈА НЕКИХ ПРЕЛАЗНИХ МЕТАЛНИХ КОМПЛЕКСА СА АСИМЕТРИЧНИМ ТЕТРАДЕНТАТИМ ШИФОВИМ БАЗАМА

ACHUT S. MUNDE¹, AMARNATH N. JAGDALE², SARika M. JADHAV³ и TRIMBAK K. CHONDHEKAR³

¹Department of Chemistry, Milind College of Science, Aurangabad-431 004(M.S), ²Department of Chemistry, D.P. College, Karjat, Dist.: Ahemdnager, (M.S) и ³Department of Chemistry, Dr. Babasaheb Ambedkar Marathwada University, Aurangabad-431 004, Maharashtra, India

Синтетисани су комплекси Cu(II), Ni(II), Co(II), Mn(II) и Fe(III) са асиметричним тетрадентатним Шифовим базама изведеним из дехидросирћетне киселине, 4- метил-о-фенилендиамина и салицил-алдехида и окарактерисани елементалном анализом, кондуктометријом, магнетном сусцептибилношћу, UV–Vis, IR, ¹H-NMR спектрима, рендгенском дифракционом анализом праха, термичком анализом и тестирали на антимикробну активност. IR спектрални подаци сугерисали су да се лиганд понаша као двобазни тетрадентатни лиганд према централном металном јону са ONNO секвенцијом донорних атома. Из микроанализе нађена је стехиометрија комплекса 1 :1 (метал:лиганд). Физичко-хемијски подаци сугерисали су квадратно-планарну геометрију за Cu(II) и Ni(II) комплексе и октаедарску геометрију за комплексе Co(II), Mn(II) и Fe(III). Термичко понашање (TGA/DTA) комплекса је проучавано и кинетички параметри су одређени Horowitz–Metzger и Coats–Redfern методама. Лиганд и његови метални комплекси су тестирали на антибактеријску активност према *Staphylococcus aureus* и *Escherichia coli* и антифунгалну активност према *Aspergillus niger* и *Trichoderma viride*. Рендгенски дифракциони подаци праха указали су на моноклинични кристални систем за Co(II), Mn(II) и Fe(III) комплексе.

(Примљено 4. априла, ревидирано 16. октобра 2009)

REFERENCES

- Y. Shibuya, K. Nabari, M. Kondo, S. Yasue, K. Maeeda, F. Uchida, H. Kawaguchi, *Chem. Lett.* **37** (2008) 78
- B. J. Gangani, P. H. Parsania, *Spectrosc. Lett.* **40** (2007) 97

3. B. Sindhu mari, G. Riju uulal, K. Mohanan , *Synth. React. Inorg., Met.-Org. Nano-Met. Chem.* **39** (2009) 24
4. M. Thankamony, K. Mohanan, *Indian J. Chem.* **46A** (2007) 247
5. N. Raman, J. Dhaveethu Raju, A. Sakthivel, *J. Chem. Sci.* **119** (2007) 303
6. D. Wang, Y. Yang, Y. Yang, T. Zhao, X. Wu, S. Wang, Y. Hou, W. Chen, *Chin. Sci. Bull.* **51** (2006) 785
7. K. Shrivakumar, Shashidhar, M. B. Halli, *Russ. J. Phys. Chem.* **82** (2008) 2269
8. S. A. Sadeek, M. S. Refat, *J. Korean Chem. Soc.* **50** (2006) 107
9. N. T. S. Pan, D. H. Brown, H. Adams, S. E. Spey, P. Styring, *J. Chem. Soc. Dalton Trans.* **9** (2004) 1348
10. S. F. Tan, K. P. Ang, *Transition Met. Chem.* **13** (1988) 64
11. D. Surya Rao, B. L. Subha Rao, V. T. John, M. C. Ganorkar, *Nat. Acad. Sci. Lett.* **1** (1978) 402
12. D. Surya Rao, C. Sadasiva Reddy, V. T. John, M. C. Ganorkar, *Curr. Sci.* **49** (1980) 511
13. B. Schleiffenbaum, O. Spertini, F. Tedder Thomas, *J. Cell. Biol.* **119** (1992) 229
14. V. G. Stanley, S. Woldesenbet, G. Cassandra, *Poul. Sci.* **75** (1996) 42
15. A. Levai, J. Jeko, *Monatsh. Chem.* **137** (2006) 339
16. M. A. Qayyoom, P. Hanumanthu, C. V. Ratnam, *Indian J. Chem.* **21B** (1982) 883
17. P. S. Mane, S. G. Shirodkar, B. R. Arbad, T. K. Chondhekar, *Indian J. Chem.* **40** (2001) 648
18. S. F. Tan, K. P. Ang, H. L. Jatchandran, *Transition Met. Chem.* **9** (1984) 390
19. P. Venkateswar Rao, A. Venkata Narasaiah, *Indian J. Chem.* **42A** (2003) 896
20. D. C. Dash, A. K. Panda, P. Je na, S. B. Patjoshi, A. Maha patra, *J. Indian Chem. Soc.* **79** (2002) 48
21. R. Natrajan, K. Antonysamy, C. Thangaraja, *Transition Met. Chem.* **28** (2003) 29
22. K. Nakamoto, *Infrared Spectra of Inorganic and Coordination Compounds*, 3rd ed., Wiley Interscience, New York, 1970, pp. 159, 167, 214
23. N. Raman, Y. Pitchaikaniraja, A. Kulandaivasamy, *Proc. Indian Acad. Sci. (Chem. Sci.)* **113** (2001) 183
24. K. M. Reddy, M. B. Halli, A. C. Hiremath, *J. Indian Chem. Soc.* **17** (1994) 118
25. M. Mokhles Abd-Elzaher, *J. Chin. Chem. Soc.* **48** (2001) 153
26. A. B. P. Lever, *Inorganic Electronic Spectroscopy*, Elsevier, Amsterdam, 1968, p. 275
27. K. C. Satpathy, A. K. Panda, R. Mishra, I. Pande, *Transition Met. Chem.* **16** (1991) 410
28. L. Sacconi, *Transition Met. Chem.* **61** (1968) 943
29. M. N. Patel, V. J. Patel, *Synth. React. Inorg., Met.-Org. Chem.* **19** (1989) 137
30. N. S. Bhave, R. B. Kharat, *J. Inorg. Nucl. Chem.* **42** (1980) 977
31. V. K. Revankar, V. B. Mahale, *Indian J. Chem.* **28A** (1979) 683
32. H. H. Horowitz, G. Metzger, *Anal. Chem.* **35** (1963) 1464
33. A. W. Coats, I. P. Redfern, *Nature* **20** (1964) 68
34. A.M. El-Awad, *J. Therm. Anal. Calorim.* **61** (2000) 197
35. A. Impura, Y. Inoue, I. Yasumori, *Bull. Chem. Soc. Jpn.* **56** (1983) 2203
36. J. R. Carvajal, T. Roisnel, *Winplotr, A Graphic Tool for Powder Diffraction*, Laboratoire Leon Brillouin (ceal/cnrs) 91191 Gif sur Yvette Cedex, France, 2004
37. D. P. Shoemaker, C. W. Garland, *Experiments in Physical Chemistry*, 5th ed., McGraw-Hill International Edition, New York, 1989
38. M. B. Deshmukh, S. Dhongade-Desai, S. S. Chavan, *Indian J. Chem.* **44** (2005) 1659
39. L. Mishra, V. K. Singh, *Indian J. Chem.* **32A** (1993) 446
40. N. Dharamraj, P. Viswanathamurthi, K. Natarajan, *Transition Met. Chem.* **26** (2001) 105.





Enumeration of a class of IPR hetero-fullerenes

ALI REZA ASHRAFI and MODJTABA GHBORBANI*

Institute of Nanoscience and Nanotechnology, University of Kashan,
Kashan 87317-51167, I. R. Iran

(Received 30 July, revised 20 August 2009)

Abstract: Hetero-fullerenes are fullerenes in which some of the carbon atoms are replaced by other atoms. This paper uses the Pólya theorem to count the number of their possible positional isomers and chiral isomers. To do this, the computer algebra system GAP was applied to compute this number for a class of IPR hetero-fullerenes with I_h point group symmetry. These fullerenes were constructed by means of the leapfrog principle.

Keywords: fullerene; hetero-fullerene; Pólya theorem; cycle index.

INTRODUCTION

Carbon exists in several forms in nature. One is the so-called fullerenes, which were discovered for the first time in 1985.¹ Fullerenes are carbon-cage molecules in which a large number of carbon atoms are bonded in a nearly spherically symmetric configuration. Let p , h , n and m be the number of pentagons, hexagons, carbon atoms and bonds between them, respectively, in a given fullerene F . Since each atom lies in exactly 3 faces and each edge lies in 2 faces, the number of atoms $n = (5p + 6h)/3$, the number of edges $m = (5p + 6h)/2 = 3n/2$ and the number of faces $f = p + h$. By the Euler formula, $n - m + f = 2$, it can be deduced that $(5p + 6h)/3 - (5p + 6h)/2 + p + h = 2$ and, therefore, $p = 12$, $v = 2h + 20$ and $e = 3h + 30$. This implies that such molecules made up entirely of n carbon atoms and having 12 pentagonal and $(n/2 - 10)$ hexagonal faces, where $n \neq 22$, is a natural number equal or greater than 20.² Hetero-fullerenes are fullerene molecules in which one or more carbon atoms are replaced by hetero-atoms, such as boron or nitrogen, the formation of which is a kind of “on-ball” doping of the fullerene cage.

Detecting symmetry of molecules is a well-studied problem with applications in a large number of areas. Randic,^{3,4} and then Balasubramanian,^{5–11} considered the Euclidean matrix of a chemical graph to find its symmetry. Here the Euclidean matrix of a molecular graph G is a matrix $\mathbf{D}(G) = [d_{ij}]$, where for $i \neq j$,

*Corresponding author. E-mail: ghorbani@kashanu.ac.ir
doi: 10.2298/JSC090730020A

d_{ij} is the Euclidean distance between the nuclei i and j . In this matrix, d_{ii} can be taken as zero if all the nuclei are equivalent. Otherwise, different weights for different nuclei may be introduced.

Suppose σ is a permutation on n atoms of the molecule under consideration. Then the permutation matrix \mathbf{P}_σ is defined as $\mathbf{P}_\sigma = [x_{ij}]$, where $x_{ij} = 1$ if $i = \sigma(j)$ and 0 otherwise. It is easy to see that $\mathbf{P}_\sigma \mathbf{P}_\tau = \mathbf{P}_{\sigma\tau}$, for any two permutations σ and τ on n objects, and hence the set of all $n \times n$ permutation matrices is a group isomorphic to the symmetric group S_n on n symbols. It is a well-known fact that a permutation σ of the vertices of a graph G belongs to its automorphism group if it satisfies $\mathbf{P}_\sigma^t A \mathbf{P}_\sigma = \mathbf{A}$, where \mathbf{A} is the adjacency matrix of G . Thus, for computing the symmetry of a molecule, it is sufficient to solve the matrix equation $P^t EP = \mathbf{E}$, where \mathbf{E} is the Euclidean matrix of the molecule under consideration and P varies on the set of all permutation matrices with the same dimension as \mathbf{E} .

A method^{12,13} has been described on how to construct a fullerene C_{3n} from a fullerene C_n having the same or even a bigger symmetry group as C_n . This method is called the Leapfrog principle. If one starts with a C_n cluster with icosahedral symmetry, all the new clusters will be of the same symmetry, since this is the biggest symmetry group in 3-dimensional space. In the first step, an extra vertex has to be put into the centre of each face of C_n . Then, these new vertices have to be connected with all the vertices surrounding the corresponding face. Then, the dual polyhedron is again a fullerene having $3n$ vertices, 12 pentagonal and $(3n/2) - 10$ hexagonal faces. Knowing the 3-dimensional cycle index of $S(C_n)$ acting on the sets of vertices, edges and faces, it is very easy to compute the cycle index for the induced action of $S(C_n)$ on the set of vertices of C_{3n} . One just has to identify the vertices of C_n with the n new hexagonal faces of C_{3n} .¹⁴ From Fig. 1, it can be seen that $\text{Le}(C_{20}) = C_{60}$.

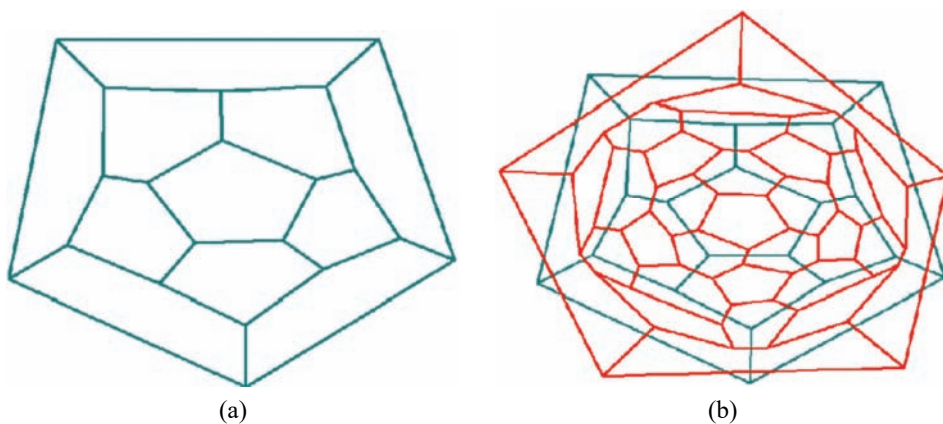


Fig. 1. The fullerene C_{20} (a) and $\text{Le}(C_{20})$ (b).

Balasubramanian¹¹ has realized a lot of work on methods for isomer counting of hetero-fullerenes and of poly-substituted fullerenes, especially, using the generalized character cycle index. Mathematically the isomer counting of poly-substituted fullerene is essentially the same as that of hetero-fullerene. Shao and Ji-ang¹⁵ discussed hydrogenated C₆₀. Furthermore, Zhang¹⁶ also studied fullerene cages. In this paper, the compute number of hetero-fullerenes, C_{3ⁿ × 20}, is computed.

MAIN RESULT AND DISCUSSION

Groups are often used to describe symmetries of objects. This is formalized by the notion of a group action. Let G be a group and X a non-empty set. An action of G on X is denoted by G_X and X is called a G-set. It induces a group homomorphism φ from G into the symmetric group S_X on X, where φ(g)x = gx for all x ∈ X. The orbit of x will be denoted by Gx, which defines as a set all φ(g)x, g ∈ G. The set of all G-orbits will be denoted by G\X := {Gx | x ∈ X}. Suppose g is a permutation of n symbols with exactly λ₁ orbits of size 1, λ₂ orbits of size 2, ..., and λ_n orbits of size n. Then the cycle type of g is defined as 1^{λ₁}, 2^{λ₂}, ..., n^{λ_n}.

Now, the notion of a cycle index is introduced. Let G be a permutation group. The cycle index of G acting on X is the polynomial Z(G, X) over Q in terms of the indeterminates x₁, x₂, ..., x_t, t = |X|, defined by:

$$Z(G, X) = \frac{1}{|G|} \sum_{p \in G} \prod_{i=1}^t x_i^{c_i(p)}$$

in which (c₁(p), ..., c_t(p)) is the cycle type of the permutation p ∈ G. The generalized character cycle index is defined as:

$$P_G^\chi(x_1, x_2, \dots, x_t) = \frac{1}{|G|} \sum_{p \in G} \prod_{i=1}^t \chi(g) x_i^{c_i(p)}$$

where χ(g) is the linear character of the irreducible representation of G. In this paper, two special cases are used: one is the anti-symmetric representation, that is:

$$\chi(g) = \begin{cases} 1 & \text{if } g \text{ is a proper rotation,} \\ -1 & \text{if } g \text{ is an improper rotation,} \end{cases}$$

and the other when χ is 1 for all g. Since, all elements of a conjugacy class of a permutation group have the same cycle type, the cycle index and the generalized character cycle index can be rephrased in the following way:

$$Z(G, x_1, \dots, x_t) = \frac{1}{|G|} \sum_{C \in \text{Conj}(G)} |C| \prod_{i=1}^t x_i^{c_i(g_C)}$$



$$P_G^\chi(x_1, x_2, \dots, x_t) = \frac{1}{|G|} \sum_{C \in \text{Conj}(G)} |C| \prod_{i=1}^t \chi(g_C) x_i^{c_i(g_C)}$$

Enumeration of chemical compounds has been accomplished by various methods. The Pólya–Redfield theorem is a standard method for combinatorial enumerations of graphs, polyhedra, chemical compounds, etc. Combinatorial enumerations have found wide-ranging application in chemistry, since chemical structural formulas can be regarded as graphs or three-dimensional objects.

Denote by $C_{m,n}$ the set of all functions $f: \{1, 2, \dots, m\} \rightarrow \{x_1, x_2, \dots, x_n\}$. The action of $p \in S_m$ induced on $C_{m,n}$ is defined by $\hat{p}(f) = f \circ p^{-1}$, $f \in C_{m,n}$. Treating the colors x_1, x_2, \dots, x_n that comprise the range of $f \in C_{m,n}$ as independent variables, the weight of f is:

$$W(f) = \prod_{i=1}^m f(i)$$

Evidently, $W(f)$ is a monomial of the (total) degree m . Suppose G is a permutation group of degree m , $\hat{G} = \{\hat{p} : p \in G\}$, \hat{p} is as defined above. Let p_1, p_2, \dots, p_t be representatives of the distinct orbits of \hat{G} . The weight of p_i is the common value of $W(f), f \in p_i$. The sum of the weights of the orbits is the pattern inventory:

$$W_G(x_1, x_2, \dots, x_n) = \sum_{i=1}^t W(p_i)$$

Theorem 1 (the Pólya Theorem¹⁷). If G is a subgroup of S_m , the symmetry group on m symbols, then the pattern inventory for the orbits of the $C_{m,n}$ modula \hat{G} is:

$$W_G(x_1, x_2, \dots, x_n) = \frac{1}{|G|} \sum_{p \in G} M_1^{C_1(p)} M_2^{C_2(p)} \dots M_m^{C_m(p)}$$

where $M_k = x_1^k + x_2^k + \dots + x_n^k$ is the k^{th} power sum of the x -es.

Theorem 2 (generalization of the Pólya Theorem¹⁶). Substituting M_i for x_i and in the generalized character cycle index, $i = 1, 2, \dots, t$, one obtains the chiral generating function $CGF = P_G^\chi(M_1, \dots, M_k)$.

To enumerate all possibilities of the hetero-fullerene structures, one has to consider the rotation group of the fullerene, and its whole automorphism group to enumerate the number of chiral isomers. Friperinger¹⁸ computed the symmetry of some fullerenes and then applied Symmetria¹⁹ to calculate the number of $C_{60}H_kCl_{60-k}$ molecules and Balasubramanian computed the number of $C_{60}H_{36}$ isomers. F. Zhang *et al.*¹⁶ used the Pólya counting theorem for calculating the possibilities of different positional isomers. He also applied the generalization of the Pólya theorem to compute the number of chiral isomers.

Now is the time to enumerate the number of hetero-fullerenes in a series of fullerenes constructed by leapfrog. From the above discussion, the problem is reduced to the coloring of the corresponding fullerene graph with $3^n \times 20$ vertices. Consider the molecular graph of the fullerene $C_{3^n \times 20}$, Fig. 2. From the leapfrog principle, it can be seen that the symmetry group G of these fullerenes is isomorphic to the group $I_h = Z_2 \times A_5$ of order 120 and the cycle types of elements of G are as given:

Fullerene	Cycle type	No. of permutations
$C_{3^n \times 20}$	$1^{3^n \times 20}$	20
	$2^{3^n \times 10}$	
	$1^{3^{n-1} \times 4} 2^{3^{n-1} \times 28}$	
	$3^{3^{n-1} \times 20}$	
	$5^{3^n \times 4}$	
	$6^{3^{n-1} \times 10}$	
	$10^{3^n \times 2}$	

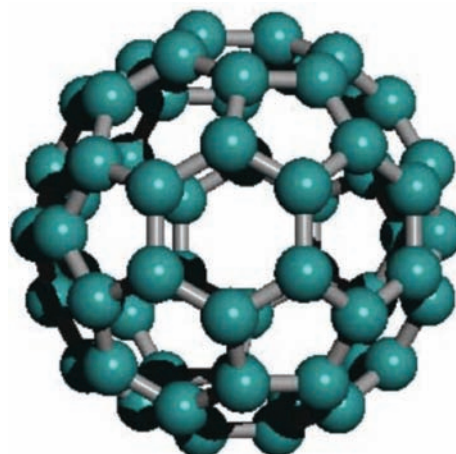


Fig. 2. The fullerene C_{60} .

Thus the cycle index of G is computed as:

$$\begin{aligned} Z(G, X) = & x_1^{20 \times 3^n} + 20(x_3^{20 \times 3^{n-1}} + x_6^{10 \times 3^{n-1}}) + 24(x_5^{4 \times 3^n} + x_{10}^{2 \times 3^n}) + \\ & + 15x_1^{4 \times 3^{n-1}} x_2^{28 \times 3^{n-1}} + 16x_2^{20 \times 3^n} \end{aligned}$$

However, from the cycle indices, the number of possible positional isomers, the number of chiral isomers and the number of orbits under the whole point

group \mathbf{I}_h can be computed. For the number of orbits under the whole point group \mathbf{I}_h , it should simply be noted that:

$$Z_{\mathbf{I}_h} - P_{\mathbf{I}_h}^{\chi} = P_{\mathbf{I}_h}^1$$

In what follows, a GAP program is prepared to compute the number of hetero-fullerenes for $C_{3^n \times 20}$. It should be mentioned here that the present computations of the symmetry properties and cycle indices of the fullerenes were realized with the use of GAP.²⁰ This software was constructed by the GAP team in Aachen. In Table I, this program is applied to compute the number of hetero-fullerenes for the case of $n = 1$.

TABLE 1. The number of $C_{60-k}B_k$ molecules

$k,60-k$	Number of $C_{60-k}B_k$ molecules for		Number of orbits under whole point group \mathbf{I}_h
	Rotational group	Symmetry group	
0,60	1	1	0
1,59	1	1	0
2,58	23	37	14
3,57	303	577	274
4,56	4190	8236	4046
5,55	45718	91030	45312
6,54	418470	835476	417006
7,53	3220218	6436782	3216564
8,52	21330558	42650532	21319974
9,51	123204921	246386091	123181170
10,50	628330629	1256602779	628272150
11,49	2855893755	5711668755	2855775000
12,48	11661527055	23322797475	11661270420
13,47	43057432740	86114390460	43056957720
14,46	144549869700	289098819780	144548950080
15,45	443284859624	886568158468	443283298844
16,44	1246738569480	2493474394140	1246735824660
17,43	3226849468425	6453694644705	3226845176280
18,42	7708584971055	15417163018725	7708578047670
19,41	17040023323785	34080036632565	17040013308780
20,40	34932048763560	69864082608210	34932033844650
21,39	66537224405790	133074428781570	66537204375780
22,38	117952355252550	235904682814710	117952327562160
23,37	194877787472550	389755540347810	194877752875260
24,36	300436595453640	600873146368170	300436550914530
25,35	432628675734195	865257299572455	432628623838260
26,34	582384767014701	1164769471671687	582384704656986
27,33	733373386161407	1466746704458899	733373318297492
28,32	864332935668892	1728665795116244	864332859447352
29,31	953746664302456	1907493251046152	953746586743696
30,30	985538239868528	1971076398255692	985538158387164



A gap program for counting the number of hetero-fullerene for $C_{3^n \times 20}$

```
f:=function(n)
local s,i,f,x,t,tt,g;
x:=Indeterminate(Rationals,"x");
f := ((1 + x)^(20*3^n) + 20*((1 + x^3)^(20*(3^(n - 1))) + (1 + x^6)^(10*(3^(n - 1)))) + 24*((1 + x^5)^(4*3^n) + (1 + x^10)^(2*3^n)) + 15*(1 + x)^(4*(3^(n - 1)))*(1 + x^2)^(28*(3^(n - 1))) + 16*(1 + x^2)^(10*(3^n))/120;
g := ((1 + x)^(20*3^n) + 20*(1 + x^3)^(20*(3^(n - 1))) + 15*(1 + x^2)^(10*(3^(n))) + 24*(1 + x^5)^(4*(3^n))/60;
t := CoefficientsOfLaurentPolynomial(f);
tt := CoefficientsOfLaurentPolynomial(g);
Print("*****\n");
Print("\n");
Print("THIS FULLERENE IS C_,"3^n*20," \n");
Print("\n");
Print("Number of Molecules for Symmetry Group ="," \n");
for i in t[1] do
Print(i," \n");
od;
Print("*****\n");
Print("Number of Molecules for Rotation Group="," \n");
for i in tt[1] do
Print(i," \n");
od;
Print("*****\n");
Print("Number of Orbits under Whole Point Group Sn="," \n");
for i in [1..Length(t[1])] do
Print("[",i-1);Print(",Length(t[1])-i);Print("]");Print(tt[1][i]-t[1][i]," \n");
od;
Print("*****\n");
return;
end;
```

CONCLUSIONS

In this paper, an efficient method is presented which is useful for computing permutational isomers of hetero-fullerenes. The method was applied on a buckminster fullerene and the number of such isomers was computed. From the cycle index of leap frog of a series of fullerenes with I_h point group symmetry, such numbers for all elements of the series can be computed. A GAP program for such calculations is also presented.

И З В О Д

ПРЕБРОЈАВАЊЕ ЈЕДНЕ КЛАСЕ ХЕТЕРО-ФУЛЕРЕНА СА ИЗОЛОВАНИМ ПЕНТАГОНИМА

ALI REZA ASHRAFI и MODJTABA GHORBANI

Institute of Nanoscience and Nanotechnology, University of Kashan, Kashan 87317-51167, I. R. Iran

Хетеро-фулерени су фулерени у којима су неки угљеникови атоми замењени другим атомима. У раду је примењена Појина (Pólya) теорема за пребројавање могућих како позиционих тако и хиралних изомера. Да би се то постигло, коришћена је компјутерска алгебра система GAP и он примењен за одређивање броја изомера за једну класу хетеро-фулерена са изолованим пентагонима (IPR), чије су групе симетрије I_h . Ови фулерени су конструисани применом “липфрг” методе.

(Примљено 30. јула, ревидирано 20. августа 2009)

REFERENCES

1. H. W. Kroto, J. R. Heath, S. C. O'Brien, R. F. Curl, R. E. Smalley, *Nature* **318** (1985) 162
2. P. W. Fowler, D. E. Manolopoulos, *An Atlas of Fullerenes*, Oxford Univ. Press, Oxford, 1995
3. M. Randić, *Chem. Phys. Lett.* **42** (1976) 283
4. M. Randić, *J. Chem. Phys.* **60** (1974) 3920
5. K. Balasubramanian, *J. Chem. Phys.* **72** (1980) 665
6. K. Balasubramanian, *Int. J. Quantum Chem.* **21** (1982) 411
7. K. Balasubramanian, *Chem. Rev.* **85** (1985) 599
8. K. Balasubramanian, *J. Chem. Phys.* **75** (1981) 4572
9. K. Balasubramanian, *Chem. Phys. Lett.* **232** (1995) 415
10. K. Balasubramanian, *J. Phys. Chem.* **108** 5527 (2004)
11. K. Balasubramanian, *Chem. Phys. Lett.* **391** (2004) 69
12. P. W. Fowler, *Chem. Phys. Lett.* **131** (1986) 444
13. P. W. Fowler, J. I. Steer, *J. Chem. Soc. Chem. Commun.* (1987) 1403
14. M. Ghorbani, A. R. Ashrafi, *Asian J. Chem.* **19** (2006) 1109
15. Y. Shao, Y. Jiang, *Chem. Phys. Lett.* **242** (1995) 191
16. F. Zhang, R. Li, G. Lin, *J. Mol. Struct. (THEOCHEM)* **453** (1998) 1
17. G. Pólya, R. C. Read, *Combinatorial Enumeration of Groups and Chemical Compounds*, Springer, New York, 1987
18. H. Fripertinger, *MATCH Commun. Math. Comput. Chem.* **33** (1996) 121
19. *Symmetrifica, A program system devoted to representation theory, invariant theory and combinatorics of finite symmetric groups and related classes of groups*, copyright by Lehrstuhl II für Mathematik, Universität Bayreuth, 95440 Bayreuth, distributed via anonymous, ftp://132.180.16.20, in dist/SYM.tar.Z.
20. The GAP Team : *GAP, Groups, Algorithms and Programming*, R WTH, Aachen, Germany, 1995
21. A. R. Ashrafi, M. Ghorbani, *MATCH Commun. Math. Comput. Chem.* **60** (2008) 359
22. A. R. Ashrafi, M. Jalali, M. Ghorbani, M. V. Diudea, *MATCH Commun. Math. Comput. Chem.* **60** (2008) 905
23. A. R. Ashrafi, M. Ghorbani, *MATCH Commun. Math. Comput. Chem.* **59** (2008) 595
24. M. Ghorbani, M. Jalali, *MATCH Commun. Math. Comput. Chem.* **62** (2009) 353
25. M. Ghorbani, A. R. Ashrafi, *J. Comput. Theor. Nanosci.* **3** (2006) 803
26. A. R. Ashrafi, M. Ghorbani, M. Jalali, *Dig. J. Nanomater. Bios.* **3** (2008) 245.





An SEM and EDS study of the microstructure of nitrate ester plasticized polyether propellants

YONG LIU^{1,2*}, LUOXIN WANG¹, XINLIN TUO¹ and SONGNIAN LI^{1,2}

¹Institute of Polymers, Department of Chemical Engineering, Tsinghua University, Beijing 100084 and ²College of Mechanical and Electrical Engineering, Beijing University of Chemical Technology, Beijing 100029, China

(Received 26 March, revised 15 July 2009)

Abstract: To probe the microstructures of nitrate ester plasticized polyether (NEPE) composite propellants and observe the morphology of each constituent in the propellant, the microstructure and elemental constituents of NEPE propellants were investigated using scanning electron microscopy and energy dispersive X-ray spectroscopy. The ammonium perchlorate (AP) grains had a scraggly surface and were difficult to disperse uniformly. The compatibility between the AP grains and the polymer binder was poor, especially for large grains. The size distribution range of the AP and octogen (HMX) grains in propellants varied from several to several hundreds μm for the former while for the latter from several to several tens μm . Contrasting images before and after dissolution of the propellant in trichloro methane showed that the degree of crosslinking of the polymer binder was low since non-crosslinked binder on the surface areas was easily removed by the solvent, and that the plasticizer was near the HMX grains and contributed more O to the element analysis of HMX.

Keywords: composite solid propellants; scanning electron microscopy; microstructure; element analysis.

INTRODUCTION

NEPE (nitrate ester plasticized polyether) propellants are a type of highly energetic, composite solid propellant.^{1–3} This type of propellant uses a polyether polymer binder, such as polyethylene glycol (PEG) or ethylene oxide (tetrahydrofuran-co-polyether), and a plasticizer of mixed nitrate (BG), usually using nitroglycerin (NG) and 1,2,4-butane triol trinitrate (BTTN).^{4–6} The balance of the propellant consists of large amounts of solid grains, including aluminum powder (Al), octogen (HMX), ammonium perchlorate (AP), etc. The interactions between the polymer binder and the other constituents, which are mostly inorganic, are not good. However, after crosslinking, the polymer binder can wrap all the

*Corresponding author. E-mail: yongsd@iccas.ac.cn
doi: 10.2298/JSC090326007L

solid grains as shown in a previous study.⁷ This type of propellant integrates the advantages of double-base propellants and composite propellants, and adds excellent low temperature mechanical properties.^{8,9} Therefore, this type of propellant has been studied extensively and applied broadly in many countries since its first development in the USA in the 1970s.^{10–12} However, the microstructure of the propellant, which decisively affects its performance, has hitherto not been clearly investigated.^{13–15} In this study, scanning electron microscopy (SEM) and energy dispersive X-ray spectroscopy (EDS) were employed to directly observe the micro-morphology and distribution of the constituents in the propellant, whereby a detailed understanding of its special microstructure was obtained.

EXPERIMENTAL

The microstructure of NEPE solid propellant, which was taken from a rocket, was observed using Hitachi S-4500 and S-6301 scanning electron microscopes (Japan). The grains in the SEM figures were measured using the measuring tool incorporated into Imagenet 2000 software. The elemental constituents of a small area were analyzed using an Inca energy dispersive X-ray spectrometer (The Netherlands) combined with the S-6301 microscope. The samples were sprayed with gold for 5 minutes before observation.

The main constituents of the NEPE propellants by mass percentage were: PEG, 6 to 9; BG, 15 to 21; Al, 19; HMX, 43 and AP, 8. The content of some other auxiliary agents were about 1–2 %. The analytical reagent trichloromethane was used to extract the plasticizer from the NEPE propellants.

RESULTS AND DISCUSSION

SEM Analyzes for Al and AP in NEPE propellants

In the NEPE propellants, the polymer binder PEG is the continuous phase while solid grains, such as Al, AP and HMX, are dispersed in the PEG. By the process of elimination, if the morphologies of any two among three kinds of solid grains are determined then the remaining kind of solid grain is also identified. Hence, first the microstructure of two raw materials, AP and Al, were observed, as shown by the images in Fig. 1. HMX was not selected for direct observation since these grains in the propellant are covered closely by bonding agent, making it difficult to obtain their real morphology.

An SEM image of several AP grains is shown in Fig. 1a. This image clearly shows that most of AP grains are anomaly shaped with a size from approximately 100–300 µm, with a few even smaller grains. The SEM image in Fig. 1b is zoomed in on a single AP grain which exhibits a dense, small protuberance on its surface. This grain has the characteristic of a scraggy morphology. Elemental analysis using EDS was performed on this same grain to determine its composition: N:O:Cl is 17:56:15 (the element H cannot be determined), which basically conforms to the molecular composition of AP (NH_4ClO_4). The SEM image in Fig. 1c shows several Al grains with not only ellipsoid shapes but also spherical shapes.¹⁵ The size of the Al grains was mostly below 15 µm, with a wide size distribution.

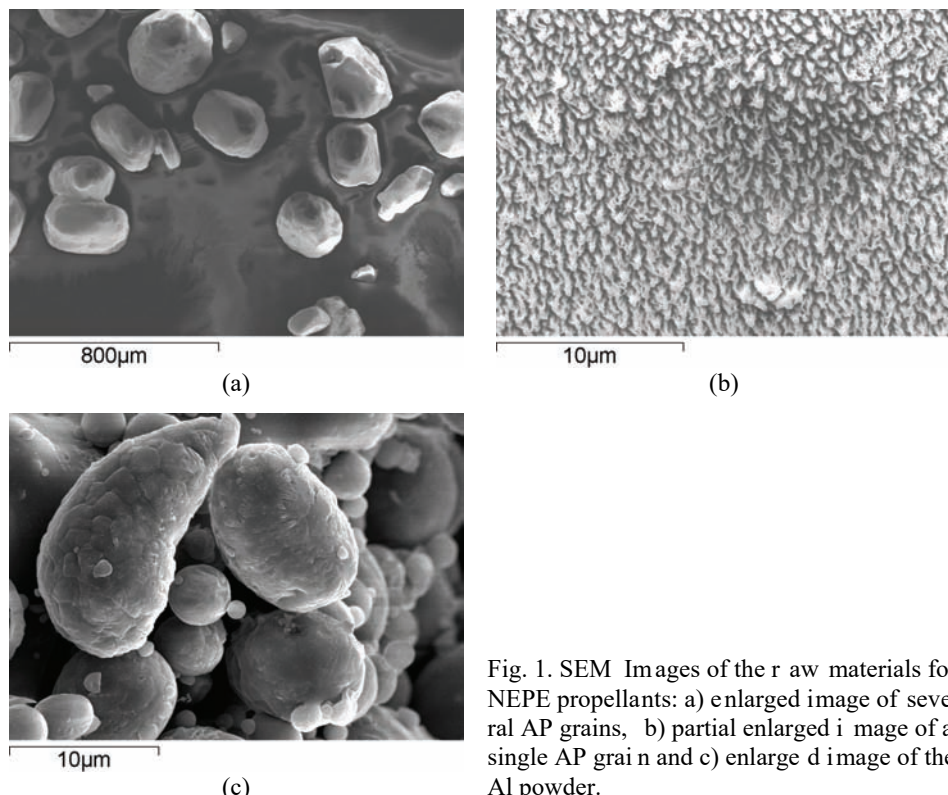


Fig. 1. SEM Images of the raw materials for NEPE propellants: a) enlarged image of several AP grains, b) partial enlarged image of a single AP grain and c) enlarged image of the Al powder.

The microstructure of the NEPE propellant was observed using SEM (Fig. 2). The wide-angle SEM image of the NEPE propellant sample in Fig. 2a clearly shows that the large grains are AP due to both their scraggy morphological characteristic and their relatively large size. The spatial distribution of this kind of grain is uneven since four can be seen located close to the top left corner of the image while none is seen in the middle. Two AP grains, the top left and the bottom ones, are obviously cracked. This cracking likely occurred during cutting the propellant using a knife to obtain the SEM samples. From the distribution of AP grains in this image, it can be inferred that the large AP grains are difficult to disperse evenly. The SEM image in Fig. 2b is zoomed in to show a smaller area of propellant. Almost all the solid grains (no bigger than approximately 30 μm) are covered with polymer binder. Only one solid grain, in the lower part of the Fig. 2b, is exposed and its surface is scraggy — perhaps a small AP grain or a corner of large one. An SEM picture of a single AP grain in the propellant is shown in Fig. 2c. Obviously the surface of this AP grain has two kinds of morphology: grooves on the left and protuberances on the right. The right morphology, grooves, is the same as those of the raw AP material. The possible reason for the two

kinds of morphology appearing simultaneously is that an AP grain, as a crystal, has several surfaces of which two of them appeared in this observation area. Different observation angles showed different morphologies. The three images in Fig. 2 show the poor compatibility of AP (especially the large grains) with the polymer binder in this propellant, since only AP grains were visible, the other solid grains being covered with binder. A further easy deduction is that the bad compatibility will result in the AP grains being the point of stress concentration within the propellant. Thus, the mechanical performance of the propellants could be improved by improving the compatibility between the AP grains and the polymer binder, possibly by using a bonding agent.

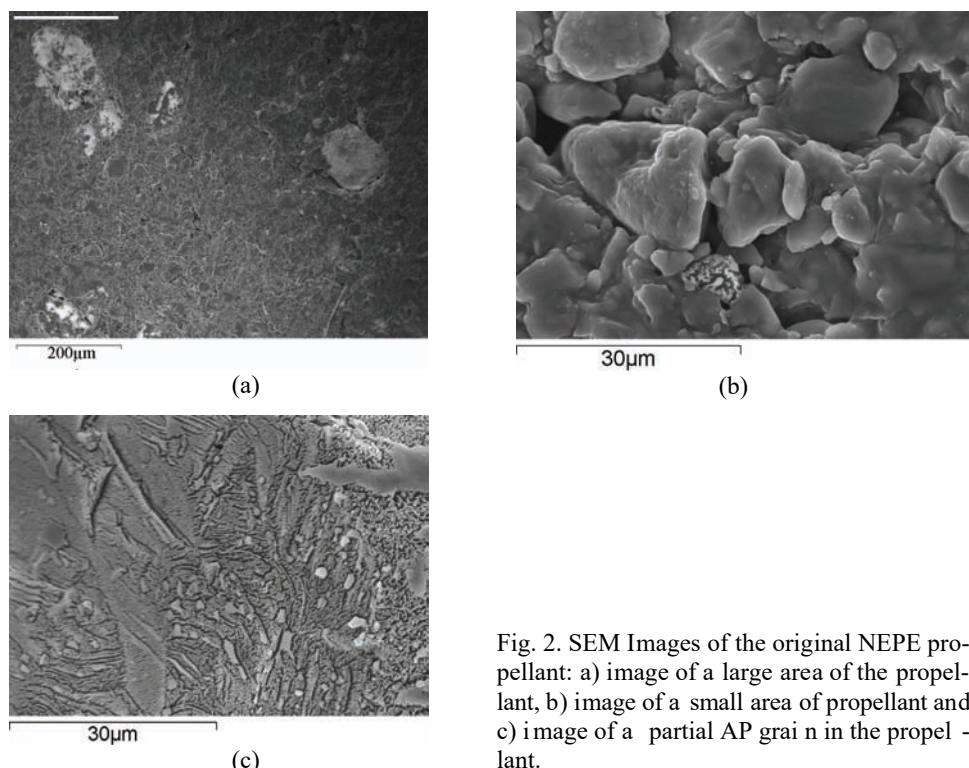


Fig. 2. SEM Images of the original NEPE propellant: a) image of a large area of the propellant, b) image of a small area of propellant and c) image of a partial AP grain in the propellant.

SEM and EDS analyses of NEPE propellants

According to the formulation of NEPE propellants, most of the solid grains in Fig. 2b should be HMX. However, the ellipsoid Al and small AP grains could possibly be covered with polymer binder, which is an additional difficulty in ascertaining whether or not a certain grain is HMX. In order to assure the material attributes of a grain in NEPE propellants and to determine the dimension distri-

bution of HMX grains, elemental analysis using EDS combined with the S-6301 SEM was performed on a few of the solid grains and some polymer binder areas.

First, a planar area to make element analysis was selected where the polymer binder seemed to be the main component, Fig. 3a. The mini cross in the image is the center of the area selected for spectrum analysis. The EDS results are listed in Table 1 and shown by Fig. 3b. Al and AP grains were possibly located under the binder area, explaining the small content of the elements Al and Cl in these results. In this area, the constitute ratio of C:O was about 69:25, which is larger than expected for the PEG polymer, the segment molecular formula of which is C_2H_4O . The deviation in the element C content possibly arises from SEM instrumental error, as about 12% C, was also measured in the element constitute results for pure AP and Al grains.

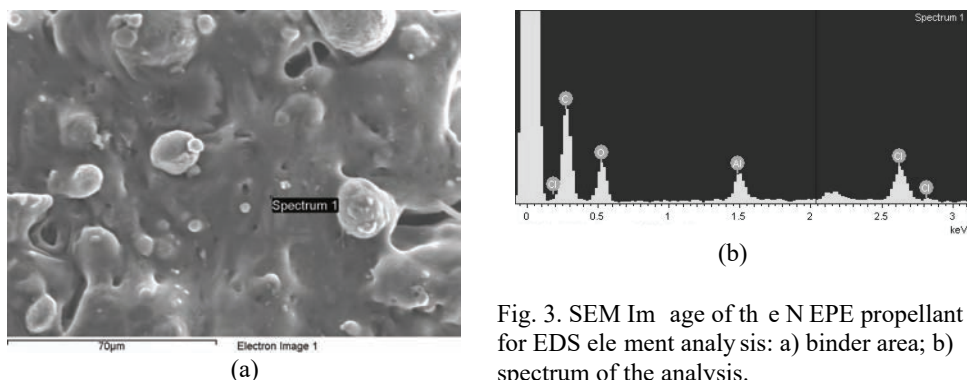


Fig. 3. SEM Image of the NEPE propellant for EDS element analysis: a) binder area; b) spectrum of the analysis.

TABLE I. Element content of the binder determined by EDS analysis

Element	Content, mass %	Content, at. %
C	59.18	69.44
O	28.69	25.27
Al	3.74	1.95
Cl	8.39	3.34

Second, a medium-sized grain having an anomalous shape, as shown in Fig. 4a, was analyzed. Elemental composition was approximately C:N:O = 10:7:8. The molecular formula of HMX is $C_4H_8N_8O_8$, while the formulae of NG and BTTN are $C_3H_5O_9N_3$ and $C_4H_7O_9N_3$, respectively. With no Cl or Al evidenced and further with the ratio of the elements N and O nearly 1:1, this solid grain can be confirmed to be HMX. The content of element O is slightly high in the results, possibly because liquid plasticizer near the HMX grain contributed more elemental O. To confirm the above hypothesis, a NEPE propellant sample was left in $CHCl_3$ for 10 days in order to extract the plasticizer. Then another EDS analysis performed on a solid grain, as shown in Fig. 4b. The elemental composition re-

sults for C:N:O was approxim ately 43:27:27. The elem ent C content was very high. Possible reasons are the SEM instrument and the bonding agent which contains a relatively large amount of element C, coating the HMX grains. The ratio of N:O was 1:1 in these elemental composition results, proving the correctness of the above hypothesis. The plasticizer w ould be near the HMX grain and would contribute a large amount of element O to EDS analysis results. Comparing images in Figs. 4a and 4b, clearly the polymer binder covering the solid grains was lower in Fig. 4b, indicating that the degree of crosslinking of the polymer binder was low and that some uncrosslinked polymer binder was dissolve by the CHCl₃.

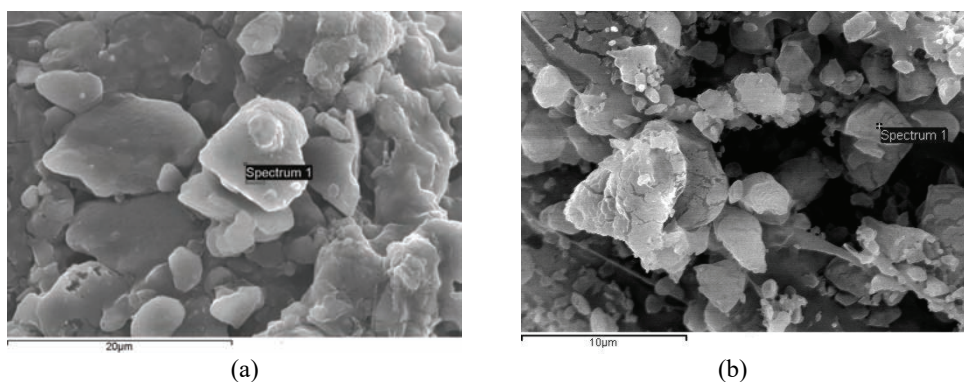


Fig. 4. SEM Images of middle size grains for EDS element analysis:
a) NEPE propellant; b) after soaking in CHCl₃.

In Fig. 5, the large grain and the small white one below it were con firmed to be HMX usi ng EDS ele ment analysis. Cracks on th e surface of t he large HM X grain were th e result of the high veloci ty electron i mpulse when observing th e microstructure. The dim ensions of the l arge and sm all HMX grains can be esti mated as about 30 and 4 µm, respectively, illustrating that the size distribution of the HMX grains was broad, from several to several tens of µm.

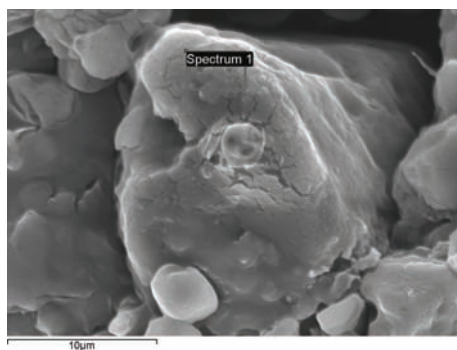


Fig. 5. SEM Im age of one large grain i n the NEPE propellant.

Using the same element analysis method, the small grain marked in Fig. 6 and the other small grain, close to the left of the marked one, were determined to be HMX and AP, respectively. The three spots in the left part of the image were the result of image distortion because when observing microstructure the polymer binder tended to flow under the action of the high velocity electrons or the electrical conductivity was bad in this area. Contrasting this image with those in Figs. 2 and 3, it is apparent that the polymer binder covered the small grains more easily than the large ones, especially the large AP grains. Another conclusion is that the size range of the AP grains was larger than that for the HMX grains, being from several to several hundreds μm in size.

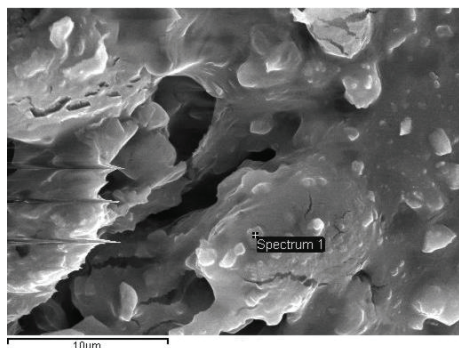


Fig. 6. SEM Image of a small grain in the NEPE propellant.

CONCLUSIONS

The microstructure morphology of AP grains observed using SEM was either dense, small protuberances or groove anomalies on the grain surface. The size distribution range of the grains was wide, from several tens to about 300 μm . The shape of the Al grains varied widely and their size was predominately less than 15 μm , with a broad distribution. Observations of the NEPE propellant using SEM evidenced that the distribution of the large AP grains was not uniform or regular, and that compatibility between the AP grains and the polymer binder was poor, making the AP grains points of stress concentration if the propellant were to be subjected to stress.

The elemental composition of the material in the NEPE propellants was determined using EDS element analysis, enabling the material attributes of the grains and binder to be established. The size range of the HMX grains in these propellants, confirmed using EDS, was from several to several tens of μm . By using CHCl_3 to extract the plasticizer from the NEPE propellants, with before and after element analysis, the plasticizer was shown to lie very close to the HMX grains. The contrasted microstructure images allowed the deduction that the degree of cross-linking of the polymer binder in the NEPE propellants is low and that the uncross-linked binder on surface parts can be readily dissolved by solvents.

Acknowledgements. This work was supported by the China Post-doctor Science Foundation (No. 20060390431).

ИЗВОД

SEM И EDS СТУДИЈА МИКРОСТРУКТУРЕ ЕКСПЛОЗИВА НА БАЗИ НИТРАТНИХ ЕСТАРА ПЛАСТИФИКОВАНИХ ПОЛИЕТРИМА

YONG LIU^{1,2}, LUOXIN WANG¹, XINLIN TUO¹ и SONGNIAN LI^{1,2}

¹*Institute of polymer, Department of Chemical Engineering of Tsinghua University, Beijing 100084* и ²*College of Mechanical and Electrical Engineering, Beijing University of Chemical Technology, Beijing 100029, China*

За анализу микроструктуре композитних експлозива на бази нитратних естара пластификованих полиетрима (NEP E) као и морфологије и елементарног састава појединачних компоненти, коришћене су скенирајућа електронска микроскопија (SEM) и спектроскопска анализа карактеристичног рентгенског енергетског зрачења (EDS). Анализа је показала да зrna амонијум-перхлората (AP) имају неравну површину и да нису равномерно распоређена по узорку. Компатибилност између AP зrna и полимерне матрице је веома лоша што је нарочито изражено код већих зrna. Широта расподеле величине зrna је била за AP и (HMX, експлозиви високе температуре топљења) у опсегу од неколико до неколико стотина μm , односно од неколико до неколико десетина μm . Анализа слике пре и после растварања експлозива у трихлорметану је показала да су брзина и степен реакције умрежавања полимерног везива мали, и то на основу чињенице да је неумрежено полимерно везиво лако уклоњено са површине зrna. На основу елементарне анализе и повећаног садржаја кисеоника закључено је да се полистарско везиво налази на површини HMX зrna експлозива.

(Примљено 26. марта, ревидирано 15. јула 2009)

REFERENCES

1. D. K. Davis, in *Proceeding of AIAA-1984-1441, 20th SAE and ASME Joint Propulsion Conference*, Cincinnati, OH, USA, 1984, p. 125
2. J. C. Hinshaw, US Patent 4804424 (1989)
3. T. H. Zhang, Y. L. Bai, S. Y. Wang, P. D. Liu, *Acta Mech. Sin.* **17** (2001) 348
4. S. N. Li, Y. Liu, X. L. Tuo, X. G. Wang, *Polymer* **49** (2008) 2775
5. X. G. Wei, G. Q. He, P. J. Liu, X. Z. Li, in *Proceeding of 57th International Astronautical Congress*, Valencia, Spain, 2006, paper No. IAC-06-C4.P.2.5
6. A. Davenas, *J. Propuls. Power* **11** (1995) 285
7. Y. Liu, L. X. Wang, X. L. Tuo, S. N. Li, X. G. Wang, *Chin. J. Explos. Propel.* **30** (2007) 53
8. A. Davenas, *J. Propuls. Power* **19** (2003) 1108
9. M. Kearns, *Mater. Sci. Eng. A* **375** (2004) 120
10. W. S. Kennedy, S. M. Kovacic, E. C. Rea, T. C. Lin, *J. Spacecr. Rockets* **36** (1999) 890
11. S. W. Beckwith, H. B. Carroll, *J. Spacecr. Rockets* **22** (1985) 156
12. F. T. Chen, Y. Q. Duo, S. G. Luo, Y. J. Luo, H. M. Tan, *Propellants Explos. Pyrotech.* **28** (2003) 7
13. P. D. Peterson, D. J. Idar, *Propellants Explos. Pyrotech.* **30** (2005) 88
14. C. L. Gallic, R. Belmas, P. Lambert, *Propellants Explos. Pyrotech.* **29** (2004) 339
15. L. Meda, G. Marra, L. Galfetti, F. Severini, L. De Luca, *Mater. Sci. Eng. C* **27** (2007) 1393.



SHORT COMMUNICATION

**Surface-charged polyacrylonitrile/poly(vinyl alcohol)
(PAN/PVA) colloids used to prepare
proton conducting materials**

JIANDONG GAO^{1,2}, ZHIGANG MA^{1,2}, JING GUO^{1,2}, YONGJIAN HUAI^{1,2},
ZHENGHUA DENG^{1*} and JISHUAN SUO¹

¹*Chengdu Institute of Organic Chemistry, Chinese Academy of Sciences, Chengdu Sichuan 610041* and ²*Graduate School of Chinese Academy of Sciences, Beijing 100039, P. R. China*

(Received 9 March, revised 20 August 2009)

Abstract: Proton exchange membranes exhibiting a well-organized structure were successfully prepared by a novel self-assembling technique using surface-charged latex nanoparticles as building blocks. The nanoparticles were synthesized in water by free-radical copolymerization. Free-standing membranes were obtained by casting the polymer emulsions followed by a cross-linking reaction. The acquired membrane exhibited a high proton conductivity of 0.04 S cm⁻¹ with an ion exchange capacity (IEC) as low as 0.48 mmol g⁻¹. The enhanced proton conductivity is thought to be derived from the formation of a co-continuous ionic network for ion channels by the closely packed surface-charged latex nanoparticles, facilitating proton transportation in the membranes.

Keywords: polyacrylonitrile; poly(vinyl alcohol); proton conductivity ; ion exchange capacity; fuel cell.

INTRODUCTION

Proton-conducting polymer electrolyte membranes (PEM) are one of the most critical components for polymer electrolyte membrane fuel cells (PEMFCs) and direct methanol fuel cells (DMFCs). Most of the PEMs are ionomers consisting of a hydrophobic backbone with pendant cation exchange sites, such as SO_3^- . The ionic aggregation and the nanoscale phase separation of ionic and nonionic components resulted in the formation of bi-continuous structures for membranes exhibiting proton conductivity.^{1,2} However, the long-range patterned organization of hydrophilic clusters into a hydrophobic phase does not exist in PEMs,³ which suggests that a low content of clusters does not induce the formation of percolation paths. Increasing the content of cation exchange site fac-

*Corresponding author. E-mail: zhengh@cioc.ac.cn
doi: 10.2298/JSC090309005G

litates the transformation from insulator to ion conductor (percolation threshold) for the polymers, which is ascribed to the formation of interconnected ionic domains. However, a continuous increment in the content of ionic sites may result in a deterioration of mechanical properties of the membranes because of the high hydrophilic property of the polymer. Therefore, it is essential to reasonably control the amount of ionic group in order to avoid a sharp decrease of the proton conductivity or a deterioration of the mechanical properties of the membranes.

Although there are many archetypal structures to choose from in order to design a polymer with a particular molecular structure which would promote phase separation, the synthetic pathways available are not quite so rich.⁴ Furthermore, membranes casting from ionomer solutions usually did not lead to a precisely controlled structure (Fig. 1) to improve proton transport by optimizing the connectivity of the ionic domains.

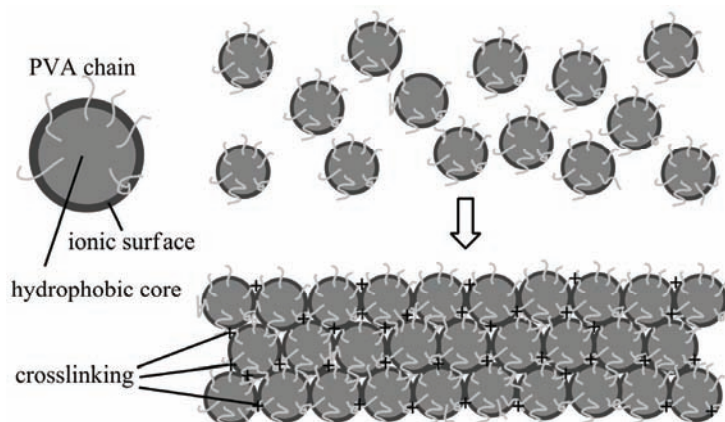


Fig. 1. Schematic diagram showing the surface-charged latex nanoparticles and membrane formation *via* the self-assembly of the nanoparticles.

Self-assembling of latex nanoparticles were applied for the preparation of templating semiconductors or conducting polymers. The polystyrene particles used to template doped π -conjugated polymers were found to decrease the percolation threshold for electrical conductivity.⁵ Surface-charged latex nanoparticles were used to build blocks for PEMs exhibiting a linear relationship between conductivity and ion exchange capacity (IEC) values even at low IEC values, probably due to the disappearance or shifting to very low of percolation thresholds for membranes with discontinuous structures.^{6,7} In this work, the efforts were mainly focused on the preparation and characterization of novel proton exchange membranes, increasing the co-continuous ionic network for ion channels and facilitating proton transportation. A novel method to prepare proton-conducting membranes *via* surface-charged polymer colloids self-assembling te-

chniques, followed by a cross-linking reaction, is demonstrated. A schematic diagram showing the surface-charged latex nanoparticles and the membrane formation is shown in Figure 1. The surface-charged latex nanoparticles were packed and linked together as building blocks medium for proton conductive membranes. In this way, a proton conductive membrane with controlled micro/nanoscale structure and optimized connectivity of the ionic domains was formed.

EXPERIMENTAL

Sample preparation

A hydrophobic monomer, acrylonitrile (AN), a cross-linker, *N,N'*-methylenebisacrylamide (BIS), and a charged monomer, sodium vinylsulfonate (SVS, 25 % content in distilled water), were chosen for the nanoparticle syntheses by free-radical emulsion copolymerization in an aqueous poly(vinyl alcohol) (PVA, degree of polymerization and saponification were 1700 and 98–99 %, respectively) solution. During the nanoparticle synthesis reaction, the PVA served as a polymeric dispersant, preventing the colloidal particles from aggregation. The PVA chains assembled the spheres to form latex films and the hydroxyl groups (–OH) in PVA were cross-linked in the following membrane preparation process, constraining the swelling of the membrane and providing mechanical strength. The synthesis in aqueous emulsions should result in charged groups being attached to the surface of the particles.⁸ Varying amounts of SVS were introduced into the system to obtain particles with different contents of charges for different membranes. AN (14.0 g), BIS (1.0 g) and SVS (1.0–4.0 g) were added into 80.0 g of an aqueous PVA solution containing 4.0 g of PVA under vigorous stirring and then heated under a nitrogen atmosphere to the incubation temperature of 65 °C. The reaction was initiated by adding dropwise an ammonium persulfate (APS) solution.

The free-standing membranes were prepared by direct casting of the emulsion onto a clean glass slide, followed by drying under normal pressure at ambient temperature. Then the membrane with a thickness of about 120 µm was immersed into an acetone solution containing 5 wt. % glutaraldehyde (GA) and 0.5 % HCl (volume fraction). The reaction was maintained at 40 °C for 4 h, whereby cross-linked membranes were subsequently obtained. In addition, the as-received membranes were treated with a 1.0 M H₂SO₄ solution overnight and then washed three times with distilled water before measurements of the proton conductivity and ionic content. Nafion® 117 (1100 EW, 177.8 µm thickness, commercially extruded film) was purchased from Aldrich and used as received without any further purification.

Measurements

The FTIR analysis was performed on a Nicolet MX-1E FTIR spectrometer. The morphology of the particle membrane was studied by scanning electron microscopy (SEM), using a Jeol JSM-5900LV electron microscope.

The proton conductivities of the particle membranes were evaluated by measuring the ac impedance spectra using a Solartron ac impedance system (1260 impedance analyzer, 1287 electrochemical interface, Zplot software) in the frequency range of 1 MHz to 1 Hz. The membranes of 0.59 cm² in area were sandwiched between two platinum blocking electrodes. All membranes were prehydrated in water for at least 24 h and then quickly enclosed in a sealable cell to maintain hydration during impedance measurements. The IEC values of the membranes were measured by the classical titration method.

RESULTS AND DISCUSSION

The FTIR spectra of the membranes before and after the cross-linking reaction are shown in Fig. 2. With respect to the membrane after cross-linking with GA, the membrane showed different absorption bands in the spectra as compared with the pristine membrane. The bands at 1000 and 1038 cm⁻¹ correspond to the vibration of C–O and C–O–C bonds due to acetal or semi-acetal formation after the cross-linking reaction, respectively. The band at 1717 cm⁻¹ was assigned to the absorption of the carbonyl groups of non-conjugated aldehydes.⁹ In addition, two important peaks at 2934 and 2862 cm⁻¹ were ascribed to the absorptions of the stretch vibration of C–H bonds related to aldehydes.¹⁰ These FTIR spectral changes shown in Fig. 2 confirm the acetalization that occurred inter molecular between PVA and GA.

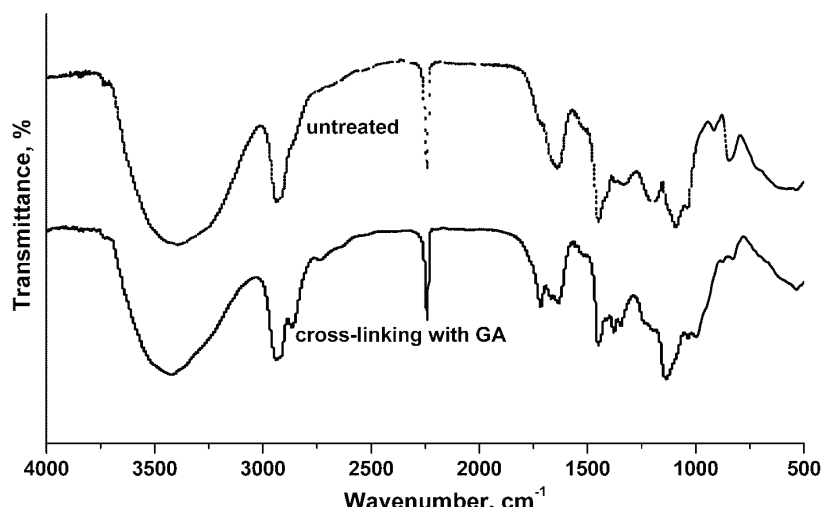


Fig. 2. FTIR Spectra of particle membranes obtained before and after the cross-linking reaction.

Before the cross-linking reaction, cohesion of the spheres was achieved mainly through intersphere chain entanglement of PVA. The water solubility of the PVA chains enabled the film to swell excessively in water, preventing measurement of the conductivity and IEC. After the cross-linking reaction, the films showed constrained swelling and adequate mechanical strength.

An SEM cross-section image of a cross-linked membrane obtained from the surface-charged polymer colloids is shown in Fig. 3. It may be observed that the particles are individually well dispersed and packed closely within the membrane, suggesting that the structure of the particles remained after the preparation and cross-linking reaction of the membrane. The well dispersed structure of the particles is believed to facilitate the formation of network for ion channels.

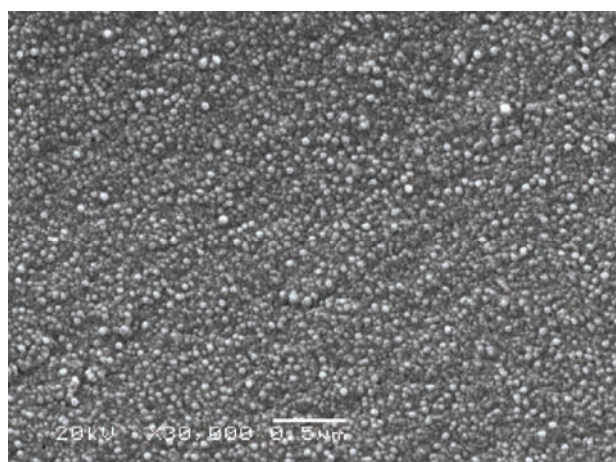


Fig. 3. SEM Cross-sectional image of a particle membrane with an *IEC* value of 0.28 mmol g⁻¹.

Proton conductivity can vary with different experimental approaches and instruments. For comparison, the proton conductivity of Nafion® 117 was measured under the same conditions and resulted in a value of 0.020 S cm⁻¹ at 20 °C. As shown in Table I, the proton conductivity of the particle membranes was high even for an *IEC* as low as 0.18 mmol g⁻¹. The values of the proton conductivity increased almost linearly with *IEC*, reaching 0.040 S cm⁻¹ for an *IEC* of 0.48 mmol g⁻¹. It is generally accepted that a higher value of the *IEC* is desirable to achieve higher proton conductivity in polymer electrolyte membranes. As compared with Nafion® 117 (*IEC* of 0.91 mmol g⁻¹) under the same condition, the particle membrane had a comparative proton conductivity, in addition to an *IEC* of 0.28 mmol g⁻¹, which is much lower than that of a Nafion 117 membrane of 0.91 mmol g⁻¹.

TABLE I. *IEC* and proton conductivity (δ) of the membranes

Membrane sample	SVS content ^a , wt. %	<i>IEC</i> / mmol g ⁻¹	δ^b / S cm ⁻¹
Membrane-1 5		0.18	0.010
Membrane-2 8		0.28	0.020
Membrane-3 12		0.36	0.028
Membrane-4 17		0.48	0.040
Nafion® 117	—	0.91	0.020

^aSVS contents in feed; ^bmeasured at 20 °C

It is believed that the difference between the conductivity of the particle membranes and the Nafion® 117 membrane lies in the connectivity of the conduction pathways. In a membrane made from random or graft copolymers, the charges are uniformly distributed resulting in a lack of phase separation. The high conductivity only occurs where there is sufficient connection between the

charged regions for a continuous pathway to exist, often associated with a high IEC. For the surface-charged latex membranes, the particles packed closely and the cation exchange sites ($-SO_3^-$) are spread among adjacent particles, facilitating phase separation during membrane drying. When the thin film swells in water, the localized charge clusters may diffuse to form a co-continuous ionic network and so provide continuous pathways, even at a low charge content. In this case, the percolation threshold shifts to much lower values. In effect, the low percolation threshold can be attributed to an efficient organization of the charges within the membrane. It is known that the proton conductivity of an ordered arrangement of proton conductive nanodomains is higher than that of a randomly arranged one.^{11–13} Thus, the particle membranes have the advantage of improving proton conductivity by the formation of a continuous conduction pathway.

CONCLUSIONS

Proton exchange membranes exhibiting well-organized structures were successfully prepared by self-assembling and cross-linking reaction of surface-charged polymer colloids. The well-organized structure as revealed by SEM facilitated the formation of continuous conduction pathways, thus improving the proton conductivity of the particle membranes. The novel method for preparing membranes with an ordered microstructure is recognized to be useful in the design of both PEMs and ion-conducting membranes for use in battery applications, electrosynthesis and water purification.

ИЗВОД

ПРИМЕНА ПОВРШИНСКИ НАЕЛЕКТРИСАНИХ КОЛОИДНИХ ЧЕСТИЦА
ПОЛИ(АКРИЛОНИТРИЛ)/ПОЛИ(ВИНИЛАЛКОХОЛА) (PAN/PVA)
У ПРОТОН ПРОВОДНИМ МАТЕРИЈАЛИМА

JIANDONG GAO^{1,2}, ZHIGANG MA^{1,2}, JING GUO^{1,2}, YONGJIAN HUAI^{1,2}, ZHENGHUA DENG¹ и JISHUAN SUO¹

¹*Chengdu Institute of Organic Chemistry, Chinese Academy of Sciences, Chengdu Sichuan 610041* и

²*Graduate School of Chinese Academy of Sciences, Beijing 100039, P. R. China*

У овоме раду је приказана израда протон проводних мембрана добро дефинисане структуре применом нове технике „само-организације“ површински наелектрисаних наночестица. Наночестице су синтетисане емулзионом кополимеризацијом у присуству слободних радикала као иницијатора. Полимерне мембрane су добијене поступком извливања латекса и накнадним умрежавањем колоидних честица. Добијене полимерне мембрane су показивале велику протонску проводљивост од око $0,04 \text{ S cm}^{-1}$ при релативно ниском јоноизмењивачком капацитету (IEC) од $0,48 \text{ mmol g}^{-1}$. Претпоставља се да је повећана протонска проводљивост мембрana последица континуалне мреже јонских канала, настале густим паковањем површински наелектрисаних наночестица, чиме је олакшан транспорт протона кроз мембрну.

(Примљено 9. марта, ревидирано 20. августа 2009)

REFERENCES

1. L. Rubatat, A. L. Rollet, G. Gebel, O. Diat, *Macromolecules* **35** (2002) 4050
2. Y. A. Elabd, E. Napadensky, C. W. Walker, K. I. Winey, *Macromolecules* **39** (2006) 399
3. K. A. Mauritz, R. B. Moore, *Chem. Rev.* **104** (2004) 4535
4. Y. Yang, S. Holdcroft, *Fuel Cells* **5** (2005) 171
5. R. Mezzenga, J. Ruokolainen, G. H. Fredrickson, E. J. Kramer, D. Moses, A. J. Heeger, O. Ikkala, *Science* **299** (2003) 1872
6. J. Gao, D. Lee, Y. S. Yang, S. Holdcroft, B. J. Frisken, *Macromolecules* **38** (2005) 5854
7. J. Gao, D. Lee, Y. S. Yang, S. Holdcroft, B. J. Frisken, *Macromolecules* **39** (2006) 8060
8. J. H. Kim, M. Chainey, M. S. El-Aasser, J. W. Vanderhoff, *J. Polym. Sci., Part A: Polym. Chem.* **30** (1992) 171
9. W. M. de Azevedo, J. M. de Souza, J. V. de Melo, *Synth. Met.* **100** (1999) 241
10. H. S. Mansur, R. L. Oréfice, A. A. P. Mansur, *Polymer* **45** (2004) 7193
11. E. M. W. Tsang, Z. B. Zhang, Z. Q. Shi, T. Soboleva, S. Holdcroft, *J. Am. Chem. Soc.* **129** (2007) 15106
12. R. Maki-Ontto, K. de Moel, E. Polushkin, G. A. van Ekenstein, G. ten Brink, O. Ikkala, *Adv. Mater.* **14** (2002) 357
13. T. Tezuke, K. Tadanage, A. Hayashi, M. Tatsumisago, *J. Am. Chem. Soc.* **128** (2006) 16470.



Preparation and morphology of porous SiO_2 ceramics derived from fir flour templates

ZHONG LI^{1,2}, TIEJUN SHI^{1*} and LIYING GUO¹

¹School of Chemical Engineering, Hefei University of Technology, Hefei 230009 and ²School of Chemical Engineering, Anhui University of Science & Technology, Huainan 232001, China

(Received 10 April, revised 25 November 2009)

Abstract: The preparation of SiO_2 ceramics with controllable porous structure from fir flour templates via sol-gel processing was investigated. The specific size of the fir flour, which was treated with 20 % NaOH solution, was infiltrated with a low viscous silica sol and subsequently calcined in air, which resulted in the formation of highly porous SiO_2 ceramics. X-Ray diffraction (XRD), Fourier transform infrared spectroscopy (FTIR) and field emission scanning electron microscopy (FESEM) were employed to investigate the microstructure and phase formation during processing as well as of the SiO_2 ceramics. N_2 adsorption measurements were used to analyze the pore size distributions (PSD) of the final ceramics. The results indicated that the surface topography was changed and the proportion of the amorphous material was increased in NaOH-treated fir flour. The final oxide products retained ordered structures of the pores and showed unique pore sizes and distributions with hierarchy on the nanoscale derived from the fir flour.

Keywords: porous silicon ceramics; microstructure; sol-gel process; calcination.

INTRODUCTION

Over the last decade, oxide ceramics with special structure and morphology have aroused widespread interest, one of which is SiO_2 with unique porous structures.^{1–5} Porous silicas have attracted considerable attention because of their distinguished performance in adsorption technology, catalysis, and medical applications. In general, biotemplating techniques, in which biological materials are used directly as template structures for high-temperature conversion into technical ceramic materials, is an ideal method to fabricate these materials.^{6–8} In recent years, different biotemplating routes have been developed for the conversion of biological materials into biomorphous SiO_2 ceramics. Shin *et al.*⁹ reported the fabrication of hierarchical porous SiO_2 ceramics from wood by a surfactant-template

*Corresponding author. E-mails: zhongli-91@163.com; stjhfut@163.com
doi: 10.2298/JSC090410010Z

sol-gel process. Davis *et al.*¹⁰ produced ordered mesoporous silica by infiltration of bacteria with an SiO₂ gel. Cook *et al.*¹¹ exactly replicated butterfly structures by chemical vapor deposition of silica. However, for the application of bio-templates, how to control the pores shape and size distribution is still a challenge.

Wood is a biodegradable, recyclable, abundant and natural composite with cellulose, hemicellulose, and lignin as the major biopolymeric constituents with additional macromolecular compounds, such as different kinds of fat, oil, wax, resin, etc., as minor constituents. Wood tissues are composed of interconnected cells (tracheids) and open spaces (lumens). These cells are glued together by an intercellular layer and are connected by openings of different shapes. These openings are called pits (bordered pits or simple pits) and are the communication channels between the cells.^{9,12} Owing to its stable and hierarchically porous characteristics, wood is an excellent template for porous structures.

In the present study, porous SiO₂ ceramics were fabricated using fir flour as the biological template structure. Fir wood (classified as coniferous) is composed of a unique cross-sectional constructed tracheidid cells and bordered pits along the tracheid walls for tangential connectivity. Fir wood exhibits a nearly bimodal pore distribution. The scales range from mm via μm to nm.¹² However, the fine structure of the cellulose materials in fir wood is composed of crystalline and amorphous regions. The amorphous regions easily absorb chemicals, whereas the compactness of the crystalline regions makes it difficult for chemical penetration. To increase the pore volume and the corresponding possible amount of the infiltrated SiO₂ precursor, the fir flour was pretreated with a NaOH solution. The sol-gel infiltration process of a low viscous oxide precursor into the fir flour was applied. During burnout of the biological preforms during the calcination process, porous SiO₂ ceramics were obtained, which maintained the morphology of the fir flour. The microstructure, crystallinity change and chemical functional groups of fir flour and porous SiO₂ ceramics were investigated using field emission scanning electron microscopy (FESEM), X-ray diffraction (XRD) analysis and Fourier transform infrared (FTIR) spectroscopy.

EXPERIMENTAL

Material preparation

Fir wood (*Cunninghamia lanceolata*) was ground into flour of approximately 200 μm and dried at 105 °C for 24 h. Dried flour (2.5 g) was treated with 20 wt. % NaOH solution (100 mL) at 30 °C for 2 h in order to remove the fats and fatty acids in the flour. The NaOH-treated flour, which possessed a better connectivity and cellular affinity for the penetration of the precursor solution, was subsequently washed with distilled water until the wash water was alkali-free and then dried at 105 °C for 24 h. The precursor solution was prepared using tetraethyl orthosilicate (TEOS), ethanol (EtOH), distilled water and hydrochloric acid (HCl) in the molar ratio 1:4:4:0.05.

The NaOH-treated flour specimens were infiltrated with the precursor solution at 60 °C for 24 h in a self-made sealed infiltration vessel. Subsequently, the specimens were removed

from the precursor solution and dried in air at 130 °C for 24 h to form *in situ* SiO₂ gels. Finally, the infiltrated specimens were calcined by heating at a rate of 10° C/min to 600, 800 or 1000 °C and held at the desired temperature for 3 h to remove the template by oxidation and then allowed to cool to room temperature.

Characterization

A Fourier transformation infrared spectrometer (Perkin–Elmer Spectrum 100) operating in the transmission mode under a dry air atmosphere was employed to record the FTIR spectra of the samples in the wavenumber range 4000–400 cm⁻¹ using the KBr pellet technique.

For crystalline phase identification, the X-ray diffraction patterns of the samples were measured on a powder X-ray diffraction meter (Rigaku D/Max-rB). The crystallinity index (I_c) was determined by using Eq. (1):

$$I_c = \frac{I_{(002)} - I_{(am)}}{I_{(002)}} \quad (1)$$

where $I_{(002)}$ is the counter reading at peak maximum at a 2θ angle close to 22°, representing crystalline material, and $I_{(am)}$ is the counter reading at peak maximum at a 2θ angle close to 18°, representing amorphous material in the cellulosic fir flour.

Field emission scanning electron microscopy (FEI Sirion 200, operated at 5 kV) was employed to observe the morphological features of the samples. For field emission scanning electron microscopy (FESEM) observations, the sample was pre-sputtered with a conducting layer of Au for 2 min at 10 kV.

The N₂ adsorption isotherms were measured with a Micromeritics ASAP 2020 adsorption analyzer. The pore size distributions (PSD) were calculated from the adsorption branches of the N₂ isotherms using the Barrett–Joyner–Halenda (BJH) method.

RESULTS AND DISCUSSION

FTIR Analysis

The spectra of fir flour, NaOH-treated flour, SiO₂ gel-treated flour composite and SiO₂ ceramics are shown in Fig. 1. In the spectra of the fir flour and NaOH-treated flour (Fig. 1, a and b, respectively), the absorption bands at 2928 and 1374 cm⁻¹ are attributed to the C–H stretching and bending vibration in cellulose. The absorption band of the C–O stretch vibrations in cellulose and hemicelluloses are at 1054 cm⁻¹, which is the highest intensity band. Furthermore, the vibration peak at 1732 cm⁻¹, attributed to the C=O stretching of methyl ester and carboxylic acid, was absent in the spectrum of the NaOH-treated flour. This indicated the removal of pectin, waxy and natural oils covering the external surface of the cell wall by the alkali treatment. The ratio of peak heights at 1374 and 2928 cm⁻¹ (H_{1374}/H_{2928}) in the FTIR spectra of the flour samples was used for the determination of the crystallinity index of cellulose in fir flour.¹³ In this study, the H_{1374}/H_{2928} ratio decreased from 1.2 for fir flour to 0.93 for the NaOH-treated flour, suggesting that the proportion of the amorphous material had increased in the NaOH-treated flour.

In the spectra of the SiO₂-gel-treated flour composite and SiO₂ ceramics calcined at 800 °C (Fig. 1, c and d, respectively), the absorption bands at 1090, 800

and 460 cm^{-1} are ascribed to the asymmetric and symmetric stretching vibrations of Si–O–Si bonds. In the FTIR absorption spectrum of the SiO_2 gel-treated flour composite (Fig. 1, c), peaks characteristic for both flour and SiO_2 absorption spectra appear, suggesting that no chemical reaction between the SiO_2 gel and the fir flour occurred during the infiltration. In the FT IR spectrum of the product obtained at a calcination temperature of $800\text{ }^\circ\text{C}$, the peaks assigned to fir flour became negligible and nearly only the peaks ascribed to the Si–O–Si asymmetric and symmetric stretching vibrations were evident, suggesting that the calcination went nearly to completion.

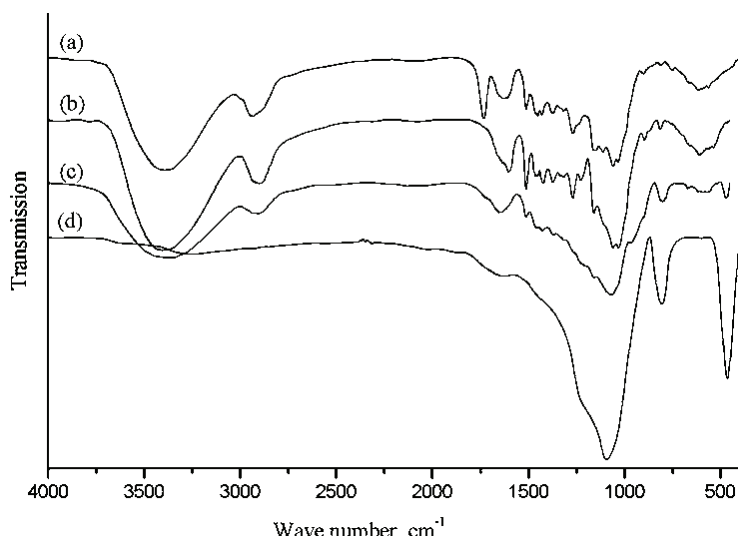


Fig. 1. FTIR Spectra of a) fir flour, b) NaOH-treated flour, c) SiO_2 gel-treated flour composite and d) SiO_2 ceramics calcined at $800\text{ }^\circ\text{C}$.

XRD Analysis

The XRD patterns of the fir flour, NaOH-treated flour, SiO_2 gel-treated flour composite and the SiO_2 gel dried at $1\text{--}10\text{ }^\circ\text{C}$ are shown in Fig. 2. The major diffraction planes of the cellulose in fir flour, namely the (101), (002) and (040) planes, are present at 2θ angles of 16.5 , 22.3 and 34.3° .¹⁴ The characteristic peak of cellulose can be seen in Fig. 2 (a and b). There was no crystalline transformation of the crystalline structure in the NaOH-treated flour. However, the NaOH treatment decreased the intensity of the (020) plane, suggesting that the degree of crystallinity of cellulose was decreased. The crystallinity index (I_c) decreased from 68 % for fir flour to 58 % for the NaOH-treated flour, suggesting that alkali treatment increased the proportion of amorphous material present in the fir flour as also suggested by FTIR results. In Fig. 2 (d), a broad peak centered at $2\theta = 23.2^\circ$ indicates that the SiO_2 gel was in the amorphous

state.¹⁵ Characteristic peaks of both fir flour and SiO₂ gel can be found in Fig. 2 (c). The broad peak at $2\theta = 23^\circ$ is formed by the overlapping the cellulose characteristic peak centered at $2\theta = 22.3^\circ$ and a SiO₂ gel relevant peak. The peak characteristic for cellulose at 16.5° has a lower intensity than that shown in Fig. 2 (b). The peak characteristic for cellulose at 34.3° was absent.

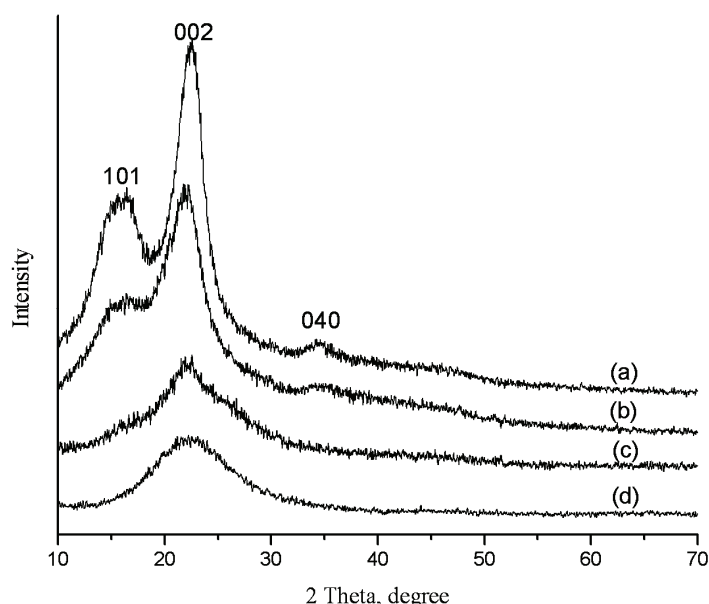


Fig. 2. XRD Patterns of a) fir flour, b) NaOH-treated flour, c) SiO₂ gel-treated flour composite and d) SiO₂ gel.

The XRD patterns of the SiO₂ ceramics calcined at 600, 800 and 1000 °C in air are illustrated in Fig. 3. According to these patterns, the original components of fir flour were completely removed. There is only one broad peak centered at $2\theta = 23.2^\circ$, suggesting that amorphous SiO₂ was formed during calcination at 600 and 800 °C in air. When the calcination temperature was increased to 1000 °C, the peak became somewhat sharper and more intense. The SiO₂ after calcination at 1000 °C in air had a typical cristobalite structure. There were eight crystal peaks at 2θ values of 21.8, 28.5, 31.1, 36.0, 42.5, 44.6, 46.8, and 48.5°, which correspond to (110), (111), (102), (200), (211), (202), (113) and (212). The calculated size of the SiO₂ using the Scherrer Equation was in the range 1.8–4.1 nm. Some amount of the tridymite structure was found as evidenced by the additional peaks at 2θ values of 20.8 and 27.5°.

FESEM Analysis

The SEM micrographs of fir flour, NaOH-treated flour, the SiO₂ gel-treated flour composite and the SiO₂ ceramics calcined at 800 °C are shown in Fig. 4.

The fir wood, which is a softwood, is composed of a unique cross-sectional constructed tracheid cell and bordered pits along the tracheid walls. Figs. 4a and 4b show that bordered pits of 5–10 μm can be observed on the cell walls, which are channels that connect the different tracheid cells and enhance their connectivity. By comparing Fig. 4b with Fig. 4d, it is evident that NaOH treatment can clean the surface of the flour, and enlarge the size of the pit pores. The highly uniform parallel tubular cellular structures and ordered arrays of bordered pits can be clearly observed (Fig. 4c). The pit pores at the tracheid walls are 10–15 μm in diameter (Fig. 4d).

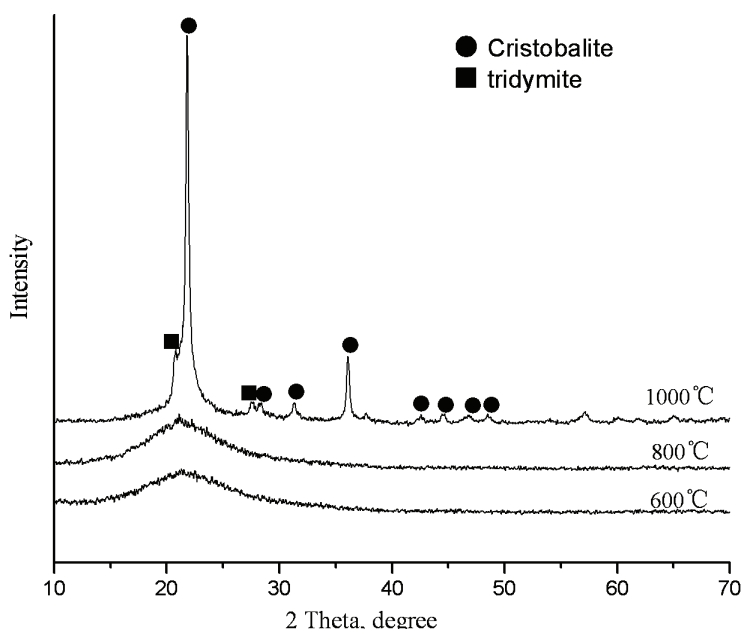


Fig. 3. XRD Patterns of NaOH-treated flour specimens infiltrated with SiO_2 ceramics calcined at various temperatures in air.

After the NaOH-treated fir flour had been infiltrated with SiO_2 sol, subsequent gelling and drying occurred, and an SiO_2 gel-treated flour composite was formed (Figs. 4e and 4f). It can be seen that the gel covered the surface of the flour and filled almost all the pores of tracheids and pits, suggesting that the SiO_2 sol penetrated the cell wall structures and condensed around the cellular tissues.¹⁶ Figures 4g and 4h show the SiO_2 ceramics calcined at 800 °C. In comparison with the fir flour, the obtained ceramic materials retained the ordered pores structure of the fir flour. The array of tubular tracheid and pit pores were retained. However, the pit pores shrank to 1–5 μm , and some cracks on the walls were created by the thermal contraction.

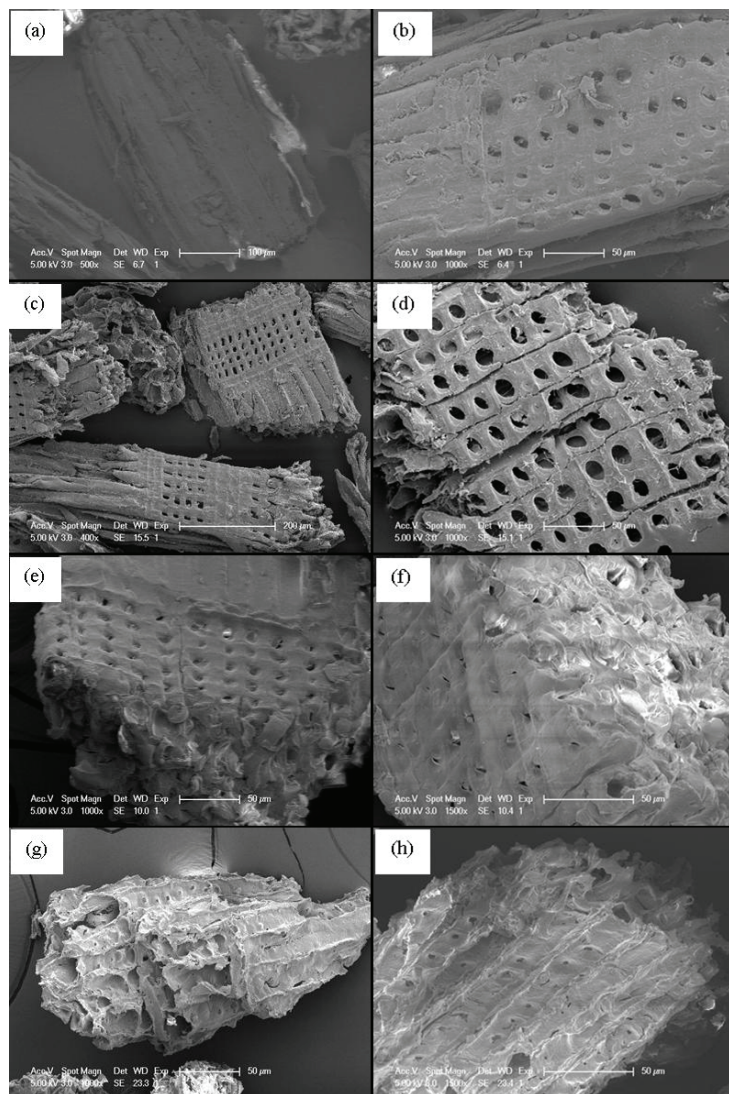


Fig. 4. SEM Micrographs of fir flour (a and b), NaOH-treated flour (c and d), SiO₂ gel-treated flour composite (e and f) and SiO₂ ceramics calcined at 800 °C (g and h).

N₂ Adsorption measurement

From the N₂ adsorption measurement, the isotherms and corresponding PSD curves for SiO₂ ceramics calcined at 800 °C are shown in Figs. 5a and 5b, respectively. The obtained isotherm can be classified as type-IV according to the IUPAC classification with an H3 hysteresis loop. According to the PSD curves, the size distribution fell in the range of mesopore (2–40 nm), as can be seen in

Fig. 5b. The adsorption–desorption hysteresis occurs in the p/p_0 range 0.41–0.99, demonstrating that the materials contained mesopores of relatively uniform pore size. The H3 hysteresis loop indicates the asymmetric slot shape of the mesopores or channels coincidence with the tubular characteristics of the pores of the fir flour. Meanwhile, a narrow hysteresis loop illustrates an interconnected mesoporous system and high pore connectivity according to the percolation theory.¹²

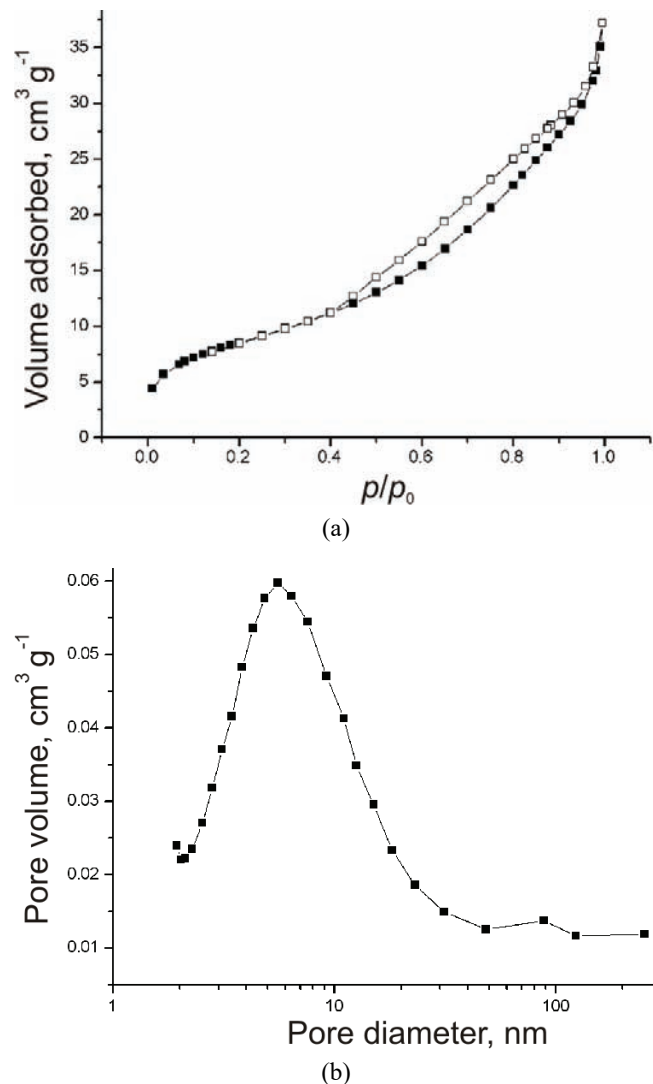


Fig. 5. N_2 adsorption results of SiO_2 ceramics calcined at 800 °C,
a) isotherm plots and b) PSD curves.

CONCLUSIONS

The structure of fir flour treated with 20 % NaOH solution was analyzed by FTIR spectroscopy, X-ray diffraction analysis and FESEM. The results show that most of the non-cellulosic components, such as pectin, waxy substances and natural oils, covering the external surface of the cell walls were removed and that the crystallinity of the fir flour was decreased after treatment, which changed the topography of the flour and increased the proportion of amorphous material present in the fir flour. The NaOH treatment was useful to achieve a net shape conversion of the complex structures and to increase the pore volume and the corresponding possible amount of the infiltrated precursor.

Porous SiO₂ ceramics were successfully prepared by a simple biotemplated process, *i.e.*, the infiltration of NaOH-treated fir flour with a low viscosity SiO₂ sol and subsequent heat treatment in air. The final oxide products retained the ordered pores structure and also exhibited unique pore size and distribution with a hierarchy on the nanoscale derived from the fir flour.

Acknowledgements. This work was supported by the National Science Foundation of China (No. 50773017).

ИЗВОД

МОРФОЛОГИЈА SiO₂ ДОБИЈЕНОГ ИЗ ШАБЛОНА ОД ПИЉЕВИНЕ ЈЕЛЕ

ZHONG LI^{1,2}, TIEJUN SHI¹ и LIYING GUO¹

¹School of Chemical Engineering, Hefei University of Technology, Hefei 23009 u ²School of Chemical Engineering, Anhui University of Science & Technology, Huainan 232001, China

Испитивано је добијање SiO₂ са контролисаном порозном структуром из шаблона од пилевине јеле сол-гел поступком. Пилевина јеле одређене крупноће, која је третирана 20 % раствором NaOH, филтрирана је SiO₂ солом мале вискозности и затим термички третирана у ваздуху, чиме се формира високопотозна структура SiO₂. Микроструктура SiO₂ и формирање фаза током поступка испитивани су дифракцијом X-зрака (XRD), инфрацрвеном спектроскопијом са Фуреовим трансформацијама (FTIR) и скенирајућом електронском микроскопијом исијавања из поља (FESEM). Расподела пора по величини у коначном производу мешана је адсорцијом N₂ (PSD). Резултати указују на то да се мења топографија површине и повећава удео аморфне фазе у пилевини третираној раствором NaOH. Коначни оксидни производ задржао је уређену структуру пора и показао је униформну расподелу пора по величини, са хијерархијом на нано-нивоу добијеном из пилевине јеле.

(Примљено 10. априла, ревидирано 25. новембра 2009)

REFERENCES

1. O. D. Velev, T. A. Jede, R. F. Lobo, A. M. Lenhoff, *Nature* **389** (1997) 447
2. B. T. Holland, C. F. Blanford, T. Do, A. Stein, *Chem. Mater.* **11** (1999) 795
3. O. D. Velev, E. W. Kaler, *Adv. Mater.* **12** (2000) 531
4. M. Kanungo, M. M. Collinson, *Chem. Commun.* **5** (2004) 548
5. M. E. Davis, *Nature* **417** (2002) 813

6. J. Cao, O. Rusina, H. Sieber, *Ceram. Int.* **30** (2004) 1971
7. Z. Liu, T. Fan, W. Zhang, D. Zhang, *Micropor. Mesopor. Mater.* **85** (2005) 82
8. A. Egelja, J. G ulicovski, A. D evecerski, B. Babić, M. Miljković, S. Bo šković, B. Matović, *J. Serb. Chem. Soc.* **73** (2008) 745
9. Y. Shin, J. Liu, J. H. Chang, Z. Nie, G. J. Exarhos, *Adv. Mater.* **13** (2001) 728
10. S. A. Davis, S. L. Burkett, N. H. Mendelson, S. Mann, *Nature* **385** (1997) 420
11. G. Cook, P. L. Timms, C. G. Spickermann, *Ang. Chem. Int. Ed.* **42** (2003) 557
12. X. Li, T. Fan, Z. Liu, J. Ding, Q. Guo, D. Zhang, *J. Eur. Ceram. Soc.* **26** (2006) 3657
13. S. Y. Oh, D. I. Yoo, Y. Shin, H. C. Kim, H. Y. Kim, Y. S. Chung, W. H. Park, J. H. Youk, *Carbohydr. Res.* **340** (2005) 2376
14. L. Y. Mwaikambo, M. P. Ansell, *J. Appl. Polym. Sci.* **84** (2002) 2222
15. J. Locs, L. Berzina-Cimdina, A. Zhurinsh, D. Loca, *J. Eur. Ceram. Soc.* **29** (2009) 1513
16. Y. Shin, C. Wang, W. D. Samuels, G. J. Exarhos, *Mater. Lett.* **61** (2007) 2814.



Supercritical CO₂ extract and essential oil of bay (*Laurus nobilis L.*) – chemical composition and antibacterial activity

JASNA IVANOVIĆ^{1*}#, DUŠAN MIŠIĆ², MIHAJLO RISTIĆ³,
OLIVERA PEŠIĆ¹ and IRENA ŽIŽOVIĆ^{1#}

¹Faculty of Technology and Metallurgy, Karnegijeva 4, 11000 Belgrade, ²Faculty of Veterinary Medicine, University of Belgrade, Bulevar Oslobođenja 18, 11000 Belgrade

and ³Institute for Medical Plant Research "Dr Josif Pančić",
Tadeuša Košćuška 1, 11000 Belgrade, Serbia

(Received 3 March, revised 26 September 2009)

Abstract: The present study deals with the supercritical carbon dioxide (SC-CO₂) extraction and hydrodistillation (HD) of dried bay leaves (*Laurus nobilis L.*). The chemical composition and antibacterial activity of the SC-CO₂ extract and essential oil (EO) from dried leaves of bay were compared to each other and literature data. Qualitative and quantitative analyses of the SC-CO₂ extract and EO were performed using GC-FID and GC-MS analytical methods. A significant difference in the chemical composition of the SC-CO₂ extract and EO was observed. The EO comprised high contents of monoterpenes and their oxygenated derivates (98.4 %), principally 1,8-cineole (33.4 %), linalool (16.0 %) and α-terpinyl acetate (13.8 %), sabinene (6.91 %) and methyl eugenol (5.32 %). The SC-CO₂ extract comprised twice less monoterpenes and their oxygenated derivates (43.89 %), together with sesquiterpenes (12.43 %), diterpenes (1.33 %) and esters (31.13 %). The major components were methyl linoleate (16.18 %), α-terpinyl acetate (12.88 %), linalool (9.00 %), methyl eugenol (8.67 %), methyl arachidonate (6.28 %) and eugenol (6.14 %). An investigation of the antibacterial activity of bay SC-CO₂ extract and EO was completed on different *Staphylococcus* strains using the broth macrodilution method. *Staphylococcus intermedius* strains were the most susceptible to both the SC-CO₂ extract and EO (*MIC* = 640 µg/ml).

Keywords: *Laurus nobilis*; bay; supercritical extraction; essential oil; antibacterial activity; gas chromatography.

INTRODUCTION

Dried leaves and the essential oil (EO) of bay (*Laurus nobilis L.*) are used extensively in the food industry for seasoning of meat products, soups, and fishes.¹

* Corresponding author. E-mail: jasnai@tmf.bg.ac.rs

Serbian Chemical Society member.

doi: 10.2298/JSC090303003I

Several studies have evaluated the potential role of bay EO as an antimicrobial and antifungal agent,^{2–4} as well as the antioxidant properties of leaves extracts.^{5–8} Recently, bay extracts obtained by solvent extraction were studied for their cytotoxic activity.^{9,10}

The EOs and plant extracts are generally obtained by hydrodistillation (HD) and solvent extraction (SE), although these methods suffer certain disadvantages. During HD, extensive hydrolysis and thermal degradation phenomena can be induced, giving in any case a product with a characteristic off-odor. SE can give an oil but, due to a high content of waxes and/or other high molecular mass compounds, often gives rise to a concentrate with a scent very similar to that of the material from which it was derived. A further drawback of SE is that small amounts of organic solvents can pollute the extraction product. Supercritical fluid extraction (SFE) can be used for the production of flavors and fragrances from natural materials and can constitute a valid alternative to both of the above-mentioned processes.¹¹ Tuning of the process parameters (pressure, temperature) enables tuning of the selectivity of supercritical carbon dioxide (SC-CO₂) towards desirable fractions as well as complete separation of the phases so that a solvent-free extract can be obtained. Several research groups investigated SC-CO₂ extraction in order to isolate biologically active compounds from *Laurus nobilis* leaves,^{4,8,12,13} berries¹⁴ and seeds.¹⁵ The chemical composition of the EO and extracts isolated from bay leaves were studied by different researchers.^{4,12,13,16–22}

Previously investigated bay EO isolated by HD was reported for its inhibitory effects on the pathogens²¹ in following order: *Escherichia coli* O157:H7 > *Staphylococcus aureus* > *Staphylococcus typhimurium* > *Listeria monocytogenes*. Bouzouita *et al.*² reported that the high content of 1,8-cineole in the EO of *L. nobilis* L. contributed to its weak antimicrobial activity on two bacteria (*Lactobacillus plantarum* and *E. coli*) and a fungus (*Geotrichum candidum*). Santoyo *et al.*⁴ reported that a SC-CO₂ extract had the strongest antimicrobial activity against *S. aureus* ATCC 25923, substantial activity against *Bacillus subtilis* ATCC 6633, *Pseudomonas aeruginosa* ATCC, 10145, *E. coli* ATCC 11 775 and *Candida albicans* ATCC 60193 strains while the fungi *Aspergillus niger* ATCC 16404 was the least susceptible.

In this study, SC-CO₂ extraction and hydrodistillation of dried bay leaves were compared with respect to their efficiency and selectivity. Thus, the yield and chemical composition of the SC-CO₂ extract and EO obtained by HD of bay leaves were investigated and are discussed herein. The antibacterial activity of bay SC-CO₂ extract and EO was investigated against chosen *Staphylococcus* strains.

EXPERIMENTAL

Plant material

Dried leaves of bay (*Laurus nobilis* L.) originating from Montenegro (2007) were used for the SC-CO₂ extraction and HD. The plant material was milled in a blender and sieved to the fraction with average particle diameter of 0.8–0.9 mm.

Supercritical carbon dioxide extraction

Extraction with SC-CO₂ was performed in a previously described²³ pilot-plant-scale supercritical fluid extractor (Autoclave Engineers SCE Screening System) with a 150 ml extraction cell. Commercial carbon dioxide (99 % purity, Messer Tehnogas, Belgrade, Serbia) was used for the extraction. The SC-CO₂ extraction was performed under a pressure of 10 MPa and at a temperature of 40 °C (density of SC-CO₂, 630 kg/m³). The initially used mass of the plant material was 24 g and the solvent rate was 0.3 kg/h.

Hydrodistillation

Plant material (24 g) and water (500 ml) were placed in a Cleaver-type apparatus. The EO was isolated by HD for 4 h. The obtained EO was kept in a sealed vial at 4 °C until required.

GC/FID/MSD

The qualitative and quantitative analyses of the SC-CO₂ extract and EO were performed using Hewlett-Packard GC-FID and GC-MS analytical methods. In the first instance, a model HP-5890 Series II chromatogram, equipped with a split-splitless injector, HP-5 capillary column (25 m×0.32 mm, film thickness 0.52 µm) and a flame ionization detector (FID), was employed. Hydrogen was used as the carrier gas (1 ml/min). The injector was heated at 250 °C, the detector at 300 °C, while the column temperature was linearly programmed from 40 to 260 °C (4 °C/min). GC-MS analysis was realized under the same analytical conditions, using a model HP G 1800C Series II GCD analytical system equipped with an HP-5MS column (30 m×0.25 mm×0.25 µm). Helium was used as the carrier gas. The transfer line (MSD) was heated at 260 °C. The EI mass spectra (70 eV) were acquired in the scan mode in the *m/z* range 40–400. In each case, the sample in a solution in hexane (1 µl) was injected in the split mode (1:30). Identification of constituents was performed by matching their mass spectra and Kovats indices (*I_K*) with those obtained from authentic samples and/or the NIST/Wiley spectra libraries, different types of search (PBM/NIST/AMDIS) and available literature data (Adams, 2007).²⁵ Area percents, obtained by the integration of corresponding chromatograms (FID), were used for quantification of the individual components.

Antibacterial activity

The investigation of the antibacterial activity of the SC-CO₂ extract and EO was performed on six *Staphylococcus* strains originating from dogs, cattle, humans and visual sources of animal origin. The investigated strains were isolated from ear and tonsils swabs and from cheese and raw milk samples. A reference strain *S. aureus* ATCC 25923 (Becton Dickinson) was also included in the investigation.

The antimicrobial effects of the plant extracts were investigated by the broth macrodilution method according to CLSI (Clinical and Laboratory Standards Institute, 2008) prescribed references^{26,27} for antimicrobial susceptibility testing. A single modification of the method concerned the fact that the plant extracts were used instead of antibiotics, but the principle of the procedure as well as the means of preparation and culture media were not altered. The antimicrobial activity of the plant extracts was investigated in concentrations (ex-

pressed in µg/ml): 1280; 640; 320; 160; 80; 40; 20 and 10. Mueller Hinton II broth (cation adjusted, CAMHB, Becton Dickinson), was used in the investigation. Bromocresol Purple 1.6 % (Merck) in a final concentration of 0.2/200 v/v for the gram-positive bacteria and Phenol Red 1 % in a final concentration of 1/200 v/v for the gram-negative bacteria were added to the CAMHB to obtain bacterial growth visibility. The desired inoculum density of 5×10^5 CFU/ml was achieved by preparing a suspension of the bacteria of approximately 1×10^8 – 2×10^8 CFU/ml, which was the same density as the McFarland standard 0.5 (Becton Dickinson). The prepared suspension was diluted 10 times to obtain a final inoculum density of approximately 1×10^7 – 2×10^7 CFU/ml and 50 µl of this suspension was applied to the CAMHB, after which the number of bacteria in the media was approximately 5×10^5 /ml. The active substance gentamicin sulfate purity 685 µg/mg (Sigma) was used for comparative antibiotic susceptibility testing. The media were incubated at 37 °C for 18 h. The MIC values were taken as the lowest extract concentration in the broth with no visible bacterial growth.

RESULTS AND DISCUSSION

The yield of the EO was 1.43 % after 4 h of HD, which has been in accordance with previously published data.^{11,12,17,18} Ozek *et al.*¹³ reported oil yields (on a dry weight basis) of 2.6 % for hydro- and 1.9 % for steam distillation after 3 h (coastal line of Turkey). Carreda *et al.*¹² isolated 0.90 % of EO from bay leaves (southern Sardinia, Italy) after 4 h. Recently, a novel microwave method was applied to the hydrothermal extraction of essential oil from bay leaves.¹⁸ This study¹⁸ revealed that the yield of EO obtained by HD in a Clevenger-type apparatus equipped with an electric mantle heater for 1 h (traditional method) was 0.784 %, while the yields of EO obtained by HD with a 200 and 300 W microwave system for 1 h were 0.813 and 1.132 %, respectively. Verdian-Rizi *et al.*¹⁹ obtained 0.654–1.132 % of EO from the aerial parts of bay in different vegetative stages after 4 h.

In the present study, the yield of bay SC-CO₂ extract obtained by a single-stage SC-CO₂ extraction was 1.37 % after 1.4 h of extraction ($m_{CO_2}/m_{solid} = 16.67$). Ozek *et al.*¹³ reported similar yields of bay SC-CO₂ extract, 1.34 % (8 MPa and 40 °C) and 1.13 % (8 MPa and 50 °C). Carreda *et al.*¹² isolated a SC-CO₂ extract by fractional separation at 9 MPa and 50 °C (waxes were entrapped in the first separator set at 9 MPa and –10 °C, the oil was recovered in the second separator at 1.5 MPa and 10 °C). In the mentioned study,¹² the authors reported a yield of essential oil fraction of 0.82 % after 4 h ($m_{CO_2}/m_{solid} = 21.44$).

The results of chemical analyses of the obtained SC-CO₂ extract and essential oil (EO) accomplished by GC-FID and GC-MSD are presented in Table I. Thirty-four components were detected and identified in the EO of bay obtained by HD. The EO comprised mostly oxygenated monoterpenes (78.77 %) and hydrocarbon monoterpenes (19.68 %). Sesquiterpenes (1.06 %) and their oxygenated (0.53 %) were also found in the EO of bay. The main components in the EO were 1,8-cineole (33.4 %), linalool (16.0 %), α-terpinyl acetate (13.8 %), sabinene (6.91 %), methyl eugenol (5.32 %), α-pinene (4.39 %) and β-pinene (3.52 %). A simi-

lar chemical composition of the oil extracted from bay leaves was observed by several authors.^{12,13,17–21} In these papers, 1,8-cineole was reported to be the main component in the bay EO isolated by HD, whereby its content was in the range of 23.51–60.72 %.

TABLE I. Percentage composition of the compounds identified in the SC-CO₂ extract and EO (mass %)

Component	<i>I</i> _K (Kovats index)	SC-CO ₂ Extract	EO
p-Xylene 871.6		0.44	—
α-Thujene 919.2		—	0.55
α-Pinene 924.8		—	4.39
Camphene 938.9		—	0.30
Sabinene 965.0		—	6.91
β-Pinene 967.2		—	3.52
Dehydro-1,8-cineole 984.4		—	0.21
β-Myrcene 985.1		—	0.14
α-Phellandrene 997.1		—	0.17
δ ³ -Carene 1002.7		—	0.24
α-Terpinene 1009.3		—	0.42
p-Cymene 1017.7		—	0.41
Limonene-β-phellandrene 1020.9		—	1.59
1,8-Cineole 1025.0		2.53	33.4
γ-Terpinene 1051.3		—	0.74
cis-Sabinene hydrate	1061.5	0.25	0.30
Terpinolene 1080.7		—	0.33
Linalool 1096.3		9.00	16.0
δ-Terpineol 1161.0		0.49	0.57
Terpinen-4-ol 1170.3		0.90	2.38
p-Cymen-8-ol 1175.5		0.23	—
α-Terpineol 1184.5		2.54	2.83
Nerol 1227.0		0.44	0.19
Linalyl acetate	1250.4	0.58	0.34
4-Thujen-2α-yl acetate	1296.1	0.20	0.28
Bornyl acetate	1278.7	0.27	0.47
δ-Terpinyl acetate	1310.1	0.55	0.68
exo-2-Hydroxycineole acetate	1335.8	0.31	0.20
α-Terpinyl acetate	1343.8	12.88	13.8
Eugenol 1352.8		6.14	1.77
β-Elemene 1383.8		0.69	—
Methyl eugenol	1400.4	8.67	5.32
β-Caryophyllene 1409.8		0.87	0.43
α-Guaiene 1429.7		0.18	—
α-Humulene 1444.1		0.71	—
allo-Aromadendrene 1451.2		0.16	—
Germacrene D	1472.0	0.55	—
β-Selinene 1476.8		0.33	—
Bicyclogermacrene 1487.3		0.72	0.36
Germacrene A	1493.0	0.39	—



TABLE I. Continued

Component	<i>I</i> _K (Kovats index)	SC-CO ₂ extract	EO
γ-Cadinene 1504.7		0.29	—
δ-Cadinene 1514.4		0.32	0.27
<i>trans</i> -Cadinene-1,4-diene 1522.5		0.41	—
α-Cadinene 1534.0		0.79	—
Dauca-5,8-diene 1565.9		0.56	—
Spathulenol 1567.9		0.79	0.27
Caryophyllene oxide	1572.7	0.46	0.26
Viridiflorol 1581.4		0.49	—
Ledol 1592.3		0.21	—
Dihydro- <i>cis</i> -α-copaene-8-ol 1608.7		0.20	—
Eremoligenol 1619.5		0.37	—
β-Eudesmol 1640.0		1.45	—
Shyobunol 1680.3		0.25	—
Sedanenolide 1712.4		1.21	—
Neocnidilide (sedanolide)	1717.7	0.36	—
Oplopanone 1729.1		0.17	—
Neophytadiene isomer I	1806.8	0.26	—
Dehydrosaussurea lactone	1823.8	0.35	—
Hexahydrofarnesyl acetone	1835.0	0.40	—
Methyl palmitate ^a 1915.4		1.49	—
Eremanthin (vanillosimin)	1981.0	0.20	—
Methyl linoleate	2087.2	16.18	—
Methyl petroselinate ^b	2092.2 5.95		—
Phytol 2102.4		1.33	—
Methyl stearate ^c 2117.5		1.23	—
Methyl arachidonate	2215.1	6.28	—

^aMethyl hexadecanoate; ^bmethyl *cis*-6-octadecenoate; ^cmethyl octadecenoate

Sixty-three components were detected of which fifty two were identified (93.0 %) in the bay SC-CO₂ extract. The supercritical extract comprised mostly oxygenated monoterpenes (43.2 %) and fatty acid esters (31.13 %), followed by sesquiterpene hydrocarbons (7.26 %) and their oxygenated derivates (5.17 %), hydrocarbons (2.60 %), phthalides (1.57 %), diterpenes (1.33 %) and monoterpene hydrocarbons (0.69 %). The most abundant components in the SC-CO₂ extract were methyl linoleate (16.18 %), α-terpinyl acetate (12.88 %), linalool (9.00 %), methyl eugenol (8.67 %), methyl arachidonate (6.28 %) and eugenol (6.14 %). A comparison of the chemical composition of the SC-CO₂ extract and that of the EO revealed significant differences. The SC-CO₂ extract comprised more than two times less monoterpene hydrocarbons and oxygenated monoterpenes (43.89 %) in comparison to EO (98.4 %). Carreda *et al.*¹² studied the chemical composition of fractions of the SC-CO₂ extract during 4 h. According to this study,¹² the lighter compounds (hydrocarbon monoterpenes) were extracted almost completely during the first extraction hour, the content of oxygenated monoter-

penes decreased to a minor extent with time, content of hydrocarbon sesquiterpenes increased significantly with time, while the content of oxygenated sesquiterpenes did not change much after the 3rd hour.

Buttery *et al.*²⁸ stated that 1,8-cineole is the major aroma component of bay oil, followed by linalool. In addition, substances present in lower concentrations, such as eugenol and (*E*)-isoeugenol, and especially the non-identified compounds at trace levels, possessing a pepper-like odor, have to be considered as key aroma compounds with a marked influence on the overall odor and flavoring quality of the leaves.²⁷ In the present study, the contents of eugenol and methyl eugenol were two times higher than in the EO. A significant difference in the 1,8-cineole content in the EO and extract was also observed. The SC-CO₂ extract in this study had a very low content of 1,8-cineole (2.53 %) and high contents of eugenol (6.14 %) and methyl eugenol (8.67 %) compared to those previously reported for an SC-CO₂ extract.¹² This can be result of the shorter extraction time applied in the present study (1.4 h), since Carreda *et al.*¹² observed remarkable differences in the contents 1,8-cineole and methyl eugenol after the first and fourth hour of extraction (1,8-cineole, 30.98 vs. 2.05 % and methyleugenol, 6.85 vs. 16.42 %). Ozek *et al.*¹³ identified high contents of 1,8-cineole (40.2–43.0 %) and low contents of eugenol and methyl eugenol (0.7–0.8 %) in SC-CO₂ extracts obtained at 8 MPa and at temperatures of 40 and 50 °C.

According to the *MIC* values given in Table II, bay EO and SC-CO₂ extract had the same antibacterial activity against the investigated *S. intermedius* and *S. aureus* strains. One of the *S. intermedius* strains was more susceptible to the presence of the SC-CO₂ extract and EO, with an *MIC* value of 640 µg/ml. However, the antibacterial activities against the other *Staphylococcus* strains were lower with an *MIC* value of 1280 µg/ml.

TABLE II. The minimum inhibitory concentrations (*MIC*) of the bay SC-CO₂ extract measured by the broth macrodilution (BMD) test

Bacterial strain	Origin of the examined strains	<i>MIC</i> / µg ml ⁻¹		
		EO SC	-CO ₂ extract	Gentamicin
<i>S. aureus</i> ATCC 25923	Reference strain	1280	1280	≤0.5
<i>S. intermedius</i>	Ear swab from dog	640	640	2
<i>S. intermedius</i>	Ear swab from dog	1280	1280	1
<i>S. aureus</i>	Feta cheese	1280	1280	1
<i>S. aureus</i>	Milk sample from cow with mastitis	1280	1280	1
<i>S. aureus</i>	Tonsil swab from human	1280	1280	2

Antibacterial activity of the SC-CO₂ extract and EO isolated from bay leaves could be the result of high contents of linalool (SC-CO₂, 9.00 %; EO, 16.00 %), α-terpinyl acetate (SC-CO₂, 12.88 % ; EO, 13.8 %), methyl eugenol (SC-CO₂,

8.67 %; EO, 5.32 %), eugenol (SC-CO₂, 6.14 %; EO, 1.77 %) and α -terpineol (SC-CO₂, 2.54 %; EO, 2.83 %), which were previously reported to have antibacterial activity.²⁹ High contents of methyl esters were identified in the SC-CO₂ extract (methyl linoleate, 16.18 %; methyl arachidonate, 6.28 %). The high antibacterial activity of eugenol was previously reported.³⁰ Fatty acids and fatty acid methyl esters were also reported to have significant antibacterial and antifungal activity.³¹ In the present study, despite the much lower content of 1,8-cineole in the SC-CO₂ extract, the high contents of eugenol, methyl eugenol, and methyl esters³¹ together with other active components (e.g., linalool, α -terpinyl acetate) could contribute to its antibacterial activity.

CONCLUSIONS

In this study, similar yields of EO and SC-CO₂ extract were observed, although the supercritical extraction was a less time-consuming process. This study reported significant antimicrobial activity of bay EO and SC-CO₂ extract against the tested *Staphylococcus* strains. Despite having much lower contents of monoterpenes and their oxygenate derivates, which are generally considered to be responsible for antibacterial activity, the SC-CO₂ extract had the same antibacterial activity as the EO. The high contents of eugenol, methyl eugenol and fatty acid methyl esters together with other active components (e.g., linalool, α -terpinyl acetate, 1,8-cineole) in the SC-CO₂ extract could contribute to its overall antibacterial activity. One of the *S. intermedius* strains was more susceptible to both bay EO and SC-CO₂ extract than the other strains. The presented results indicate that bay EO and SC-CO₂ extract could be considered for use not only as a spice and flavoring agent but also as preservative in the food industry.

Acknowledgments. Financial support of this work by the Ministry of Science and Technological Development of the Republic of Serbia (Project TR 19037) is gratefully acknowledged.

ИЗВОД

НАТКРИТИЧНИ ЕКСТРАКТ И ЕТАРСКО УЉЕ ЛОВОРА (*Laurus nobilis* L.) – ХЕМИЈСКИ САСТАВ И АНТИБАКТЕРИЈСКА АКТИВНОСТ

ЈАСНА ИВАНОВИЋ¹, ДУШАН МИШИЋ², МИХАИЛО РИСТИЋ³, ОЛИВЕРА ПЕШИЋ¹ и ИРЕНА ЖИЖОВИЋ¹

¹Универзитет у Београду, Технолошко-металуршки факултет, Карнегијева 4, 11000 Београд, ²Институт за проучавање лековитог биља „Др Јосиф Панчић“, Тадеуша Кошчушки 1, 11000 Београд и ³Универзитет у Београду, Факултет ветеринарске медицине, Булевар Ослобођења 18, 11000 Београд

У раду је испитана надкритична екстракција и хидродестилација осушених листова ловора (*Laurus nobilis* L.). Приказана је упоредна анализа хемијског састава и антибактеријске активности надкритичног екстракта и етарског уља као и поређење истих са литературним подацима. За квалитативну и квантитативну анализу хемијског састава надкритичног екстракта и етарског уља коришћене су GC-FID и GC-MS аналитичке методе. Хемијски састав надкритичног екстракта и уља ловора био је веома различит. Најзаступљеније компоненте у етарском уљу били су монотерпени и њихови кисеонични деривати (98,4 %), пре свега 1,8-

-цинеол (33,4 %), линалоол (16,0 %), α -терпинил-ацетат (13,8 %), сабинен (6,91 %) и метил-еугенол (5,32 %). Надкритични екстракт ловора садржао је два пута мању количину монотерпена и њихових кисеоничних деривата у односу на етарско уље (43,89 %) поред сескви-терпена (12,43 %), дитерпена (1,33 %) и естра (31,13 %). У надкритичном екстракту најзаступљеније компоненте били су метил-линолеат (16,18 %), α -терпинил-ацетат (12,88 %), линалоол (9,00 %), метил-еугенол (8,67 %), метил-арахидонат (6,28 %) и еугенол (6,14 %). Антибактеријско деловање надкритичног екстракта и етарског уља ловора испитивано је на сојевима *Staphylococcus* применом макродилуционе методе у бујону. Сојеви *Staphylococcus intermedius* били су најосетљивији на надкритични екстракт и етарско уље ловора при чему су вредности MIC биле 640 µg/ml.

(Примљено 3. марта, ревидирано 26. септембра 2009)

REFERENCES

1. H. Surburg, J. Panten, *Common Fragrance and Flavor Materials, Preparation, Properties and Uses*, 5th ed., Wiley-VCH Verlag, Weinheim, 1985, p. 212
2. N. Bouzouita, F. Kachouri, M. Hamdi, M. M. Chaabouni, *Flavour Fragr. J.* **18** (2003) 380
3. A. Si mić, D. Soković, M. Ristić, S. Grujić-Jovanović, J. Vukovićević, P. D. Marin, *Phytother. Res.* **18** (2004) 713
4. S. Santoyo, R. Lloría, L. Jaime, E. Ibanez, F. J. Senorans, G. Reglero, *Eur. Food Res. Technol.* **222** (2006) 565
5. M. Simić, T. Kundaković, N. Kovačević, *Fitoterapia* **74** (2003) 613
6. M. Skerget, P. Kotnik, M. Hadolin, A. R. Hras, M. Simonic, Z. Knez, *Food Chem.* **89** (2005) 191
7. A. Demo, C. Petrakis, P. Kefalasa, D. Boskoub, *Food Res. Int.* **31** (1998) 351
8. D. J. M. Gomez-Coronado, C. J. Barbas, *J. Agric. Food Chem.* **51** (2003) 5196
9. A. Barla, G. Topcu, S. Oksuz, G. Tumen, D. G. I. Kingston, *Food Chem.* **104** (2007) 1478
10. B. Kılçak, T. Mert, *Fitoterapia* **73** (2002) 242
11. H. Hafizoğlu, M. Reunanen, *Lipid-Fett* **95** (1993) 304
12. A. Caredda, B. Marongiu, S. Porcedda, C. Soro, *J. Agric. Food Chem.* **50** (2002) 1492
13. T. Ozek, B. Bozan, and K. H. C. Baser, *Chem. Nat. Comp.* **34** (1998) 668
14. H. Marzouki, A. Piras, B. Marongiu, A. Rosa, A. M. Dessì, *Molecules* **13** (2008) 1702
15. S. H. Beis, N. T. Dunford, *J. Am. Oil Chem. Soc.* **83** (2006) 953
16. A. Kilic, H. Hafizoglu, H. Kollmannsberger, S. J. Nitz, *J. Agric. Food Chem.* **52** (2004) 1601
17. H. Yalçın, M. Anik, M. A. Sanda, A. J. Cakir, *J. Med. Food* **10** (2007) 715
18. G. Flaminio, T. Marianna, P. L. Cioni, L. Ceccarini, A. S. Ricci, I. J. Longo, *J. Chromatogr. A* **1143** (2007) 36
19. M. Verdian-Rizi, *J. Environ. Agric. Food Chem.* **7** (2008) 3321
20. F. J. Müller-Riebau, B. M. Berger, O. Yegen, C. Cakir, *J. Agric. Food Chem.* **45** (1997) 4821
21. I. Dadaliolu, A. Evrendilek, *J. Agric. Food Chem.* **52** (2004) 8255
22. M. C. Diaz-Ma roto, M. S. Prez-Coello, M. D. J. Cabezudo, *J. Agric. Food Chem.* **50** (2002) 4520
23. I. Žižović, M. Stamenić, J. Ivanović, A. Orlović, M. Ristić, S. Djordjević, S. Petrović, D. Skala, *J. Supercrit. Fluids* **43** (2007) 249



24. *Automated Mass Spectral Deconvolution and Identification System software (AMDIS ver.2.1.)*, National Institute of Standards and Technology (NIST), Standard Reference Data Program, Gaithersburg, MD, 2005
25. R. P. Adams, *Identification of Essential Oil Components by Gas Chromatography/Mass Spectrometry*, 4th ed., Allured Publishing Corporation, Carol Stream, IL, 2007
26. Clinical Laboratory Standards Institute, *Performance standards for antimicrobial susceptibility testing*, 16th Informational Supplement, Vol. 26, No.3, Wayne, PA, 2006
27. H. D. Isenberg, *Antimicrobial susceptibility testing*, in: *Clinical Microbiology Procedures Handbook*, Vol. 2, H. D. Isenberg, Ed., American Society for Microbiology Press, Washington DC, 2004
28. G. R. Butterly, D. R. Black, G. D. Guadagni, L. C. Ling, G. Connolly, R. Teranishi, *J. Agric. Food Chem.* **22** (1974) 773
29. H. J. D. Dorman, S. G. Deans, *J. App. Microbiol.* **88** (2000) 308
30. A. M. Leite, E. O. Lima, E. L. Souza, M. F. F. M. Diniz, V. N. Trajano, I. A. Medeiros, *Braz. J. Pharm. Sci.* **43** (2007) 121
31. G. Agoramoorthy, M. Chandrasekaran, V. Venkatesalu, M. J. Hsu, *Braz. J. Microbiol.* **38** (2007) 739.



On the removal of *s*-triazine herbicides from waters using commercial low-cost granular carbons

F. J. ROJAS MORENO¹, J. M. CARDENETE LÓPEZ¹, R. MARÍN GALVÍN^{1,2},
M. J. MARTÍNEZ CORDÓN³ and J. M. RODRÍGUEZ MELLADO^{4*}

¹Empresa Municipal de Aguas de Córdoba, S.A, C/ De los Plateros, 1, E-14006-Córdoba,

²Departamento de Química Inorgánica e Ingeniería Química, Facultad de Ciencias, Campus Universitario Rabanales, edificio Marie Curie, Universidad de Córdoba, E-14014-Córdoba,

³Departamento de Edafología y Química Agrícola, Facultad de Ciencias, Campus Universitario Rabanales, edificio Marie Curie, Universidad de Córdoba E-14014-Córdoba and

⁴Departamento de Química Física y Termodinámica Aplicada, Facultad de Ciencias, Campus Universitario Rabanales, edificio Marie Curie, Universidad de Córdoba, E-14014-Córdoba, Spain

(Received 7 March 2009)

Abstract: The adsorption capacities of three low-cost granular active carbons, used in a water treatment facility for the removal of the triazine herbicides propazine, prometryn and prometon, was evaluated. Kinetic studies showed that the three carbon samples used could be suitable in practice for the treatment of moderate contents of the herbicides in contaminated waters. The apparent adsorption rate constants were calculated. Equilibrium studies showed that the data fit the Frumkin isotherm. The results show that in the adsorption process there are repulsive lateral interactions that depend mainly on the adsorbate molecules rather than the nature or distribution of the adsorption sites. Such lateral interactions seem to be established mainly between the isopropyl groups of adjacent molecules, being of the same order for the three molecules.

Keywords: granular carbon; adsorption; triazine herbicides; herbicide removal; propazine; prometryn; prometon.

INTRODUCTION

For several decades, active granular carbon has been used in water treatment in the filtration units of landfills because of their known adsorbent properties.¹ There are several parameters on which the efficiency of the different types of granular carbon assets depend: the adsorbent properties of the type of carbon used, grain size and distribution, filter bed depth, treatment applied to the water

*Corresponding author. E-mail: jmrodriguez@uco.es
doi: 10.2298/JSC090307004M

before arriving at the coal filters and finally, but very important, on the concrete compound (or compounds) to be eliminated from the treated water.²

The adsorbent properties of carbons depend on the type of carbon itself, its origin (either vegetable, such as coconut, wood or rubble, or mineral, both in mineral form or coke), and on the exact thermal and/or chemical activation. These properties are standardized according to the adsorption of iodine, of Methylene Blue or of more specific substances, such as atrazine, toluene or trichloroethylene.³ In addition, the practical performance is determined not only by the granulometry (mean particle diameter, effective size, coefficient of uniformity and abrasion) and the depth of the employed filter bed, but also by the purely filtering capacity.⁴

The purely adsorbent activity of an activated carbon (granular or as powder) is related to the presence of "pores" in its surface, which are responsible of the adsorptive process. Although active carbon is an amorphous substance and is essentially apolar, it has surface functional groups (mainly carboxyl-, carbonyl- and phenol-) that are responsible for the adsorption capacity.⁵

On the other hand, the main field of activity in water treatment in which the use of active carbon is increasingly demanded is that of the minimization of synthetic organic compounds, which are difficult to remove by conventional treatments, and that appear with increasing frequency in the waters habitually used for human consumption.

The *s*-triazine herbicides are continuously accessing the environment due to their persistence in soils and hydric sediments, caused by their low solubilities in water, and their strong sorption on carbonous materials and clays.⁶

Wood charcoal was used as an effective low-cost adsorbent for the removal of contaminants, such as endosulfan,⁷ from waters. Other waste activated carbons (granular and powder) were studied for the removal of atrazine.⁸

In a previous paper, the adsorption capacities of three low-cost granular active carbons used in a water treatment facility were evaluated for the removal of simetryn, a triazine herbicide.⁹

The aim of this work was to compare the adsorption capacities of such low-cost granular active carbons for the removal of propazine, prometryn and prometon, three triazine herbicides having the same basic chemical structure but with different substituents, as shown in Fig. 1.

EXPERIMENTAL

In all cases, Merck analytical grade reagents were used with the exception of the triazine herbicides, which were from Polyscience (HPLC standard quality). All reactants were used without further purification.

Commercial active carbons used were provided by Aguas de LevanteTM, GallaquimTM and KemiraTM, having the characteristics given in Table I.

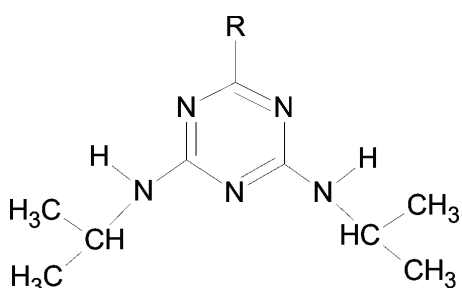


Fig. 1. Chemical structures of the investigated herbicides. Propazine, R = -Cl; prometryn, R = -SCH₃; prometon, R = -OCH₃.

The analyses were made using a Varian GC 3800 gas chromatograph coupled with a n Autodrive 8200 autosampler. The pH of the samples was adjusted to 6.5 by adding HCl or NaOH prior to preconcentration using C18 packed cartridges (Supelco 505471). Such cartridges were connected to a vacuum generator (Supelco 57030-U) equipped with a pump (Millipore XX 55 220 50) and activated by the successive addition of 3 mL hexane, 3 mL ethyl acetate and 2 mL deionized water. The samples were then slowly passed through the cartridges. Dry argon was passed during 20 min through the cartridges. The elution was performed with 2 mL ethyl acetate and 2 mL hexane. The solvent was evaporated from the 4 mL of eluted samples with dry nitrogen and the residual was dissolved in 500 μL hexane. Then, the samples were processed in the gas chromatograph. The calibration of the method was made with standards of the herbicide. When the concentrations of herbicide were very high, the initial samples were diluted with deionized water to suitable volumes.

TABLE I. Characteristics of the studied active carbons

Material	AC1 AC2		AC3
	Coconut	Vegetable	Mineral
Superficial area, m ² g ⁻¹	1000	950	900
Iodine index, mg g ⁻¹	1000	900	950
Methylene Blue index, mg g ⁻¹	260	265	255
Atrazine adsorption (1 μg L ⁻¹), mg g ⁻¹	40	35	30
Toluene adsorption (1 mg L ⁻¹), mg g ⁻¹	100	110	90
Trichloroethylene adsorption (50 μg L ⁻¹), mg g ⁻¹	20	25	25
Abrasion minimum coefficient	75	75	70
Effective size, mm	0.9–1.1	0.9–1.1	0.9–1.1
Particle mean diameter, mm	1.4	1.4	1.35
Uniformity coefficient	1.4	1.3	1.4

For kinetic studies, glass bottles (Schott Duran GL45) of 100 mL capacity were used. A suitable adsorbent dose and 75 mL of solution of simetryn were introduced into such bottles and placed in a thermostated linear bath shaker (from Ovan model Ovantherm 100). Samples of 1 mL were taken at intervals of 15 min. The filtrates of such samples were stored in the dark at 4 °C and analyzed for the residual herbicide concentration as described above. Blank samples consisting of the same solutions but without the herbicide were treated in the same manner.

The equilibrium studies were performed at constant temperature using the data obtained in the previous kinetic study. The same type of samples were placed on the shaker and agitated for a period of 36 h, which was found in the kinetic experiment to be sufficient for

equilibrium to be attained. The filtrates of the samples were stored in the dark at 4 °C and analyzed for residual herbicide concentration. Blank samples consisting of the same solutions but without the herbicide were treated in the same manner.

RESULTS AND DISCUSSION

Typical decreasing curves of the residual herbicide concentration with time were obtained for the three studied samples of carbon. The kinetics of herbicides adsorption by one of the assayed activated carbons is given in Fig. 2 as an example. It can be seen that the equilibrium was attained faster for propazine than for the other two herbicides. In all cases, around a 75 % was removed after 3 h and the maximum removal was reached after 8–12 h, being around 80 %. The extension of the experiments to 36 h showed that a very slight increase in the removal was obtained, although on some occasions, a very slight decrease in the removal was observed. Since the industrial filters have residence times of 1.5 to 2 h, the use of two filtration units mounted in series (or even using only one unit) could be suitable in the practice for the treatment of moderate contents of herbicide in contaminated waters, this being the case for the three studied carbon samples as well as for the three investigated herbicides.

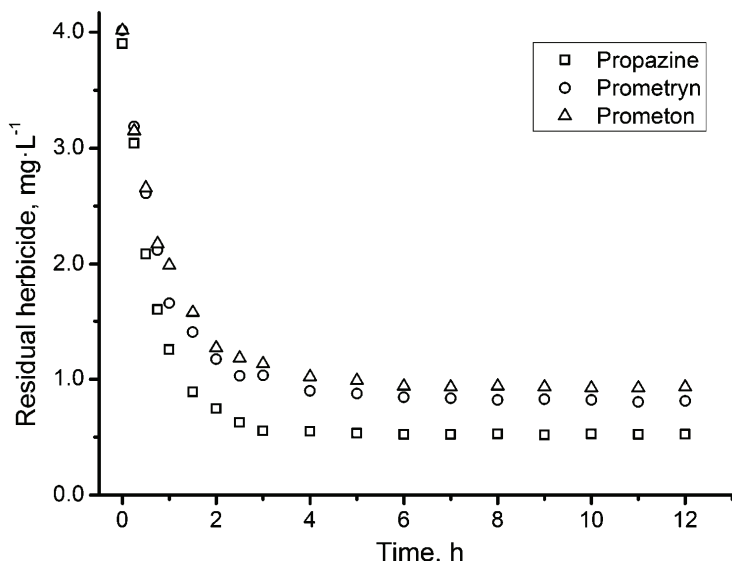


Fig. 2. Adsorption kinetics on carbon AC3 as the residual herbicide concentration vs. time at 25 °C. Initial herbicide concentration, 4 mg mL⁻¹.

Though 12 h seem enough to reach equilibrium conditions, the equilibrium study was performed, as stated above, for 36 h.

Adsorption kinetics can be attributed to the occupation of the available adsorbent sites by the adsorbate molecules. Although the adsorption process could

be complex due to the non-equivalence of the adsorption sites arising from the pore and particle size distributions and differences in the chemical affinities, a simple model can be assumed to compare the adsorption kinetics of the herbicides onto the samples. At infinite time, it could be supposed that all the available sites had been occupied and the number of available sites must be proportional to the difference between the initial and the residual concentrations of adsorbent. If a second-order adsorption kinetics is assumed (first-order in both the adsorbate and the sites of adsorption), it is easy to show that the following equation is fulfilled:

$$\ln \frac{c - c_\infty}{c} = \ln \frac{c_0}{c_0 - c_\infty} - kt$$

where c_0 , c and c_∞ are the initial and residual herbicide concentration at the instant and at infinite time, respectively, and k is the apparent rate constant.

Plots corresponding to the studied three carbons are shown in Fig. 3. As can be seen, the plots are linear, indicating that the above equation can be considered as a good approximation for the adsorption process.

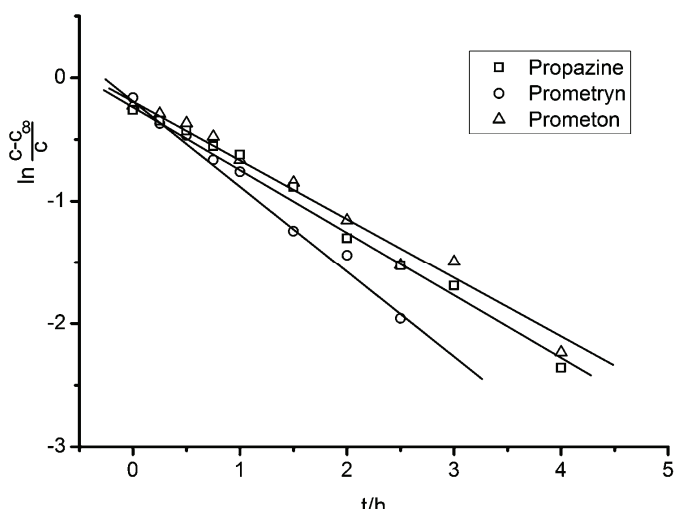


Fig. 3. Plots corresponding to the kinetic model; Carbon AC2.

The apparent rate constants for the three carbons used are given in Table II. As can be seen, although the AC1 carbon leads in all cases to the maximum removal, the other carbons reached equilibrium more rapidly. In general, the AC3 carbon approached equilibrium with an apparent rate constant similar to that of AC2 but giving a maximum removal similar to that of AC1. In addition, the adsorption of propazine occurred faster than the adsorptions of the two other compounds and equilibrium was reached at *c.a.* 45 min, 1 h prior that for propazine.

TABLE II. Apparent rate constants ($k / \text{mg g}^{-1} \text{h}^{-1}$) for the adsorption processes

Sample	Propazine	Pro mtryn	Prometon
AC1	0.66	0.47	0.46
AC2	0.78	0.63	0.61
AC3	0.76	0.59	0.56

The adsorption of the herbicides onto granular active carbons from solutions in distilled water does not fit the Langmuir isotherm. Nevertheless, it fits well with the Freundlich isotherm, as is shown by the fact that the plots of $\ln q$ vs. $\ln c$ were linear (q being the amount of adsorbed herbicide). This isotherm is useful for practical work with the herbicide-adsorbent system.

In addition, if it is assumed that at the tested concentrations the maximum adsorption was not reached (which seems logical because the maximum concentration of the herbicide samples is limited by the low solubility of these substances in water), the fitting with the Frumkin isotherm is good. Hence, using the data obtained at the lowest concentrations, the values of q_{\max} , K and a/q_{\max} can be estimated from the intercept and the slope of the plot of $\ln(q/c)$ vs. q , respectively, as shown in Fig. 4. Thus, q_{\max} was obtained using the higher concentrations and the estimated parameters, and fitting the experimental data to the Frumkin equation.

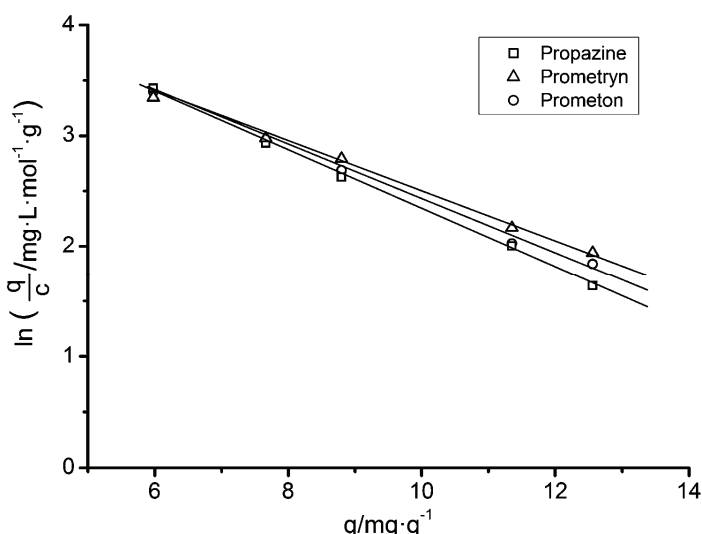


Fig. 4. Plot of the linearized Frumkin isotherm for AC1 carbon.

The results show that in the adsorption process there are repulsive lateral interactions, because the exponential parameters of the isotherm are negative. The results obtained for the three carbons and the three herbicides investigated are given in Table III.

Table III. Isotherm parameters; q – adsorbed herbicide (mg g^{-1}), K – adsorption constant, a – adsorption parameter, q_{\max} – maximum specific adsorption capacity (mg g^{-1}); Freundlich: $q = Kca$; Frumkin: $(q/(q_{\max} - q))\exp(-2aq/q_{\max}) = Kc$

Herbicide Sample	$K_{\text{Freundlich}}$	$a_{\text{Freundlich}}$	K_{Frumkin}	a_{Frumkin}	q_{\max}
Propazine	AC1 10.21	0.31	122.2	-3.13	27.15
	AC2 9.32	0.39	109.7	-3.27	25.62
	AC3 9.12	0.37	115.3	-3.37	25.05
Prometryn	AC1 9.87	0.30	121.9	-3.09	26.32
	AC2 8.66	0.38	108.9	-3.21	23.92
	AC3 8.82	0.36	114.1	-3.34	24.75
Prometon	AC1 9.82	0.30	120.9	-3.09	26.02
	AC2 8.63	0.37	108.6	-3.20	23.51
	AC3 8.79	0.35	112.3	-3.31	24.58

As can be seen, the calculated maximum specific adsorption capacity was similar for the three investigated carbons, although it was slightly higher for AC1. On the other hand, the repulsive lateral interactions arising from the exponential parameter of the Frumkin isotherm are very similar for the three samples. This indicates that these repulsive lateral interactions depend mainly of the adsorbate molecules rather than the nature or distribution of the adsorption sites. Moreover, such lateral interactions are very similar for the three herbicides. This could easily be explained if it is assumed that the adsorption of the three compounds occurs with the triazine ring parallel to the carbon surface, as is the case on mercury electrodes.^{10–12} Hence, the main lateral interactions must be established mainly between the isopropyl groups of adjacent molecules, and these interactions must be of the same order for the three molecules.

Acknowledgements. Financial support from Junta de Andalucía (Research Group FQM-0198) and DGICYT (Project CTQ2006-07224/PPQ) is gratefully acknowledged.

ИЗВОД

УКЛАЊАЊЕ *s*-ТРИАЗИНСКИХ ХЕРБИЦИДА ИЗ ВОДА ПОМОЋУ КОМЕРЦИЈАЛНИХ ГРАНУЛИСАНИХ УГЉЕВА

F. J. ROJAS MORENO¹, J. M. CARDENETE LÓPEZ¹, R. MARÍN GALVÍN^{1,2},
M. J. MARTÍNEZ CORDÓN³ и J. M. RODRÍGUEZ MELLADO⁴

¹Empresa Municipal de Aguas de Córdoba, S.A, C/ De los Plateros, 1, E-14006-Córdoba, ²Departamento de Química Inorgánica e Ingeniería Química, Facultad de Ciencias, Campus Universitario Rabanales, edificio Marie Curie, Universidad de Córdoba, E-14014-Córdoba, ³Departamento de Edafología y Química Agrícola, Facultad de Ciencias, Campus Universitario Rabanales, edificio Marie Curie, Universidad de Córdoba E-14014-Córdoba and ⁴Departamento de Química Física y Termodinámica Aplicada, Facultad de Ciencias, Campus Universitario Rabanales, edificio Marie Curie, Universidad de Córdoba, E-14014-Córdoba, Spain

Испитиван је адсорpcionи капацитет три комерцијална гранулисана активна угља. Они су коришћени у третману вода за уклањање триазинских хербицида, пропазина, прометрина и прометона. Кинетичка испитивања су показала да три употребљена узорка активних угљева могу бити корисни у пракси за третман вода са умереним садржајем хербицида.

Израчунате су константе брзине адсорпције. Добијени резултати су у сагласности са Фрумкиновом изотермом. Резултати показују да током адсорпције постоје одбојне бочне интеракције које знатно више зависе од карактеристика адсорбата, а мање од расподеле и типа активних места на адсорбенсу. Таква бочна интеракција се остварује углавном између изопропил група суседних молекула који су истом положају код сва три испитивана хербицида.

(Примљено 7. марта 2009)

REFERENCES

1. R. Marín Galvín, *Equipamientos y Servicios Municipales* **34** (1990) 65
2. D. Lemarchand, A. Le Marechal, G. Martin. *TSM-L'eau* **11** (1981) 561
3. *Commercial information from Aguas de Levante™, Galaquim™ and Kemira™*, 2006
4. R. Marín Galvín, *Análisis de Aguas y Ensayos de Tratamiento: Principios y Aplicaciones*, Ed. G. P. E., S.A., Barcelona, Spain, 1995
5. P. Y. Divet. *Ingeniería Química*, octubre 1976, 123
6. J. Ayele, P. Levavasseur, M. Mazet, *J. Water-SRT Aqua* **45** (1996) 28
7. Y. Sudhakar, A. Dikshit, *J. Environ. Sci. Health* **34** (1999) 587
8. P. K. Gosh, L. Philip, *J. Environ. Sci. Health* **40** (2005) 425
9. L. Alonso, M. González Jiménez, J. M. Cardenete López, R. Marín Galvín, J. M. Rodríguez Mellado, *VirtualPro* **86** (2009)1
10. M. J. Higuera, M. Ruiz Montoya, R. Marín Galvín, J. M. Rodríguez Mellado, *J. Electroanal. Chem.* **474** (1999) 174
11. M. J. Higuera, M. Ruiz Montoya, R. Marín Galvín, J. M. Rodríguez Mellado, *Bull. Electrochem.* **19** (2003) 513
12. J. M. Rodríguez Mellado, R. Marín Galvín, M. Ruiz Montoya, in *New trends in electrochemistry research*, M. Núñez, Ed., Nova Science Publishers Inc., New York, 2007, p. 187.



Humic acid from Shilajit – a physico-chemical and spectroscopic characterization

SURAJ P. AGARWAL¹, M. D. KHALID ANWER^{1,3*}, RAJESH KHANNA²,
ASGAR ALI¹ and YASMIN SULTANA¹

¹Dept. of Pharmaceutics, Faculty of Pharmacy, Jamia Hamdard (Hamdard University), New Delhi-110062, ²Dabur Research Foundation, 22, Site IV, Sahibabad, Ghaziabad, Uttar Pradesh-201010, India and ³College of Pharmacy, Al-kharj, King Saud University, K.S.A.

(Received 16 March, revised 22 June 2009)

Abstract: Shilajit is a blackish-brown exudation, consisting of organic substances, metal ions and minerals, from different formations, commonly found in the Himalayan region (1000–3000 m) from Nepal to Kashmir. Shilajit can also be collected throughout the mountain region in Afghanistan, Bhutan, China, Bajkal, throughout Ural, Caucasus and Altai mountains also, at altitudes between 1000 to 5000 m. The major physiological action of shilajit has been attributed to the presence of bioactive dibenzo- α -pyrones together with humic and fulvic acids, which act as carrier molecules for the active ingredients. In this work, the aim was to extract humic acid from Shilajit from various sources and characterised these humic acids based on their physicochemical properties, elemental analysis, UV/Vis and FTIR spectra, X-ray diffraction pattern and DSC thermograms. The spectral features obtained from UV/Vis, FTIR, XRD and DSC studies for samples of different origins showed a distinct similarity amongst themselves and in comparison to soil humic acids. The surfactant properties of the extracted fulvic acids were investigated by determining the effect of increasing concentration on the surface tension of water. The study demonstrated that humic acids extracted from shilajit indeed possessed surfactant properties.

Keywords: Shilajit; humic acid; FTIR spectra; DSC; XRD; surfactant properties.

INTRODUCTION

Shilajit, also known as salajit, shilajatu, mumie or mummiyo, is a blackish-brown exudate coming out from layer of rocks in many mountain ranges, especially in the Himalayas and Hindukush ranges of the Indian subcontinent.¹ It is also found in Russia, Tibet, Norway and other countries, where it is collected in small quantities from steep rock faces at altitudes between 1000 and 5000 m. Shi-

*Corresponding author. E-mails: -manwer@ksu.edu.sa; mkanwer2002@yahoo.co.in
doi: 10.2298/JSC090316006A

lajit samples from different regions of the world, however, vary in their physiological properties.²

It mainly consists of p alaeohumus (around 80–85 %) and organic compounds derived from vegetation f ossils that were compressed under la yers of rocks for hundreds of years and underwent significant metamorphosis due to the prevalent high temperature and pressure conditions.⁵

Extensive research has been performed to determine the exact chemical nature of Shilajit. Earlier work on shilajit showed that its major organic constituents included benzoic acid, hippuric acid, fatty acids, resin and waxy materials, gu ms, albuminoids and vegetabl e matter with benzoic acid being the active substance.^{6,7} Extensive research in the eighties showed that the major organic mas s of Shilajit was comprised of hum us (60–80 %) along with other com ponents, such as benzoic acid, hippuric acid, fatty acids, ichthyol, ellagic acid, resin, triterpenes, sterol, aromatic carboxy lic acid , 3,4-be nzocoumarins, amino acids and phen olic lipids.⁸ The major physiological action of Shilajit was found to be due to the presence of bioactive dibenzo - α -pyrones along with humic and fulvi c acids, which acted as the carrier molecules for the active substances.^{9–11} Recently, the physico-chemical, spectral and thermal properties of shilajit and its humic substances were reported, which further confirmed its humic nature.^{12–15} Elemental analysis and spectroscopic techniques, such as UV/Vis, FTIR and X-ray diffraction and DSC analyses have been widely used for the characterization of hum ic acids obtained from lignite, charcoal, soil, sewage sludge and compost.^{16,17} In this study, these methods were applied for t he first time to humic acids extracted from Shilajit from different sources.

EXPERIMENTAL

Materials and methods

An authentic sample of rock Shilaj it (RS) w as obtain ed from Da bur Re search Foundation, Ghaziabad, India. Dried Shilaj it extracts were also obtained from three different commercial sources in India, *viz.*, Pioneer Enterpris es (PE) – Mumbai, Natural Remedies (NR) – Bangalore and Gurukul Kangri (GK) – Haridwar. The humic acid was extracted from all the samples of Shilajit and characterised based on their physico-chemical properties and their elemental analysis. Scanning electron microscopy and spe ctal analysis, such as UV/Vis, FTIR, DSC and X-ray diffraction, were perfor med. The E_4/E_6 ratio was al so determined. The spec tral properties were compared with a humic acid standard from Sigma Aldrich.

Extraction of humic acid from Shilajit

Finely powdered shilaj it was succe ssively extracted¹⁸ with 5 00 ml each of hot organic solvents of increasing polarity, *i.e.*, chloroform, ethyl acetate and methanol, to remove the bio-active co mponents, specific ally oxygenated dibenzo- α -pyrones. The so-ob tained extracted Shilajit was taken and dispersed in 0.10 M aqueous sodium hydroxide with intermittent shaking under nitrogen at room temperature for 24 h. The suspension was filtered to remove humin (insoluble in water at all pH values) and the filtrate was acidified with dilute HCl to a pH of less than three. The solution was allowed to stand at room temperature (25 °C) overnight. The humic acid, which separated out as a coagulate, was filtered, dried and pulverized.

Elemental analysis

The C, H, N and S contents were determined by packing the fulvic acid powder in tin boats after careful weighing (Balance – Mettler Toreto, MX5) with the aid of a CHNS analyzer (Vario EL-III). The obtained values are expressed as dry weight of powder, in mass %.

UV/Vis Spectroscopy

The UV/Vis spectra of various HA extracts from shilajit of different origins were obtained on a Shimadzu, 1601 UV/Vis spectrophotometer by dissolving the various HA samples in water and recording the spectra in a 1 cm quartz cuvette in the wavelength range 200–800 nm. Since humic substances usually yield uncharacteristic spectra in the UV and visible, the E_4/E_6 ratio (ratio of the absorbance of the solution at 465 and 665 nm)¹⁹ was determined for the various samples.

Fourier transform infrared spectroscopy (FTIR)

The FTIR spectra of HA samples were recorded on a W in-IRrez (Bio-Rad, Hercules, CA, USA) using the potassium bromide (KBr) disc technique. The samples (2 mg) were mixed with potassium bromide (about 100 mg) in a clean glass pestle and mortar and compressed to obtain a pellet. The base line was corrected and scanning was performed from 4000–400 cm^{-1} .

Powder X-ray diffraction

Powder X-ray diffraction patterns of powdered samples of HA were obtained using a Panalytical X-ray diffractometer, PW3719. All the samples were treated according to the following specifications: target/filter (monochromator), Cu; voltage/current, 40 kV/50 mA; scan speed, 4 °/min.

Differential scanning calorimetry (DSC)

A Perkin–Elmer Pyris 6 instrument was used for recording DSC thermograms of the HA samples obtained from different shilajit sources. Samples (2–8 mg) were accurately weighed and heated in closed aluminium crimp cells at a rate of 10 °C/min under a dynamic nitrogen atmosphere (flow rate 20 ml/min) over the 50–300 °C temperature range.

Scanning electron microscopy

Scanning electron micrographs of the powdered samples were obtained using a Joel JSM-840 scanning electron microscope with a 10 kV accelerating voltage. The surface of samples for SEM was made electrically conductive in a sputtering apparatus (Fine Coat Ion Sputter JFC-1100) by evaporation of gold.

Surfactant properties

The surfactant properties of the humic acids were investigated by determining the effect of increasing the concentration of humic acid on the surface tension of water. The surface tension of the solutions was determined by the drop-weight method using a stalagmometer. Solutions of fulvic acids in the concentration range 0–1.4 % w/v were prepared. Each solution was separately sucked into the stalagmometer and allowed to drop slowly from it. The drop rate was adjusted to approximately 2–3 drops/min. and the weight of 10 drops was measured.

RESULTS AND DISCUSSION

Extraction of humic acid from shilajit

The yields obtained at the different stages of the earlier reported method and the improved method for the extraction of humic acid from shilajit are compared in Table I. The yields of HA extracted from shilajit from Dabur, Gurukul Kangri,

Natural Remedies and Pioneer Enterprises were 2.5, 9.2, 8.7 and 8.7 %, respectively. These are high proportion compared with those reported in the literature.¹⁸ The maximum yield of HA was obtained from the Gurukul Kangri shilajit.

TABLE I. Comparison of the yields of humic acid from Shilajit obtained from different sources

Shilajit	Yield of fulvic acid, %								
	Reported method			Improved method					
	I	II	III	Mean ± SD	I	II	III	Mean ± SD	
RS	1.2	1.0	1.4		1.2 ± 0.2	2.2	2.8	2.6	2.5 ± 0.3
GK	7.5	7.8	7.3		7.5 ± 0.3	9.2	8.9	9.5	9.2 ± 0.3
NR	5.8	6.2	6.9		6.3 ± 0.6	8.1	8.9	9.1	8.7 ± 0.5
PE	6.9	6.4	7.1		6.8 ± 0.4	9.3	8.8	8.5	8.9 ± 0.4

Physical characteristics

The physical characteristics of the humic acids extracted from Shilajit of different origin are listed in Table II. The extracted HA from shilajit of different origins exhibit very similar physico-chemical characteristics, indicating no qualitative variation in the Shilajit samples and in their extraction procedure.¹⁸ Slight variations are to be expected and were seen in these HA samples. All the HA samples were brownish black in colour and had a typical characteristic odour and taste. The pH of 2 % aqueous solutions ranged from 3.46 to 3.86. The ratio of the absorbance at 465 and 665 nm (E_4/E_6) has been widely used by soil scientist for characterization purposes. The E_4/E_6 ratio for all the examined HA samples ranged from about 3.0 to 4.0, which are consistent with those reported in the literature.¹⁷

Elemental analysis

Elemental analysis of humic substances is generally used to establish their nature and origin.²⁰ As shown in Table III, a comparison of carbon, hydrogen, ni-

TABLE II. Comparison of the physical characteristics of humic acid from Shilajit of different origins

Characteristic	Humic acid (RS)	Humic acid (GK)	Humic acid (NR)	Humic acid (PE)
Nature	Dark brown powder	Dark brown powder	Dark brown powder	Dark brown powder
Colour	Dark Brown	Dark Brown	Dark Brown	Dark Brown
Odour Charact	eristic	Characteristic	Charact eristic	Characteristic
Taste Charact	eristic	Characteristic	Charact eristic	Characteristic
pH of 2 % aq. solution	3.86 3.77 3.46			3.68
Absorbance at 465 nm (E_4)	0.513 0.542		0.284	0.222
Absorbance at 665 nm (E_6)	0.144 0.180		0.072	0.072
E_4/E_6 ratio	3.56 3.01 3.94			3.08

trogen and sulphur contents of the humic acids extracted from Shilajit of different origins with those of soil humic acids²¹ and the Sigma Aldrich standard humic acid revealed that the content of C, H, N and S were very low in the case of the humic acids extracted from the pioneer shilajit. The carbon, hydrogen, nitrogen and sulphur contents also varied significantly among the samples of humic acids. These differences may be due to differences in the origin, different isolation techniques and error in sampling and analysis. The C/N ratio also varied among the samples of humic acids.

TABLE III. Elemental analysis of humic acids extracted from shilajit of different origins

Source of humic acid	% C	% H	% N	% S	C/N ratio
Rock Shilajit (Dabur)	36.46	5.15	3.03	0.70	12.0
Shudh Shilajit (Gurukul Kangri)	45.36	5.92	2.31	0.39	19.63
Shilajit extract (Natural Remedies)	51.48	5.89	3.27	0.81	15.73
Shilajit extract (Pioneer Enterprises)	27.44	2.90	1.24	0.26	22.10
Sigma Aldrich (Std. HA)	42.28	4.25	0.57	0.81	73.09

UV/Vis Spectra

The UV/Vis spectra of the various samples of humic acids extracted from Shilajit of different origin were recorded in water from 200 nm to 800 nm are shown in Fig. 1. The samples did not exhibit any sharp maxima but exhibited a slight hump near 260–280 nm, which is characteristic of humic substances.¹⁹ As discussed previously, this hump is attributed to the absorption of radiation by the double bonds C=C, C=O and N=N of the aromatic or unsaturated components of humic

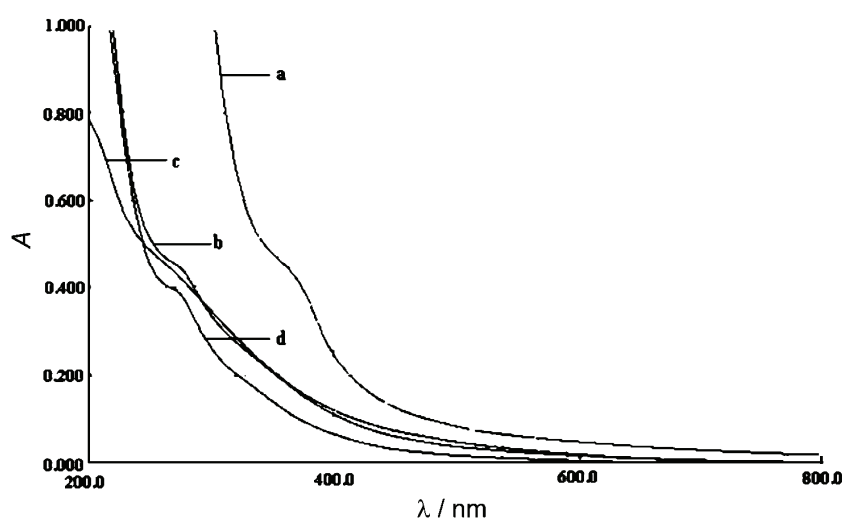


Fig. 1. UV/Vis Spectra of humic acid extracted from Shilajit of different origins:
a) RS, b) GK, c) NR and d) PE.

substances.²² The variation in the humic acid observed with the different samples of Shilajit could be attributed to variations in the concentrations of aromatic compounds, which in turn is characteristic of the difference in the humification process.

FTIR Spectra

The FTIR spectra (Fig. 2) of the extracted humic acids were characterised by relatively few broad bands. All the humic acid samples exhibited broad bands at about 3400, 1725 and 1630 cm⁻¹, which can be attributed to hydrogen bonded OH groups, C=O stretching of COOH groups and C=C double bonds, respectively. Sharp bands were observed in the region of 2925, 1400 and 1050 cm⁻¹, which can be attributed to the bending vibration of aliphatic C—H groups, the O—H bending vibrations of alcohols or carboxylic acids and the OH bending deformation of carboxyl groups, respectively.¹⁹

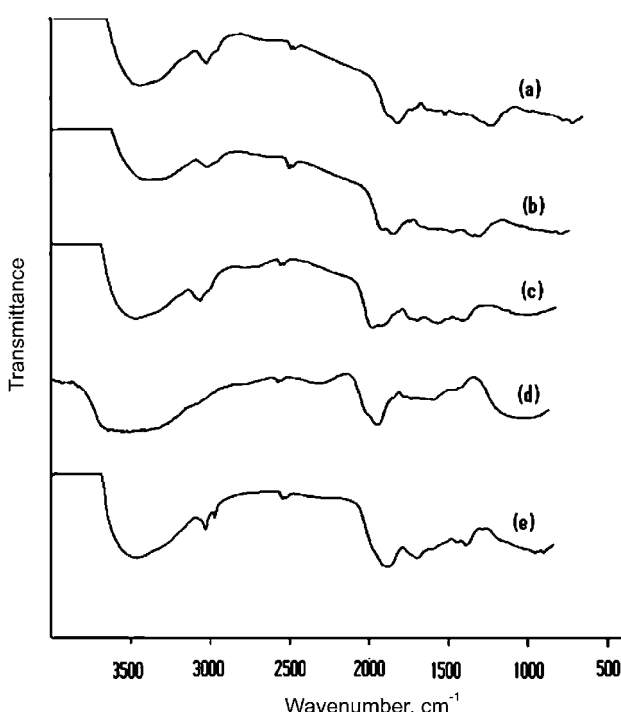


Fig. 2. FTIR Spectra of humic acid extracted from Shilajit of different origins:
a) RS, b) GK, c) NR, d) PE and e) Laurentian humic acid.

X-Ray diffraction pattern

The X-ray diffraction pattern in the 2θ range from 10 to 70° of humic acid extracted from rock shilajit sample (Fig. 3) exhibited very small diffuse peaks with a few intense peaks, implying its non-crystalline nature. This behaviour is

consistent with the behaviour observed in the case of humic substances from other sources.^{23,24}

Differential scanning calorimetry (DSC)

The humic acid of pioneer Shilajit exhibited no sharp endothermic peak, indicating that it does not have any defined melting point (Fig. 4). A shallow endotherm could be observed near 100 °C, which could be attributed to dehydration of the sample. On the other hand, it showed an exothermic peak near 331 °C, which could be attributed to the thermal degradation of carbohydrides, dehydration of aliphatic structures and decarboxylation of carboxylic groups.²⁴

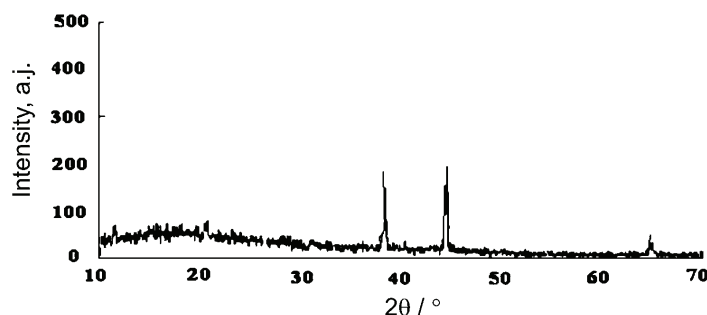


Fig. 3. XRD Pattern of humic acid extracted from the rock Shilajit.

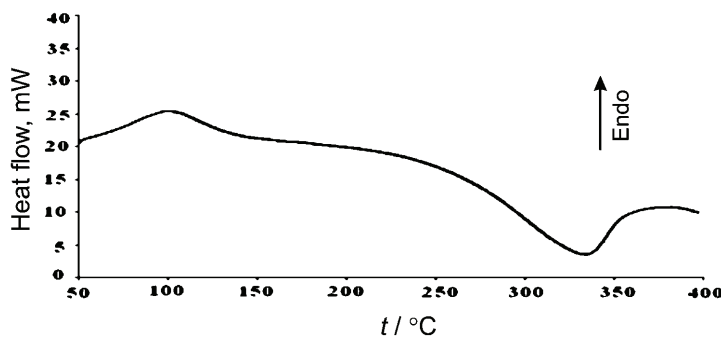


Fig. 4. DSC Spectra of humic acid extracted from the Pioneer Shilajit.

Scanning electron microscopy

The scanning electron micrographs (Fig. 5) of humic acid extracted from rock Shilajit of Dabur showed a loose spongy structure of humic acids with the particles tending to aggregate to each other.

Surfactant properties

As can be seen in Fig. 6, increasing the concentration of extracted humic acids in water clearly led to a decrease in the surface tension. The decrease was ini-

tially gradual until a concentration of about 0.8 %, w/v, after which it rose slightly and then became almost constant. This could be due to the formation of micelle at this concentration. This demonstrates that humic acids extracted from Shilajit indeed possess surfactant properties. The value of 0.8 %, w/v, for the critical micelle concentration (CMC) is in agreement with the reported value of 0.7 %, w/v, for humic acids extracted from soil.²⁶

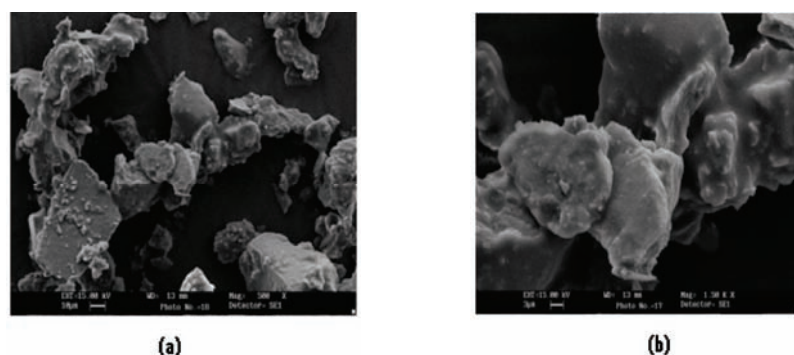


Fig. 5. Scanning electron micrographs of humic acid from rock shilajit; a) 500 \times ; b) 1500 \times .

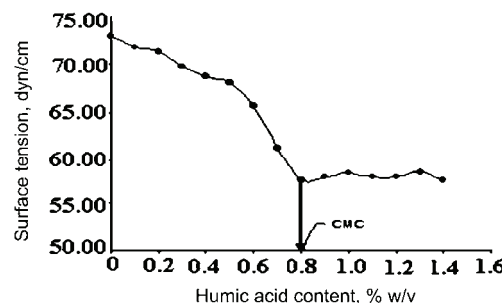


Fig. 6. Effect of humic acid concentration on the surface tension of water.

CONCLUSIONS

Humic acids from the various samples of shilajit were characterised and their physico-chemical and spectral properties compared. Such results are presented for the first time herein. The spectral features obtained from UV/Vis, FTIR, XRD and DSC studies for samples of different origins showed a distinct similarity amongst themselves and in comparison to soil humic acids. The surfactant properties of humic acids were investigated by determining the effect of increasing concentration of humic acids on the surface tension of water. The study demonstrated that the humic acids extracted from shilajit indeed possessed surfactant properties.

Acknowledgements. Our thanks go to the Hamdard National Foundation, Jamia Hamdard, New Delhi, for a fellowship and the financial aid given for the project. The authors are also grateful to Dr. G. N. Qazi, vice chancellor, Jamia Hamdard, for providing the facilities.

ИЗВОД

ХУМИНСКА КИСЕЛИНА ИЗ ШИЛАЦИТА – ФИЗИЧКО–ХЕМИЈСКА И СПЕКТРОСКОПСКА КАРАКТЕРИЗАЦИЈА

SURAJ P. AGARWAL¹, M. D. KHALID ANWER^{1,3}, RAJESH KHANNA², ASGAR ALI¹ и YASMIN SULTANA¹

¹Dept. of Pharmaceutics, Faculty of Pharmacy, Jamia Hamdard (Hamdard University), New Delhi-110062,

²Dabur Research Foundation, 22, Site IV, Sahibabad, Ghaziabad, Uttar Pradesh-201010, India и

³College of Pharmacy, Al-kharj, King Saud University, K.S.A

Шилацит је црно-мрк ексудат, који се састоји од органских супстанци, металних јона и минерала, различитог састава. Широко је распрострањен у хималајској регији (на висинама 1000–3000 m) од Непала до Кашмира. Шилацит се такође може наћи у планинским регијама Авганистана, Бутана, Кине, Бакала, као и на Уралу, Кавказу и Алтају, на висинама између 1000 и 5000 m. Основна физиолошка активност шилацита приписана је присуству биоактивних дibenzo- α -пирона поред хуминске и фулвинске киселине, које делују као носећи молекули активних саставака. У овом раду, циљ је био да се екстражују хуминске киселине из шилацита различитог порекла и да се оне окарактеришу на основу физичко–хемијских својстава, елементалне анализе, UV/Vis и FTIR спектара, дифрактограма X-зрака и DSC термограма. Спектралне карактеристике узорака различитог порекла добијене UV/Vis, FTIR и XRD методама, као и информације добијене DSC техником, показале су очигледну међусобну сличност узорака и сличност са хуминским киселинама из земљишта. Испитивана је и површинска активност екстражованих фулвинских киселина одређивањем утицаја њихове концентрације на површински напон воде. Испитивања су показала да су екстражоване хуминске киселине заиста површински активне.

(Примљено 16. марта, ревидирано 22. јуна 2009)

REFERENCES

- Y. C. Kong, P. P. H. Butt, K. H. Ng, K. F. Cheng, R. C. Cambble, S. B. Malla, *Int. J. Crude Drug Res.* **25** (1987) 179
- S. Ghosal, *Shilajit in perspective*, Narosa Publishing, New Delhi, 2006, p. 1
- S. Ghosal, J. Lal, S. K. Singh, *Soil Biol. Biochem.* **23** (1991) 673
- S. Ghosal, J. Lal, K. Ravi, K. Yatendra, *Soil. Biol. Biochem.* **25** (1993) 377
- S. Ghosal, V. Muruganandam, M. Biswajit, S. K. Bhattacharya, *Indian J. Chem.* **36** (1997) 596
- S. P. Agarwal, R. Khanna, R. Kar markar, M. K. Anwer, R. K. Khar, *Phytother. Res.* **21** (2007) 401
- S. Ghosal, J. P. Reddy, V. K. Lal, *J. Pharm. Sci.* **65** (1976) 772
- R. N. Chopra, I. C. Chopra, K. L. Handa, L. D. Kapoor, *Indigenous Drugs of India*, U. N. Dhar & Sons, Calcutta, 1958, p. 457
- S. P. Agarwal, M. Aqil, M. K. Anwer, *Drug Dev. Indust. Pharm.* **34** (2008) 506
- S. Ghosal, J. Lal, S. K. Singh, G. Dasgupta, M. Bhaduri, M. Mukhopadhyay, S. K. Bhattacharya, *Phytother. Res.* **3** (1989) 249
- S. P. Agarwal, M. Aqil, M. K. Anwer, *Asian J. Chem.* **19** (2007) 4711



12. S. P. Agarwal, R. Khanna, R. Karmarkar, M. K. Anwer, R. K. Khar, *Asian J. Chem.* **20** (2007) 209
13. S. P. Agarwal, M. Aqil, M. K. Anwer, in *Proceeding of 13th Meeting of the International Humic Substances Society*, Karlsruhe, Germany, 2006, p. 465
14. R. Khanna, R. Karmarkar, M. K. Anwer, S. P. Agarwal, R. K. Khar, in *Proceeding of 13th Meeting of the International Humic Substances Society*, Karlsruhe, Germany, 2006, p. 345
15. R. Khanna, M. Witt, M. K. Anwer, S. P. Agarwal, B. P. Koch, *Org. Geochem.* **39** (2008) 1719
16. F. Martin, *Fuel* **54** (1975) 236
17. P. M. Trompowsky, V. D. M. Benites, B. E. Madari, A. S. Pimenta, W. C. Hockaday, P. G. Hatcher, *Org. Geochem.* **36** (2005) 148
18. S. Ghosal, in *Research and Development of Indigenous Drugs*, S. B. Vohara, P. C. Dandiya, Eds., Institute of History of Medicine and Medical Research, New Delhi, 1989, p. 72
19. M. Schnitzer, in *Proceeding of Int. Meeting of Humic Substances*, Nieuwersluis, Pudoc, Wageningen, 1972, p. 293
20. R. McDonnell, N. M. Holden, N. M., S. M. Ward, J. F. Collins, E. P. Farrell, M. H. B. Hayes, *Bio. Environ.* **101** (2001) 187
21. Y. Chen, N. Sensi, M. Schnitzer, *Soil Sci. Soc. Am. J.* **41** (1977) 352
22. M. Domeizel, A. Khalil, P. Prudent, *Bioresource Technol.* **94** (2004) 177
23. G. Chilom, J. A. Rice, *Org. Geochem.* **36** (2005) 1339
24. S. A. Visser, H. Mendel, *Soil Bio. Biochem.* **3** (1971) 259
25. M. Pietro, C. Paola, *Thermochim. Acta* **413** (2004) 209
26. J. S. Gaffney, N. A. Marley, S. B. Clark, *ACS Symp. Ser. 651*, American Chemical Society, Washington DC, 1996.